STUDIES INTO THE MOLECULAR BASIS OF CHLOROPLAST DIVISION

A Dissertation

by

AARON GENE SMITH

Submitted to the Office of Graduate Studies of
Texas A&M University
in partial fulfillment of the requirements for the degree of

DOCTOR OF PHILOSOPHY

May 2011

Major Subject: Biochemistry

Studies into the Molecular Basis of Chloroplast Division

STUDIES INTO THE MOLECULAR BASIS OF CHLOROPLAST DIVISION

A Dissertation

by

AARON GENE SMITH

Submitted to the Office of Graduate Studies of
Texas A&M University
in partial fulfillment of the requirements for the degree of

DOCTOR OF PHILOSOPHY

Approved by:

Chair of Committee,	Andreas Holzenburg
Committee Members,	Tatyana Igumenova
	Timothy Devarenne
	David Stelly
Head of Department,	Gregory Reinhart

May 2011

Major Subject: Biochemistry

ABSTRACT

Studies into the Molecular Basis of Chloroplast Division.

(May 2011)

Aaron Gene Smith, B.S., Oakland University

Chair of Advisory Committee: Dr. Andreas Holzenburg

Chloroplasts are the powerhouses of plants and also perform important storage functions. Chloroplast division is an essential process that involves proteins that are conserved from prokaryotic fission and proteins evolved in eukaryotes. Due to their endosymbiotic origin, the division machineries of chloroplasts and all plastids share some core similarities with the bacterial division apparatus, but during evolution some prokaryotic components of the division machinery were not conserved and some novel components evolved to fulfill new functions. The components of the division apparatus and their interactions are being elucidated, but relatively little is known about the mechanism and dynamics of the first protein families to localize to the division site, FtsZ1 and FtsZ2. This work details a thorough investigation of the biochemical characterization of *Arabidopsis thaliana* FtsZ proteins and begins to determine the mechanism of FtsZ assembly. To achieve these ends a number of techniques were incorporated including: electron microscopy, protein purification, sedimentation and image processing.

Following expression of FtsZ and subsequent purification, experiments aimed at assessing the activity were conducted. These included determining whether the protein

was an active GTPase and capable of self-assembly as the bacterial FtsZ homolog displayed these characteristics. The recombinant protein displayed both of these activities and this result allowed for further characterization. The co-assembly critical concentration and assembly efficiency were determined by sedimentation and were 82.75 μg/ml and 33.4 ± 0.9%, respectively.

Bacterial FtsZ assemblies have been reported to be in dynamic exchange with a soluble pool of FtsZ and the existence of a similar pool in plants has been discussed in the literature. Part of this work undertook the investigation of the composition of the soluble pool in *Arabidopsis* chloroplasts. Gel chromatography revealed that prior to FtsZ assembly initiation the pool consists solely of dimers. Image processing and native PAGE results suggest that at least one assembly intermediate exists between the dimer and mature filamentous assemblies. The most common intermediate observed in assembly reactions is a tetramer. Three-dimensional renderings of the dimer and tetramer are presented and suggest that these oligomeric forms may represent consecutive steps in the assembly mechanism of *Arabidopsis* FtsZ.

DEDICATION

For those no longer with us.

ACKNOWLEDGEMENTS

Those who are important to me already know it and don't need their names in print.

Thank you for the support. It is greatly appreciated.

NOMENCLATURE

ARC	accumulation of replicating chloroplasts
ARTEMIS	*Arabidopsis thaliana* envelope membrane integrase
ATP	Adenosine Triphosphate
BCIP	5-Br-4-Cl-3-indolyl-phosphate
BSA	Bovine Serum Albumin
CCD	Charge-Coupled Device
CMWA	cold microwave-assisted
CRISP	crystallographic image processing on a personal computer
DNA	Deoxyribonucleic acid
EDTA	Ethylenediaminetetraacetic acid
EGTA	ethylene glycol tetraacetic acid
EM	electron microscopy
EMAN	electron micrograph analysis
FFT	Fast Fourier Transform
FRAP	Fluorescence recovery after photobleaching
FSC	Fourier shell correlation
Fts	Filamenting temperature sensitive
FtsZ	Filamentation temperature sensitive Z
G	Gibbs free energy
GMPPCP	β-γ-methyleneguanosine 5' triphosphate

GMP-PNP	guanylyl-imidodiphosphate
GDP	Guanosine diphosphate
GTP	Guanosine triphosphate
H	Enthalpy
LM	light microscopy
MCD1	MULTIPLE CHLOROPLAST DIVISION SITE 1
MEMK	100 mM MES, 1 mM EGTA, 5 mM Mg acetate, pH 6.5
MES	2-(*N*-morpholino) ethanesulfonic acid
Min	Minicell
MWA	Microwave-assisted
NBT	nitroblue tetrazolium
Ni–NTA	nickel-nitriloacetic acid
PAGE	polyacrylamide gel electrophoresis
PARC6	paralog of ARC6
PDV1	PLASTID DIVISION1
PDV2	PLASTID DIVISION2
PEG	polyethylene glycol
PMSF	phenyl-methylsulfonyl fluoride
S	entropy
SDS	sodium dodecyl sulfate
TAIR	The *Arabidopsis* Information Resource
TBST	Tris buffered saline plus tween-20

TEM	Transmission electron microscopy
YPD	yeast extract peptone dextrose

TABLE OF CONTENTS

LIST OF FIGURES

FIGURE Page

FIGURE Page

LIST OF TABLES

CHAPTER I

INTRODUCTION

1.1 INTRODUCTION TO BACTERIAL AND PLASTID DIVISION

Chloroplasts are organelles that house the photosynthetic machinery and are derived from proplastids which are small and undifferentiated plastids that possess the capability of becoming several types of plastids including chloroplasts (1). Chloroplasts evolved as a result of an endosymbiotic event between a cyanobacterial-like photosynthetic prokaryote being engulfed by a non photosynthetic eukaryote and is supported by the hypothesis of Mereschkowsky in 1905 that plastids are reduced forms of cyanobacteria (2,3). In addition, chloroplasts perform important storage functions and measure five μm in diameter and two-thirds of a μm thick. Chloroplasts and all plastids only arise by division of existing plastids. A complex division process occurs in chloroplasts that critically depends on two families of proteins that are homologous to the prokaryotic cell division protein FtsZ (Filamentation temperature sensitive Z), a self-assembling GTPase. The history and significance of FtsZ in chloroplast division will be discussed in the second section of chapter I. Proper function of the division machinery is necessary for maintaining a high number of small chloroplasts in leaf mesophyll cells, a determining factor for photosynthetic competence (4) and for phototropic movements of chloroplasts, a coping mechanism in high-light stress conditions (5). Deciphering the

---

This dissertation follows the style of the *Journal of Biological Chemistry*.

functional characteristics of plastid division proteins is important not only from an evolutionary and cell biological perspective, but also has applied science aspects. For example, recent studies regarding altered expression levels of specific plastid division genes were shown to affect the size of the starch-storing plastids, amyloplasts, and in turn the size of starch granules in rice (6) and potato (7) (Fig. 1.1). Large granules are favored for baking because they produce softer-texture flour, while small granules are desired for fat replacements in foods, manufacture of paper, biodegradable films and as a carrier material in cosmetics. Furthermore, increased starch granule size leads to more efficient wet-milling in corn, which subsequently improves starch yields leading to gross value gains in the region of $280 million per year domestically (8).

Milling processes enable the extraction of economically useful products and the wet-milling process for corn separates the product into its four basic components: starch, germ, fiber, and protein (9). Valuable by-products of wet-milling include ethanol and corn oil. Estimated ethanol production in the United States used in gasoline mixtures was 3.4 billion gallons in 2004 and is expected to increase in the future (10). Conventional wet-milling of corn uses a five step process and begins with an initial steep of 24 to 40 hours in a mixture of water and the hazardous chemical sulfur dioxide to begin the separation of the starch and protein bonds. Next, the germ is separated from other kernel components by grinding allowing a subsequent step to extract starch and convert it to sweeteners or ethanol. A protocol that represents a substantial decrease in the amount of sulfur dioxide needed and is less expensive has been introduced by Ramirez and colleagues (11). The process substitutes proteases for the large amounts of

sulfur dioxide previously used and repeats the same downstream steps as conventional wet milling.

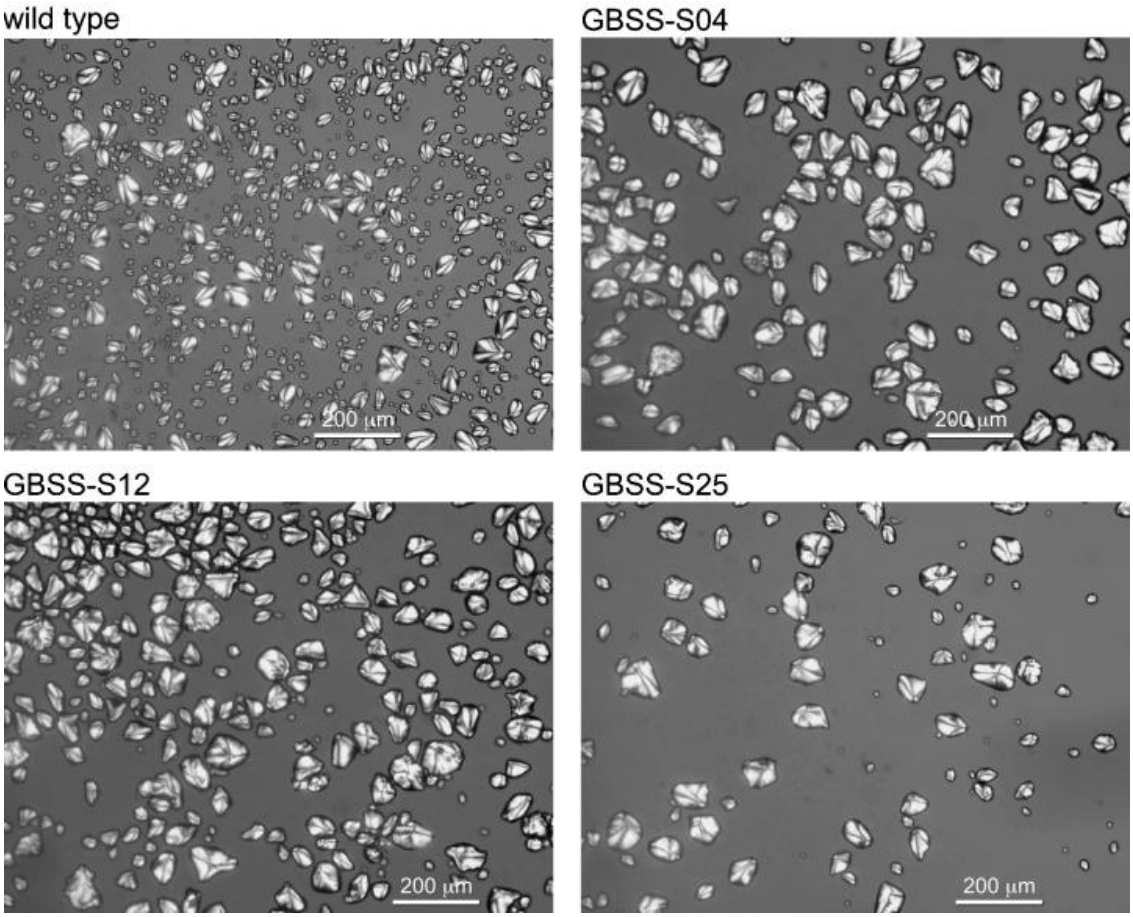

Figure 1.1. Starch granules isolated from wild-type potato tubers and from tubers from three transgenic lines GBSS-S04, GBSS-S12 and GBSS-S25 analysed by light microscopy. The transgenic lines each have increased FtsZ expression relative to wild-type. The scale bars correspond to 200 µm. GBSS, granule-bound starch synthase (7).

Another option for removing valuable products from corn is dry milling. Initial dry milling capital costs are less than wet-milling, usually smaller in scale and represent the majority of new milling facilities (12). The hardness of the corn kernel also determines which type of milling is used as studies have shown large and hard kernels

are preferable for dry milling and softer kernels are useful for wet-milling as they require less steeping time (13,14). The steps for dry milling begin with a coarse grind and then mixing with water, adjusting pH to 5.8 and adding α-amylase to break down the long chains to dextrins (15). Glucoamylase is also added to convert the dextrins to glucose and yeast is introduced to begin fermentation and eventual distillation of the alcohol. Remnants from the distillation tank can be centrifuged to yield wet distillers grain that can be dried and used as a high protein component of cattle feed (16). Manipulating plants to produce traits beneficial to the milling process requires a robust model system for basic research prior to application in economically important crops.

Arabidopsis thaliana is a member of the Brassicaceae family and is a popular model system for plant research. Johannes Thal discovered the plant in the Harz mountains (located in present day central Germany) in the sixteenth century and phenotypes deviating from the wild-type strain were first reported by Braun in 1873 (17). Friedrich Laibach first suggested using the plant as a genetic model system in 1943 and one of his students subsequently reported first mutants induced by x-ray radiation (18). There are many ecotypes classified though only three are commonly used in research, Landsberg erecta, Columbia and Wassilewskija. Chloroplast number varies among the ecotypes with Landsberg having an average of 120 chloroplast per cell and Wassilewskija having 60-80 per cell (19). A regularly updated website, The *Arabidopsis* Information Resource (TAIR), catalogs data about the model system including DNA and protein sequences. In addition, DNA clones, libraries and seeds are available to the

research community through the TAIR website for a nominal cost (www.arabidopsis.org).

Advantages of the model system include having the smallest sequenced genome in the plant kingdom, ease and speed of growth for wild-type plants (approximately six week life cycle), harboring only five chromosomes and the ability to introduce mutations (17,20). A time intensive plant regeneration and tissue culture protocol using vacuum filtration had been the predominant method for introducing recombinant DNA into *Arabidopsis* until the "floral dip" method was published (21). Studies have reported that seed yields are increased in floral dip as compared to tissue culture and plant regeneration. Floral dip is accomplished by growing a culture of *Agrobacterium tumefaciens* containing a gene of interest and then dipping plants into the bacterial solution containing a detergent and 5% (w/v) sucrose as an osmoticum. Following growth of the plants, transformants are selected using an herbicidal or antibiotic marker.

Arabidopsis thaliana has been used extensively to investigate plastid division. The similarities that plastid division share with bacterial cell division makes understanding the mechanism of binary division an important research goal. Plastid and bacterial division both polymerize FtsZ to create a Z ring at mid-plastid or mid-cell (22,23). Research has shown that some bacterial FtsZ accessory proteins have been conserved in plastid division. Most bacteria contain a single ring-shaped division machinery, whose assembly is initiated by polymerization of a tubulin-like GTPase protein, FtsZ, into a ring (Z-ring) at mid-cell (Fig. 1.2). Due to the early localization of

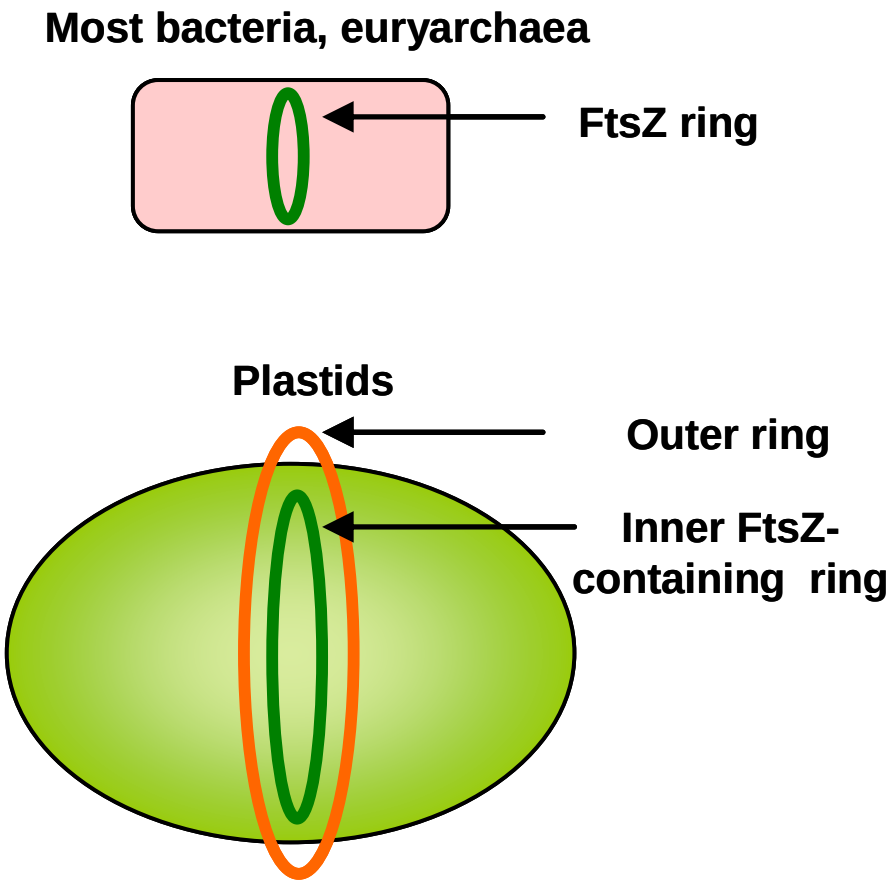

Figure 1.2. FtsZ and cell/plastid fission. FtsZ localizes to the inner side of the inner membrane as the Z-ring (green). In plastids, dynamin-like protein rings (red) localize to the cytoplasmic face while the stromal dividing ring (green), contains the FtsZ1 and FtsZ2 families and is localized along the inner envelope membrane.

FtsZ to mid-cell and its essential role in cell divsion FtsZ is an attractive antibiotic target. Completely sequenced genomes of bacteria, including cyanobacteria, contain only one FtsZ family and upon assembly into the Z-ring recruit additional components to assemble the functional division machinery and to remodel the peptidoglycan cell wall (24,25). Chloroplasts in plants, green and red algae lost the peptidoglycan wall and many of the peptidoglycan synthesis genes are either absent from their genomes (26) or

perform different functions (27). Two previously undiscovered members of the FtsZ-tubulin superfamily have recently been described in bacteria and archaea though the authors suggest that it is highly unlikely they play a role in cell division (28). Recent reports show that some archaea are capable of maintaining division without FtsZ and use an alternate division machinery (29).

The position of the division site and Z-ring is determined by the bacterial Min (Minicell) system consisting of the MinC, MinD and MinE proteins that allow destabilization or disassembly of FtsZ filaments and rings at improper sites via a coordinated mechanism (30,31). MinD recruits MinC and MinE to the membrane and a helical MinCDE structure is formed and bound to the membrane at one of the polar regions via MinD. The helical structure terminates in an E-ring composed of MinE that contracts and moves towards the pole resulting in breakdown of the MinCDE structure (Fig. 1.3). The MinCDE structure is then reassembled at the opposite pole and this oscillation occurs several times before cell division ensues. This process ensures a higher concentration of MinC in the polar regions and allows proper cell division at mid-cell as high concentrations of MinC inhibits polymerization of the Z-ring (32).

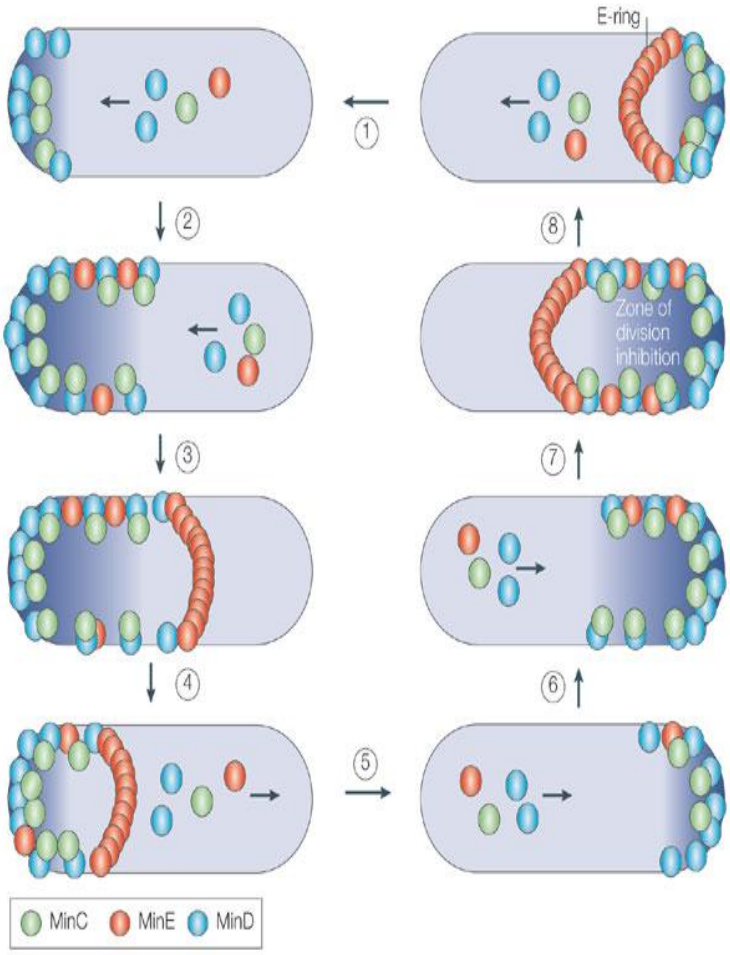

Figure 1.3. Overview of bacterial Min system. The MinCDE polar zone begins assembling at a cell pole and grows towards midcell (1–2 and 5–6). The MinE ring then assembles at the leading edge of the polar zone (3 and 7). The polar zone then disassembles, releasing MinC, MinD and MinE molecules, shrinking back to the pole, and finally releasing MinE from the E-ring (4–5 and 8–1). Because of the rapid oscillation, a zone of division inhibition (dark blue shading) is present near the two ends of the cell for a large portion of the cell cycle (33).

A system for ring placement at proper sites in plastids has been described and shares some similarities with the bacterial system (34). Homologs of cyanobacterial

MinD (*At*MinD) and MinE (*At*MinE) are present in *Arabidopsis* chloroplasts (34) and work in concert with proteins not found in bacterial division systems to accomplish proper chloroplast Z-ring placement. One of these proteins, ARC3, localizes to the division site and chloroplast poles. ARC3 also directly interacts with *At*MinD, *At*MinE and FtsZ1 and overexpression inhibits ring formation (35-37). These observations have lead to the conclusion that ARC3 fulfills a similar role to MinC in the bacterial Min system. The chloroplast Min system also contains the MCD1 (MULTIPLE CHLOROPLAST DIVISION SITE 1) protein that directly interacts with *At*MinD and as a result recruits *At*MinD to the division site. MCD1 is found only in land plants while ARC3 is conserved in land plants and green algae (38). Null mutants of *Atmind/e*, *mcd1* and *arc3* promote asymmetric chloroplast division and the formation of several FtsZ rings (Figs. 1.4 and 1.5, respectively) (38).

Both bacterial and plant FtsZ have several accessory proteins that play critical roles in the division mechanism. Assembly of the Z-ring requires three essential proteins in *E. coli*: FtsZ, FtsA and ZipA (24). FtsA acts as a membrane tether, has a role in recruiting downstream proteins and is well conserved in bacteria (39-41). ZipA has been identified as a secondary membrane anchor and promotes assembly of FtsZ protofilament bundles and sheets (42,43). While ZipA is conserved in gammaproteobacteria, a study has demonstrated that a single amino acid substitution in

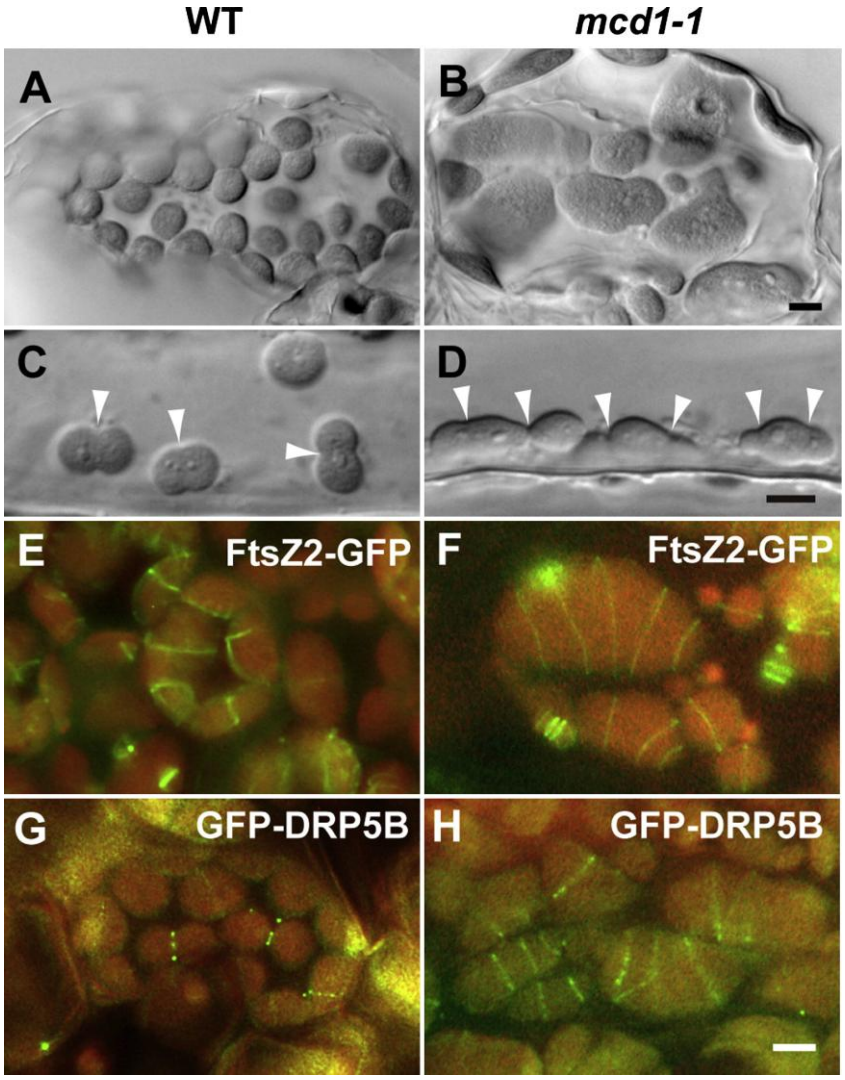

Figure 1.4. Multiple chloroplast division in *mcd1* mutants.
(A–D) Chloroplasts were observed by Nomarski optics in leaf mesophyll cells (A, B) and in petiole cells (C, D). Wild-type (A, C) and *mcd1-1* mutant (B, D) are shown. Arrows indicate the constriction sites of dividing chloroplasts. (E–H) Localization of FtsZ2-GFP (E, F) and GFP-DRP5B (G, H) in wild-type (E, G) and *mcd1-1* mutant (F, H). The fluorescence of GFP is green and the autofluorescence of chlorophyll is red. Each set of images (A and B, C and D, and E–H) are shown at the same magnification. Scale bars correspond to 5 μm (38).

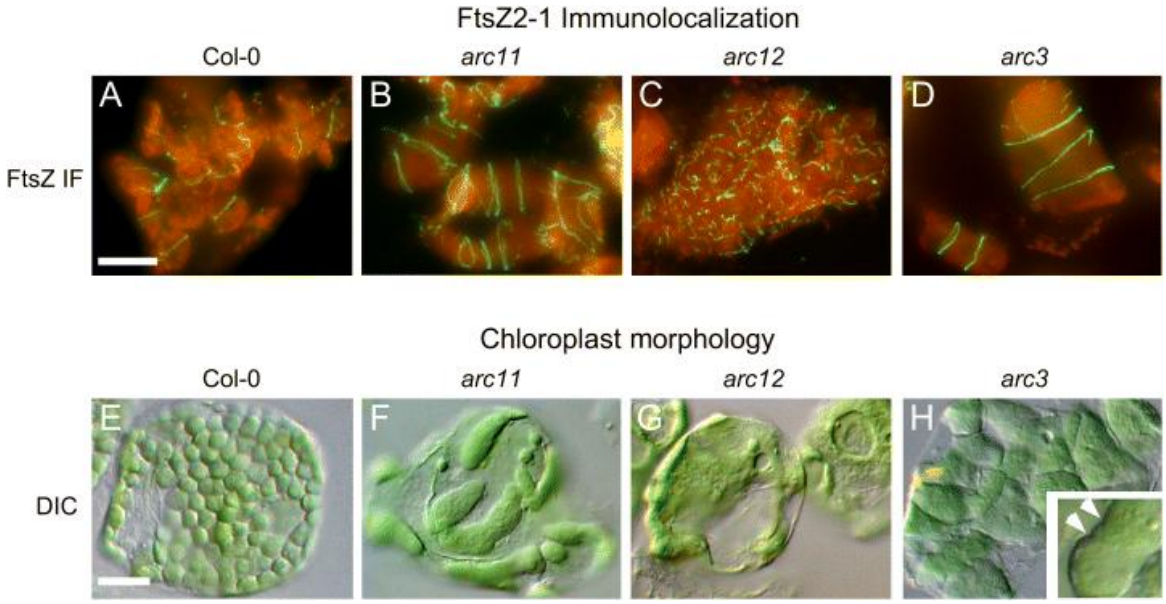

Figure 1.5. Phenotypes associated with *arc3* and *AtMinD/E* alleles. Top panel. A–D) Immunofluorescent micrographs of *At*FtsZ2-1 filament morphology in chloroplasts of mature leaf mesophyll cells from wild-type Columbia ecotype (Col-0) (A), *arc11* (an allele of *AtMinD*) (B), *arc12* (an allele of *AtMinE*) (C) and *arc3* (D). Bottom panel. E–H) Light micrographs of chloroplast morphology in mature leaf mesophyll cells from wild-type Col-0 (E), *arc11* (an allele of *AtMinD*) (F), *arc12* (an allele of *AtMinE*) (G) and *arc3* (H). Arrowheads in (H) show points of constriction in *arc3* that are probable sites of Z-ring formation. The mutant *arc12* harbors a lesion in *AtMinE* creating a frameshift and premature stop. Scale bars correspond to 20 μm (37).

E. coli FtsA renders ZipA non-essential and permits efficient growth and division (44). Several regulators of Z-ring dynamics are found in bacterial genomes though these proteins are not essential for cell division. ZapA is a small protein that promotes Z-ring assembly and stability though no phenotypes are observed in null mutations except in some sensitive backgrounds where the mutation is lethal (45-47). Some gammaproteobacteria harbor ZapB that has a redundant role with ZapA (48). EzrA is constitutively expressed in gram-positive bacteria with a low GC content and is a negative regulator of Z-ring assembly (49). Gram-positive bacteria and cyanobacteria

require SepF for proper septal morphology and in some bacteria may have a role similar to FtsA (46). Three proteins have been identified that are negative regulators of cell division under certain conditions. UgtP acts as an inhibitor of cell division in nutrient rich media by destabilizing interactions between FtsZ protofilaments and is downregulated under non-nutrient rich media conditions (50). During DNA damage in *E. coli,* SulA is expressed as part of the SOS response and inhibits assembly of new Z-rings and promotes disassembly of active Z-rings (51-54). The critical concentration of FtsZ assembly increases five fold in the presence of SulA (55). *B. subtilis* expresses the MciZ protein during sporulation and this protein directly interacts with FtsZ and inhibits polymerization. During the period of inhibition the GTPase activity of FtsZ is significantly reduced (56).

Bacterial cell division is not directly applicable to chloroplast division owing to some prokaryotic components of the division machinery being lost during evolution. Consequently, chloroplasts harbor a selection of evolutionary conserved proteins homologous to bacterial division proteins and have evolved some completely novel components to fulfill newly required functions (37,57-60). Unlike the single ring found in bacteria, chloroplasts have two ring-shaped division machineries, one on the outer, cytosolic side of the double envelope membrane and one on the inner, stromal side (Fig. 1.2). Following the sequencing of the *Arabidopsis thaliana* genome, gene homology searches were initiated to look for conserved genes. Two families of FtsZ are present in higher plants and the FtsZ2 family contained more similarity to bacterial FtsZ and parts of the Min system were conserved (34,61).

Studies by Pyke and colleagues using ethyl-methyl sulfate, a non-specific mutagen, described several accumulation of replicating chloroplasts (ARC) mutants that would later be confirmed as components of the division machinery (19,62-65). A later report outlined some roles using double mutants and analyzing their effects on plastid division (66). In addition to the role of ARC3 described above, these studies included phenotypes for ARC5, ARC6, ARC10, ARC11, ARC12 and ARC1. The first protein to be described as part of the cytosolic ring was the dynamin-like ARC5 which does not have a homolog present in bacterial cell division (67). ARC6 provides a membrane tether for the Z ring, is a positive stabilizing factor for FtsZ polymers and shares similarities on the gene level with the bacterial cell division gene *Ftn2* (68). ARC6 also coordinates positioning of PLASTID DIVISION2 (PDV2) which is part of the cytosolic ring. These initial results did not explain positioning of another component (PDV1) as PDV1 and ARC6 has no direct interaction. A paralog of ARC6 (PARC6) was identified in vascular plants and determines positioning of PDV1 which is another member of the cytosolic ring and at least one of the PDV proteins must be present to recruit ARC5 to the cytosolic ring during the late stages of chloroplast constriction (69,70). Mapping experiments have shown that ARC10 is located in the same area on chromosome five as FtsZ1 and that ARC10 is a missense mutation of FtsZ1 (G366A) (71,72). Wild-type FtsZ1 was able to complement the *arc10* null mutant (71). ARC11 and ARC12 are members of the Min system in chloroplasts and are homologs of MinD and MinE respectively (37,73). Currently, no information is available for ARC1 except for the observed decrease in chloroplast number and division defects (66). A separate search for

components of the chloroplast division machinery yielded *Arabidopsis thaliana* envelope membrane integrase (ARTEMIS) (74). Experiments using severely reduced levels of ARTEMIS resulted in *Arabidopsis* that had similar growth patterns to wild-type plants though undivided chloroplasts were observed (74). ARTEMIS is nuclear encoded, but localizes to the inner envelope membrane and may coordinate envelope constriction events (74).

Plastid division is studied in other photosynthetic model systems in addition to *Arabidopsis* and includes *Cyanidioschyzon merolae* (a unicellular red alga) and *Physcomitrella patens* (a multicellular moss) (37). Additionally, mitochondrial division research is represented in the literature and similar to chloroplasts an endosymbiotic event occurred involving an α-protobacterium and a non-photosynthetic eukaryote (3,75). *C. merolae* has one plastid and one mitochondria and the divisions can be synchronized using light and dark cycles (76,77). Three distinct rings have been identified in *C. merolae* chloroplast division including a FtsZ ring, a plastid dividing ring and a dynamin ring (78). *Physcomitrella patens* requires simple growth conditions, is recognized as the first land plant and was the first moss to be successfully transformed (79). Early studies established this moss as a model genetic system (80-82). Subsequent studies have shown that a third FtsZ family is present in *Physcomitrella* and five isoforms are present though recent gene knockout experiments suggest that the isoforms have overlapping functions (83). While the mitochondria of some lower eukaryotes such as the golden brown algae *Mallomonas splendens* retain FtsZ isoforms, the mitochondria of yeast and higher eukaryotes do not harbor FtsZ and use dynamin rings in division

events (22,84). A mutational analysis studying the dynamin-related GTPase protein found in the yeast *Saccharomyces cerevisiae*, Dnm1p, reported that mutations caused collapse of the mitochondrial membranes towards one side of the mitochondria. Two unicellular algae and a protist later had mitochondrial FtsZ identified (84-86).

The generation of the constriction force necessary for division is provided by different mechanisms in plant and bacterial division. Cell division in bacteria is powered by energy resulting from guanosine triphosphate (GTP) hydrolysis and an accompanying transition in FtsZ filaments from a straight to curved conformation (87,88). An elegant set of experiments reconstituted the essential components to generate bacterial constriction force in liposomes and confirmed that hydrolysis is necessary to generate the constriction force (89). Chloroplasts do not appear to use this mechanism as results presented herein and those of Olson *et al.* do not report significant curvature in the presence of guanosine diphosphate (GDP) (90,91). Further supporting these results, ARC5 is a dynamin-like protein that has been suggested to power the division process and *arc5* mutants arrest late in chloroplast division (67). A dynamin present in red algae, CmDnm2, has a role in the late division events of chloroplasts and is thought to provide the mechanical force required for constriction (92). Phylogenetic analysis determined that CmDnm2 is a close match to ARC5 (92). Whether FtsZ1 or FtsZ2 play a role in generating the force for chloroplast division is currently unclear.

The work presented here furthers the understanding of plastid division by examining chloroplast processes at a molecular level that was previously largely absent in the literature. Results presented here include the only published results of expression

of plant FtsZs in a eukaryotic system. Previous reports and one subsequent to this work expressed plant FtsZ in a bacterial expression system containing endogenous FtsZ. Biochemical characteristics of FtsZ are investigated and information about the oligomeric states of FtsZ involved in the assembly mechanism are provided.

1.2 INTRODUCTION TO FILAMENTOUS TEMPERATURE SENSITIVE Z (FTSZ) PROTEINS

FtsZ proteins are ancestral structural homologs of eukaryotic tubulin found in the endosymbiotic ancestors of chloroplasts, cyanobacteria and are the first proteins to locate mid-cell/plastid prior to a division event. Several members of the *Fts* (Filamenting temperature sensitive) gene family were discovered by Hirota and his colleagues in a screen for bacterial cell division mutants and included FtsZ (93). The conserved N-terminal domain of FtsZ forms a Rossman fold and contains a tubulin signature motif, GGGTG(T/S)G where S represents either a G or C, that allows for binding of GTP and has been a hallmark of all FtsZ genes found in other species (94,95) (Fig.1.6). A separate region, the T7 loop, is highly conserved in all FtsZ and is required for GTP hydrolysis (91). Due to the presence of this motif, bacterial FtsZ was expected to be an active GTPase and this notion was confirmed experimentally *in vitro* (22,96). The C-terminal portion of FtsZ is more variable than the N-terminus although the C-terminal core domain is highly conserved in bacterial FtsZ and the FtsZ2 family but absent in FtsZ1 (97). The C-terminal core domain allows specific interaction of proteins that anchor the Z-ring to the membrane and the absence of the domain in FtsZ1 suggested functional differences for the two families present in plants (98). In 1991 it was demonstrated that

bacterial FtsZ assembled into the Z-ring located at mid-cell (99). The Z-ring is most likely composed of relatively short FtsZ filaments, termed protofilaments (88).

While FtsZ accessory proteins are required for recruiting additional components to assemble functional division machinery, the assembly of FtsZ *in vitro* in the absence of these accessory proteins has been investigated. Electron microscopy (EM) has been used extensively to visualize *in vitro* FtsZ assemblies in the bacterial system (87,100-102). Sheets, filaments and mini-ring assemblies have been found depending on the experimental conditions used (Fig. 1.7). The availability of soluble and active protein allowed for structural determination of prokaryotic FtsZ. The crystal structure of FtsZ with a bound GDP from *Methanococcus jannaschii* revealed dimensions of 6 x 4 x 3.5 nm at a resolution of 2.8 Å and the structure was similar to tubulin (94). This observation further suggested that FtsZ is a tubulin homolog. A helix connects the two domains of *Methanococcus jannaschii* FtsZ and the N-terminal portion is the GTPase domain and contains a six stranded parallel β-sheet and five helices. A four strand parallel β-sheet and two helices compose the C-terminal FtsZ domain. Hydropathy plots of FtsZ proteins reveal several hydrophobic regions that are present in *Arabidopsis* FtsZ families and *Methanococcus jannaschii* FtsZ (Fig. 1.8).

The GTPase activity of bacterial FtsZ is correlated with the dynamics of protofilament assembly *in vitro* and *in vivo* (100,103-107). The FtsZ molecules outside the bacterial Z-ring are most likely in the monomeric oligomeric state (108,109). The exchange of molecules may be possible not only from the ends of protofilaments as end-to-end joining of filaments and depolymerization from internal zones were also observed

in vitro, suggesting that fragmentation and reannealing may contribute significantly to the dynamics of FtsZ assembly (109,110). When the prokaryotic FtsZ filaments hydrolyze GTP, they switch from a straight to a curved shape endowing the FtsZ assembly with a constrictive force sufficient to 'power' the binary fission process (87-89). A study has reported that a missense mutation (FtsZ84) in *E. coli* FtsZ converts the protein from a GTPase to an ATPase (104) and that a GTPase inactive mutant assembles into double stranded filaments (100).

Arabidopsis thaliana FtsZ2
GGNPEIGMNAARESKEVIEEALYGSDMVFVTAGMGGGTGTGAAPVIAGIAKAMGILTVGI 240

Staphylococcus aureus FtsZ
GANPEIGKKAAEESREQIEDAIQGADMVFVTSGMGGGTGTGAAPVVAKIAKEMGALTVGV 131

Arabidopsis *thaliana* FtsZ1
GGNPLLGEQAAEESKDAIANALKGSDLVFITAGMGGGTGSGAAPVVAQISKDAGYLTVGV 193

E. coli FtsZ
GANPEVGRNAADEDRDALRAALEGADMVFIAAGMGGGTGTGAAPVVAEVAKDLGILTVAV 130

Figure 1.6. Sequence alignment of tubulin signature motif from FtsZ in different species. Sequence alignment at the protein level from *Arabidopsis* FtsZ1, *Staphylococcus aureus* FtsZ, *Arabidopsis* FtsZ2 and *E. coli* FtsZ. The tubulin signature motif is highlighted in light green.

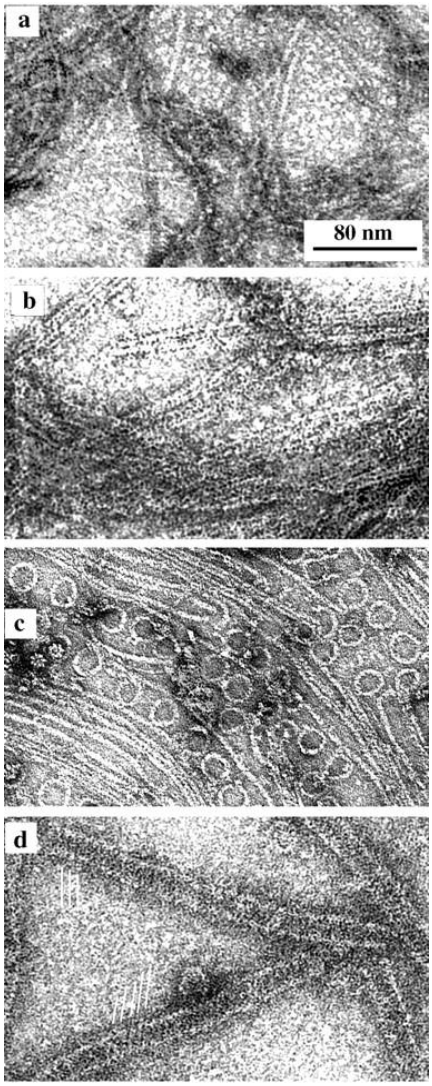

Figure 1.7. The four types of polymers formed by FtsZ in MEMK6.5. (a) Straight protofilaments formed with GTP but without DEAE-dextran; (b) sheets of straight protofilaments assembled from FtsZ plus DEAE-dextran; (c) minirings assembled with GDP and adsorbed onto a cationic lipid monolayer; (d) FtsZ tubes assembled with GDP and DEAE-dextran. The parallel white lines indicate the helical protofilaments in these tubes (87).

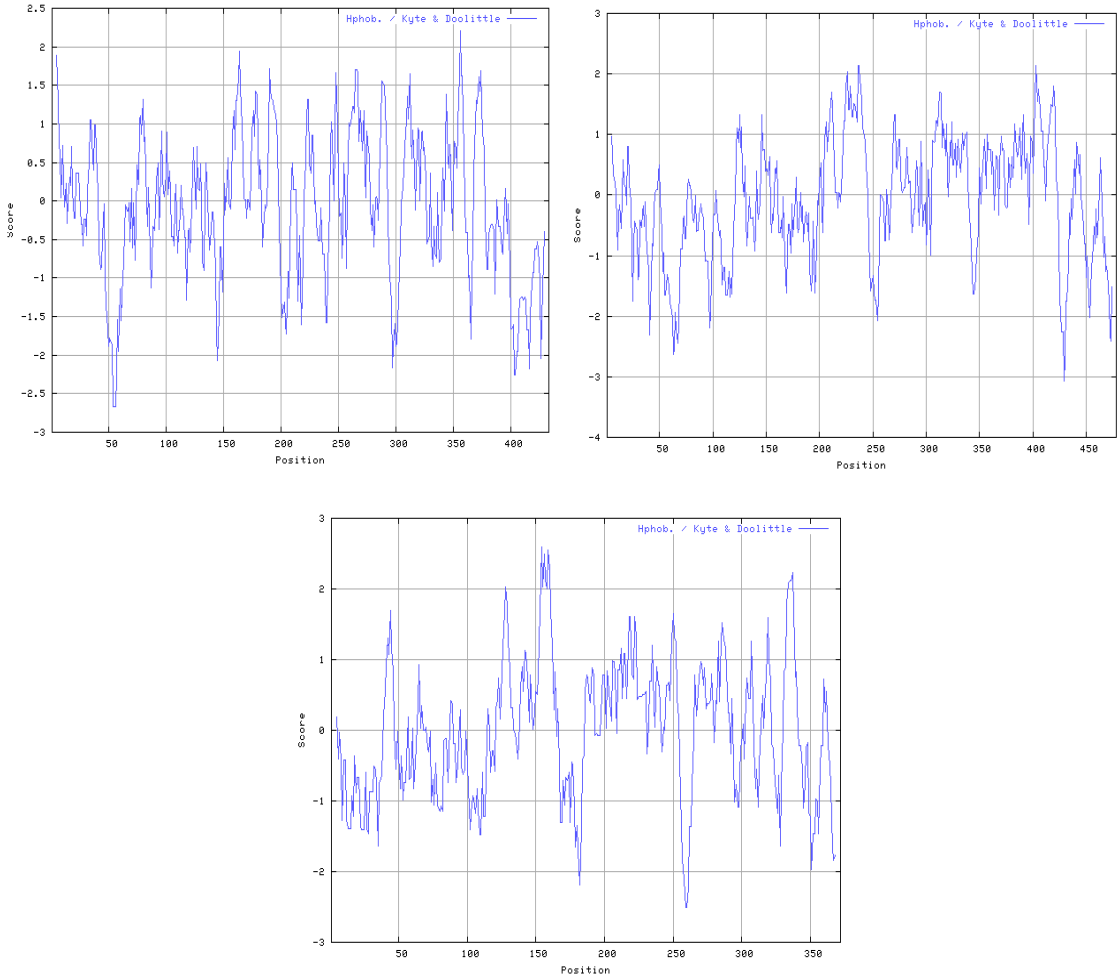

Figure 1.8 FtsZ hydropathy plots. Left panel is FtsZ1, right panel is FtsZ2-1 and bottom panel represents *Methanococcus jannaschii* FtsZ. Kyte and Doolittle hydropathy plots that measure hydrophobicity of the FtsZ proteins. The X-axis is position of the amino acid in the protein and Y-axis is relative score. The positive scores represent hydrophobic regions.

In 1995, Osteryoung and Vierling identified a nuclear encoded gene in *Arabidopsis thaliana* which shared significant sequence homology to *E. coli* FtsZ and in 1998 a second family of FtsZ in higher plants was discovered (61,111). These families both retain the conserved tubulin signature motif and have a highly conserved N-terminus but FtsZ1 lost the C-terminal core domain and both families are necessary for proper chloroplast division (71,111,112). FtsZ1 and FtsZ2 interactions promote the formation of the Z-ring structure at the mid-plastid division site (23,113). Overexpression or antisense suppression of either FtsZ1 or FtsZ2 cause severe defects in plastid division, which led to the conclusion that they are both essential for normal plastid division (111). Recent analysis, however, showed that inactivation of *Arabidopsis* FtsZ1 does not completely block plastid replication, indicating that the chloroplast division apparatus can function without FtsZ1, albeit less efficiently (71). Bacterial FtsZ studies demonstrated that some accessory proteins directly interact with FtsZ via the C-terminal core domain (41). The fact that FtsZ1 does not have this domain suggested that the families perform different functions (114). Initial models suggested that FtsZ1 could form a stromal ring and FtsZ2 would form a cytosolic ring based on observations that FtsZ1 could be imported into the stroma while FtsZ2 could not be imported into the stroma (114). Later work refuted this result and demonstrated that the FtsZ2 used in the earlier study lacked a proper transit peptide and the new construct could be imported into the stroma (115). The FtsZ1 family has a single member, *At*FtsZ1-1, while two proteins, *At*FtsZ2-1 and *At*FtsZ2-2 comprise the FtsZ2 family (111,116). A recent report showed

that *At*FtsZ2-2 is redundant with *At*FtsZ2-1 and that either can restore chloroplast division in *ftsz2-1*, *ftsz2-2* double mutants (117). Therefore, the research presented is focused on *At*FtsZ1-1 and *At*FtsZ2-1 only. The following convention is adhered to: FtsZ1 stands for *At*FtsZ1-1 and FtsZ2 for *At*FtsZ2-1.

Evolutionary history of the two FtsZ families was investigated due to the distinct functionality of the two families present in plants and algae. Phylogenetic analysis determined that the chloroplast FtsZ families diverged before the appearance of land plants and that the gene duplication event occurred before divergence among mosses, seed plants and ferns (72,118). Following the endosymbiotic event that gave rise to the chloroplast, the single *ftsz* gene of the cyanobacterial endosymbiont evolved into two structurally distinct families occurring independently three times in different clades of the evolutionary tree (Fig. 1.9) (116). The evolutionary divergence from prokaryotes, FtsZ1 and FtsZ2 specific interactions and overall greater complexity of the chloroplast division process suggests that the large body of work that has been done on the single FtsZ protein of prokaryotes is not sufficient for complete understanding of how FtsZ1 and FtsZ2 interact and function in chloroplasts.

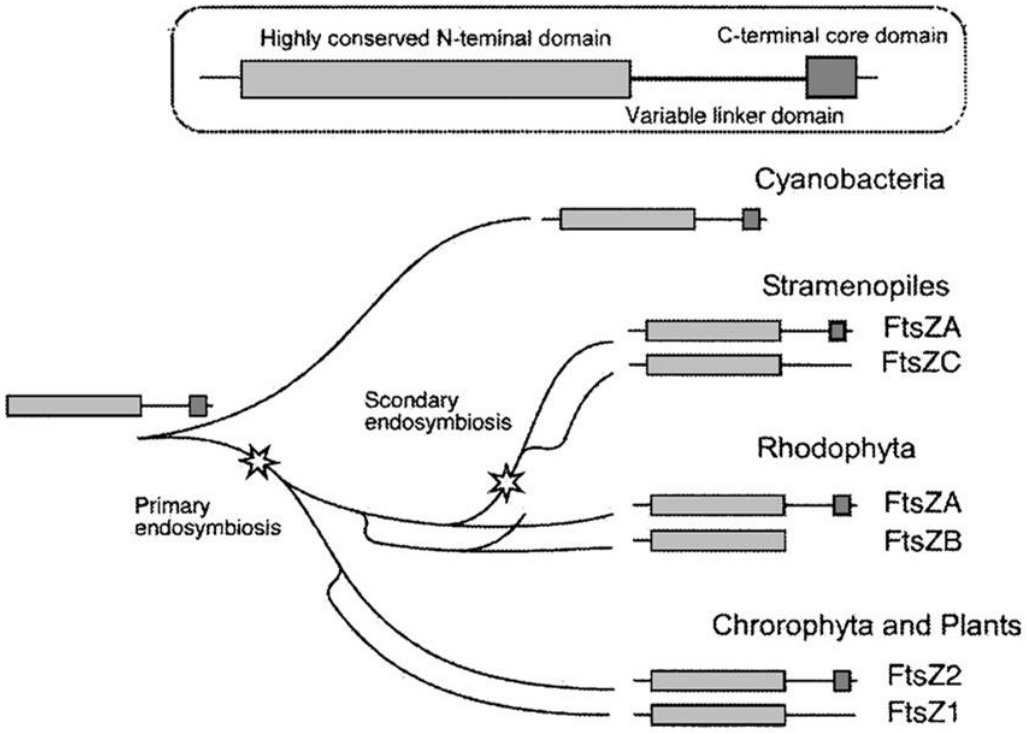

Figure 1.9. Schematic representation of the origin and evolution of the plastid FtsZ families (116).

A large body of *in vivo* FtsZ work has revealed information about chloroplast division. Fluorescently tagged FtsZ1 and FtsZ2 were shown to colocalize at the division site (Fig. 1.10) (23,115). Overexpression of FtsZ1 and FtsZ2 leads to excessive FtsZ assembly and disruption of normal division in chloroplasts (119). The relative ratio of FtsZ1:FtsZ2 in chloroplasts is maintained at 1:2 even after total FtsZ levels decline as plants age (117). This result does not address the ratio in the filaments and that ratio is currently unknown. Normal division occurs with up to 2-fold overexpression of FtsZ1

(119), while FtsZ2 is required at closer to wild-type levels (120). FtsZ1 has been shown to specifically interact with ARC3 and FtsZ2 interacts with ARC6, but not ARC3, providing further evidence of their divergent functions (36,68,121). A recent report has shown that double knockouts (FtsZ1 and FtsZ2-1) and triple knockouts (FtsZ1, FtsZ2-1 and FtsZ2-2) are viable and that chloroplast partitioning occurs (112). This suggests that a currently unknown mechanism lacking FtsZ may participate in plastid partitioning in higher plants.

Following identification of the FtsZ families in plants attempts were made to purify the proteins for *in vitro* experiments. Recombinant *Arabidopsis thaliana* FtsZ proteins proved difficult to purify from *E. coli* due to an unfavorable codon bias, toxicity to the host and formation of inclusion bodies (100-102). Despite these limitations, recombinant expression of plant FtsZ has been accomplished in *E. coli* using *Arabidopsis* (91) and *Nicotiana tabacum* FtsZ (122). El-Kafafi and colleagues concluded that *Nicotiana tabacum* FtsZ1 is able to assemble into filamentous structures while FtsZ2 did not assemble into organized polymers and this result is in contrast to Olson *et al.* and work in our laboratory demonstrating that both FtsZ1 and FtsZ2 are capable of self-assembly into filaments (90,91,122). Our work and that of Olson *et al.* concluded that both FtsZ families are active GTPases albeit with different rates of hydrolysis while El-Kafafi did not address GTP hydrolysis experimentally (91,122). It should be noted that the studies using bacterial expression systems have endogenous FtsZ present and use affinity tags to purify the recombinant protein. However, it is unknown if the endogenous FtsZ could interact with the recombinant FtsZ via the conserved self-

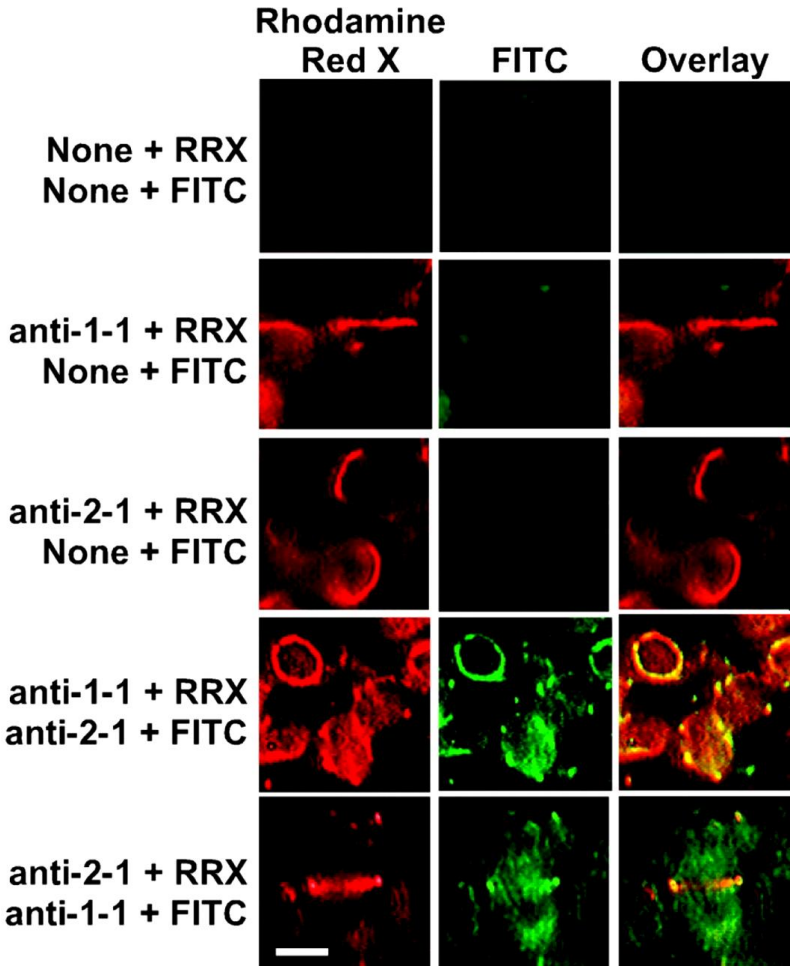

Figure 1.10. ***At*FtsZ1-1 and *At*FtsZ2-1 rings are colocalized.** Leaf sections from wild-type *Arabidopsis* plants were subjected to sequential, double immunofluorescence labeling of *At*FtsZ1-1 and *At*FtsZ2-1. The order of antibody application is indicated on the left. Tissue sections were incubated first with no antibodies (None), anti-*At*FtsZ1-1 antibodies (anti-1-1), or anti-*At*FtsZ2-1 antibodies (anti-2-1), followed by monovalent anti-rabbit antibody conjugated to Rhodamine red-X (RRX). Sections were treated with no, anti-*At*FtsZ1-1, or anti-*At*FtsZ2-1 antibody, followed by anti-rabbit FITC conjugate. The labeled sections were viewed using FITC (green) and Texas red (red) filter sets. The yellow color in the overlay of the red and green signals indicates colocalization of *At*FtsZ1-1 and *At*FtsZ2-1. Scale bar corresponds to 2 µm (23).

interaction domains. The work of Olson *et al.* uses a strain of *E. coli* that overexpresses the endogenous FtsZ copy as an expression system. To avoid this potential pitfall, our work employs the *Pichia pastoris* yeast expression system as this system lacks endogenous FtsZ.

The data demonstrated in this work includes the biochemical characterization of FtsZ1 and FtsZ2 including GTPase activities. These results are presented and discussed in chapter II. Several outstanding questions remain in the field including the effects of GTP hydrolysis on plant FtsZ assemblies and whether FtsZ1 or FtsZ2 contribute to the constriction force in plastids.

Chapter III describes experiments that address the nature of the FtsZ assembly mechanism. In particular, discussion centers around the composition of a stromal pool of soluble FtsZ molecules that is thought to be in dynamic exchange with the assembled filaments. This area of research has been discussed in the literature though no experimental data has confirmed the oligomeric identity of the components (83,112,117). Collected micrograph data of FtsZ assembly intermediates were subsequently subjected to image processing to render low resolution three-dimensional reconstructions. Detailed structure of FtsZ assemblies and the complete assembly dynamics of FtsZ1 and FtsZ2 remain to be elucidated.

1.3. INTRODUCTION TO IMAGE PROCESSING

Prior to the research presented and discussed in chapter III of this work, little structure-function data was available for *Arabidopsis thaliana* FtsZ. In large part this is a consequence of the plant FtsZ cloning problems described earlier. Several research groups, including our own laboratory, have successfully purified recombinant FtsZ and this may indicate that structural studies will become more frequent in the field. One goal of this research is to provide structural data for plant FtsZ using EM and subsequent image processing as the primary tools. Previously, a crystal structure has been solved for *Methanococcus jannaschii* FtsZ (94).

Image processing has been in use for decades and has proven valuable for generating three-dimensional structures from collected two-dimensional data (Fig. 1.11). The reconstruction process is initiated by recording images of the relevant particles and aligning them to common views (Fig 1.11 A-C). Aligned particles are subsequently assigned to classes and averages are used to generate a three-dimensional reconstruction (Fig. 1.11 D-F). Several programs have been developed for reconstructions including SPIDER, IMAGIC and electron micrograph analysis (EMAN) (123-128). EMAN was selected for use in this work and is a free to download suite of reconstruction programs and is capable of reading SPIDER, IMAGIC and several other file types. Three-dimensional reconstructions generated by EMAN include the model protein GroEL (Fig. 1.12), the protein translocation channel protein SecY and the ATP synthase in mitochondria (129-131). The software is capable of refining asymmetric particles though symmetry is preferable. In addition, an active on-line community is available to

aid in solving processing problems that arise and informative workshops are hosted on a regular basis.

The protein of interest is prepared for data collection by either negative staining or cryo-EM methods. Transmission electron microscopy (TEM) micrographs are recorded at a minimum of 3 times oversampling. This exceeds the Nyquist criterion which is the minimum sampling density needed to capture all information present in the micrograph. Before beginning the reconstruction steps, the quality of the micrographs are evaluated using the Fast Fourier Transform algorithm (FFT) in the image analysis program CRISP (132). Those micrographs containing no drift or astigmatism and bearing similar defocus values are chosen for particle selection using Boxer (123).

Boxer is a program included in the EMAN software package that allows the user to manually or semi-automatically select the desired particles for reconstruction. The semi-automatic routine requires the user to select several particles as references and then manually change thresholds that discriminate between good and bad particles. Areas of poor contrast or otherwise undesirable locations of the micrograph can be excluded from the semi-automatic boxing.

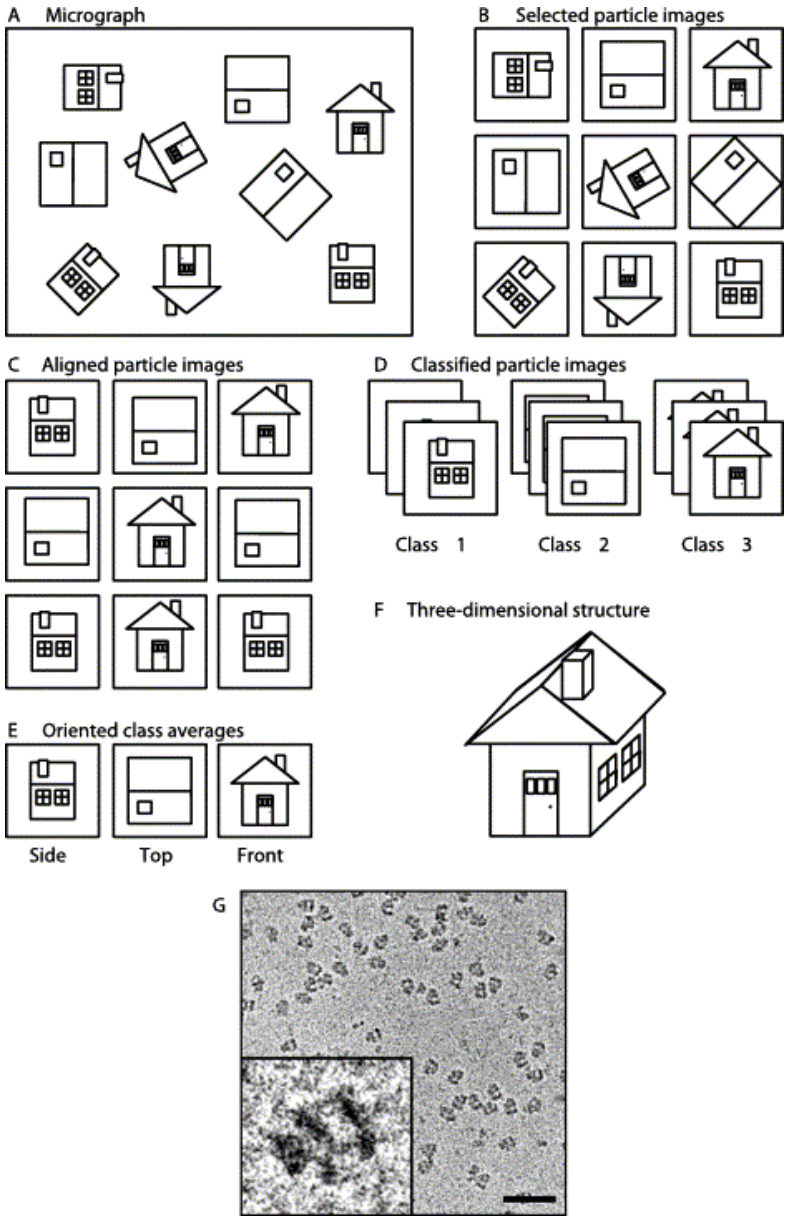

Figure 1.11. Depiction of single particle structure determination. A: Cartoon representation of a sample micrograph with three unique views of the object under study. B: Nine selected particle images from the micrograph shown in A. C: Aligned particle images. D: Classified particle images. E: Determined orientations. In this cartoon example, the orientations correspond to the side, front, and top of the object. F: Three-dimensional reconstruction. G: Sample of a real electron cryomicroscopy image. Shown is a digital micrograph of DNA-dependent kinase (133) with the inset depicting one individual selected particle image. Scale bar corresponds to 50 nm (134).

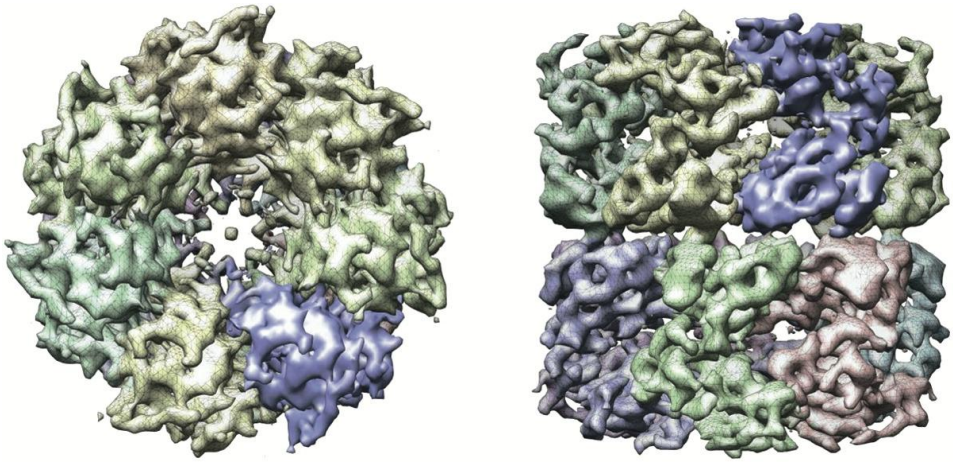

Figure 1.12. Final reconstruction of GroEL structure at ~6 Å resolution. Each monomer has been colored to make the structure easier to visually interpret (129).

A low pass filter can be applied to the particle set to attenuate high spatial frequency contributions as these represent mostly noise. Some reconstructions also use a high pass filter that highlights details in the micrographs and is referred to as a sharpening filter. Filtering out very low spatial frequencies leads to a suppression of unwanted information resulting from non-uniform specimen illumination or stain background. The particle sets are centered before additional processing steps are performed.

Similar particles can be grouped together in the absence of references and two dimensional class averages produced that represent distinct orientations of the particle.

These averages should reflect individual particles represented in the data set and an appropriately diverse data set will represent most of the possible particle orientations. Once the averages are obtained an initial three-dimensional model must be determined. Particles with known symmetry are preferable as the program encourages imposing symmetry in the reconstruction steps. EMAN allows the user to select the class averages used in forming the initial model and a Fourier common-lines routine determines the orientations of the class averages and combines them into a three-dimensional model. Alternatively, an initial model can be generated using a program other than EMAN and imported for the later refinement steps.

After obtaining a suitable initial model, the iterative refinement process is used to produce a final reconstruction. This process begins by generating a set of classes with different orientations. Each raw particle is evaluated and the similarity of the particle to each class is determined. The particles are then aligned and averaged for each assigned class. At this point a determination of the quality of each particle in the class is determined and those particles least similar to the average are not included in the new average used in the next iteration. The user defines the number of iterations that occur with the goal of obtaining a self-consistent reconstruction.

The validity of three-dimensional reconstructions can be determined by several methods and the models should converge during the final rounds of refinement. Convergence is defined differently depending on the program employed. EMAN defines convergence as when the Fourier shell correlation (FSC) curves do not move between iterations although some programs have more stringent conditions (123). Generally these

curves begin at a value of one which denotes perfect correlation between the two averages and decline to zero as this value represents no correlation (135,136). Depending on noise in the micrographs, this may mean that some FSC curves will remain above 0.5 at all spatial frequencies. The FSC cutoff of 0.5 is useful in determining the resolution of the reconstruction though it should be noted that several other criteria are employed in the field (137,138). Asymmetric triangles constitute a graphic aid in which the three points of the triangle represent orthogonal views of the particle and the interior points represent intermediate projections of the particle (139). They are useful in determining whether a sufficient number of views are present in a data set for calculating a three-dimensional structure.

A qualitative process to determine accuracy of the model is to examine back projections. This method displays two-dimensional projections used to create the final reconstruction. Comparing these projections to the class-averages, the user should be able to identify the projections represented in the class-averages.

The Even/Odd (E/O) test is a tool that essentially splits the data set of raw particles into two groups (135). The program will then create two additional three-dimensional models, one for the even data set and one for the odd data set. These reconstructions should be similar to each other and if they are significantly different there is probably bias in the final reconstruction and the data should be re-evaluated or a new data set should be obtained. The E/O test also indicates resolution of the reconstructions though EMAN has been reported to overestimate the resolution in some cases.

CHAPTER II

EXPRESSION AND BIOCHEMICAL CHARACTERIZATION OF *Arabidopsis thaliana* FtsZ1-1 AND FtsZ2-1

2.1 INTRODUCTION

FtsZ was initially discovered in bacteria and plays a critical role by being the first protein to locate to mid-cell prior to a binary fission event where it recruits several essential accessory proteins. Plants have retained FtsZ as an important factor in plastid division though multiple families evolved. In our model system, *Arabidopsis thaliana*, two families of FtsZ (FtsZ1 and FtsZ2) are present and essential for proper chloroplast division. Chloroplast division is not directly comparable to bacterial binary fission due to some bacterial accessory proteins being lost in evolution while novel proteins were evolved in chloroplasts. The resulting chimerical mix in chloroplasts resulted in a more complex division system that involves more than one ring and is not yet completely understood. Past biochemical approaches aimed at characterization have been hampered by the lack of soluble expressed FtsZ. Expression in systems containing endogenous FtsZ were not able to delete the endogenous copy and resulted in inclusion bodies, though some reports did obtain yields sufficient for research. This chapter discusses the expression of *Arabidopsis thaliana* FtsZ families in a system that does not contain endogenous FtsZ and the subsequent biochemical characterization assays.

2.2 RESULTS

2.2.1 *Arabidopsis thaliana* FtsZ can be expressed in a system lacking endogenous FtsZ

The presence of bacterial FtsZ is required for viable cell cultures and proper cell divison. As a result, bacterial expression systems carrying an FtsZ transgene also require the endogenous FtsZ. Two reports, one prior and one subsequent to our work, used plant FtsZ expressed in a bacterial expression system (91,122). The work presented here and previously published work from our laboratory use *Arabidopsis* FtsZ expressed in a methylotrophic, eukaryotic system lacking endogenous FtsZ, *Pichia pastoris* (90,140,141). Many useful techniques developed in *Saccharomyces* expression systems are applicable in *Pichia* such as gene disruption and gene replacements. In addition, 10 to 100 fold increases in expression levels have been observed in *Pichia* as compared to *Saccharomyces* systems.

The transformation vector pPICZ was used for this work and allowed for ample transgene expression and suitable tags for purification and detection. An alternate vector, pPICZα, was constructed that secretes the expressed protein directly into the media, but was not used in the experiments presented. Expression is driven by the alcohol oxidase 1 gene and periodic supplements of methanol were added during growth due to evaporation. Transformation of the vectors into *Pichia* utilized chemically competent cells supplied by the manufacturer initially and later cells made competent in the laboratory. Transformants were selected on yeast extract peptone dextrose (YPD) medium supplemented with Zeocin as an antibiotic selection marker. Following the

selection of transformants, culture size was increased from 5 ml to 250 ml to generate sufficient biomass for purification. *Arabidopsis* FtsZ sequences were submitted to ChloroP, a program that predicts the size of the chloroplast targeting sequence (142). This step was essential as previous work demonstrated that functional FtsZ is transported from the nucleus to the chloroplast and the targeting sequence is cleaved before division events proceed (114).

The manufacturer supplied three *Pichia* strains (X33, GS115, KM71H) and pPICZ bearing FtsZ1 and FtsZ2 on separate plasmids were transformed and each of the three strains were tested for expression. Two FtsZ1 constructs were used, the wild-type and a construct carrying a S115F substitution that was present in the cDNA clone used to create the original construct. The correct clone was subsequently obtained and transformed into *Pichia* strain X33. Experiments revealed biochemical properties to be similar for the wild-type and S115 FtsZ1 mutant. These results were surprising given that the serine at this position is close to residues that in *Methanococcus jannaschii* are known to contact guanine nucleotides (97). The serine is conserved in most plant and many bacterial FtsZ sequences.

Our results indicated that the X33 strain supported expression at levels deemed appropriate for further processing while the GS115 and KM71H strains demonstrated lower expression and were not used for experimentation. Optimization of expression levels in the X33 strains included using various amounts of methanol (1-5% (v/v)) every 12 h (up to 72 h) and taking a sample for protein isolation. Cells were pelleted, washed and lysed using breaking buffer (see section 2.4.2) and 0.5 μm glass beads. Samples

were assayed by sodium dodecyl sulfate polyacrylamide gel electrophoresis (SDS-PAGE) and those with the most biomass were selected for large scale cultures. The optimal growth conditions were slightly different for each strain and concentrated FtsZ protein solution was routinely 1-3 mg/ml. FtsZ purification was achieved via a nickel coated column affinity resin (nickelnitriloacetic acid (Ni-NTA), Invitrogen) that exploited the 6xHis tag. Protein was removed from the resin by increasing concentrations of imidazole (see section 2.4.2).

2.2.2 SDS-PAGE, dot and Western blotting confirm the presence of FtsZ

Protein detection assays have become an indispensible tool for several fields of research. Molecular biology has greatly benefited from the ability to specifically identify a desired protein from heterogeneous mixtures (e.g. cell extracts). The most common form of detection is the Western blot and this technique is derived from Laemmli's description of SDS-PAGE (143) and Towbin's method for electrophoretically transferring proteins from polyacrylamide gels to membranes (144). Following protein transfer the desired protein is detected using an antibody (the primary antibody) which is in turn detected by a secondary antibody conjugated to a molecule that allows signal visualization (e.g. alkaline phosphatase, horseradish peroxidase, etc.). Dot blots achieve protein detection in a similar manner but do not require SDS-PAGE or an electrophoretic transfer as protein is directly spotted onto a membrane. This technique does not allow for determination of protein size or whether multiple proteins were detected by the antibody. For these reasons, Western blotting is needed for most research applications although dot blotting is an important tool that affords a significant reduction in experiment time.

Subsequent to protein elution from the Ni-NTA column, fractions were subjected to SDS-PAGE analysis to monitor transgene expression for FtsZ1 (Fig. 2.1) and FtsZ2 (Fig. 2.2). The gels indicate that the wash steps removed loosely bound protein from the column and the first two to three elution fractions contained protein other than FtsZ and were not used for experimentation. Later elution fractions were resolved as a single band and were dialyzed to remove residual imidazole before further investigation.

Dot and Western blotting were used to confirm the identity of the band observed in the SDS-PAGE gels. Dot blots were used to detect the protein by the c-myc tag on the C-terminal end of the FtsZ constructs. The secondary antibody was conjugated with alkaline phosphatase and developed using aqueous 5-Br-4-Cl-3-indolyl-phosphate (BCIP) and nitroblue tetrazolium (NBT) and the same recognition and development schemes were employed in Western blots. Single bands were detected for both FtsZ1 (Fig. 2.1) and FtsZ2 (Fig. 2.2) in Western blot elution fractions.

Concurrent to these experiments a control using identical procedures was carried out using a non-transformed X-33 *Pichia* strain. No protein in the appropriate range for FtsZ was found on SDS-PAGE gels following affinity purification and no signal was detected on immunoblots probing with the anti-c-myc antibody. These results suggest that the purification protocol was specific for FtsZ and the protein purified was free of potential *Pichia* contaminants.

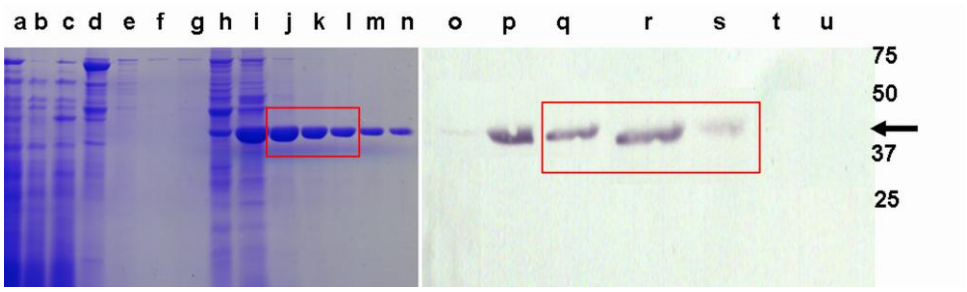

Figure 2.1. Purification of recombinant FtsZ1 expressed in *Pichia pastoris*. Coomassie stained FtsZ1 SDS-PAGE (a-n) and Western blot (o-u) probed with anti-c-myc antibody. (a) Diluted whole cell lysate, (b) flowthrough, (c-g) wash fractions (h-n) eluate fractions 1-7 and (o-u) Western blot corresponding to eluate fractions 1-7. Molecular mass marker positions are given in kDa. The arrow indicates the FtsZ1 band. The box indicates fractions that were used for dialysis and subsequent experiments (90).

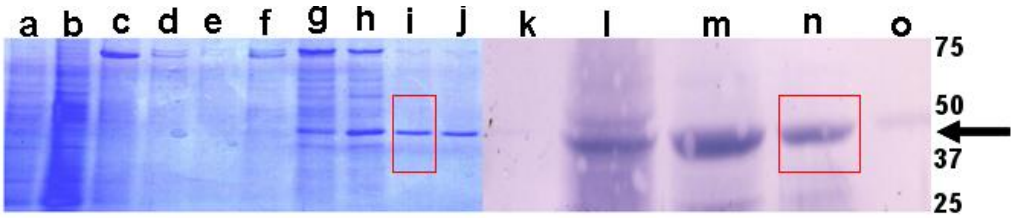

Figure 2.2. Purification of recombinant FtsZ2 expressed in *Pichia pastoris*. Coomassie stained FtsZ2 SDS-PAGE (a-j) and Western blot (k-o) probed with anti-c-myc antibody. (a) Diluted whole cell lysate, (b) flowthrough, (c-e) wash fractions (f-j) eluate fractions and (k-o) Western blot corresponding to eluate fractions. Molecular mass marker positions are given in kDa. The arrow indicates the FtsZ2 band. The box indicates the fraction used for dialysis and subsequent experiments.

2.2.3 Microwave-assisted protocols reduce blotting times

Cold Microwave-assisted (CMWA) research has been employed in laboratories for over thirty years and originated in histological studies (145). The ability of CMWA protocols to preserve cell structure made the technology a valuable tool for EM and light microscopy (LM) (146). CMWA research overcame the problem of poor heat conduction in biological materials and allowed the penetration of microwave energy several centimeters into histological samples (147). Early attempts lead to reductions in experiment time though a thorough study into experimental variables was needed for results to become reproducible (148). Studies aimed at understanding microwave energy behavior and microwave effects on chemical reagents were largely responsible for greater sample reproducibility (149). For example, a study comparing conventional (56-72 hours) and CMWA (4 hours) tissue processing protocols concluded that CMWA protocols performed equally well or surpassed conventional protocols (150). Microwave-assisted (MWA) protocols have previously been successful in several fields of research including resin polymerization for electron microscopy (151) and antibody labeling of fixed biological tissue (152). Improvements in protocols made it possible to use less chemical reagents and increase the number of specimens that can be processed simultaneously saving significant time and resources.

During the development of the FtsZ purification strategy a line of experiments were pursued that led to shortened protein detection times using CMWA protocols (140,141). The protocol does not use additional chemicals that may interfere with conventional steps suggesting that CMWA protocols may be applicable to other

techniques. Conventional protocols require total blotting times of several hours to overnight while the CMWA protocol reduces the time to approximately 45 minutes (Table 2.1). The basic steps of protein detection described in the conventional approaches have been preserved in CMWA protocols.

Table 2.1. Comparison of the traditional and the CMWA dot and Western blot protocols. The six minute cycle consists of 2 minutes on, 2 minutes off and 2 minutes on at 37°C and at a calibrated power of 220 Watts. Wash steps are at 37°C and a power of 220 Watts.

	Traditional	CMWA
Blocking	Overnight at 4°C (or 2 h at 21°C)	6 min cycle
Primary antibody	Overnight at 4°C	6 min cycle
Wash (TBS+ 2% (v/v) Tween)	4 times for 10 min each (21°C)	4 times for 1 min each
Secondary antibody	1 h at 21°C	6 min cycle
Wash (TBS+ 2% (v/v) Tween)	2 times for 10 min each (21°C)	2 times at 1 min each
Wash (TBS)	2 times for 10 min each (21°C)	2 times at 1 min each

While heat-sealed bags were used in the conventional protocol, the proper vessel for CMWA protocols required microwave compatibility and minimum volume capacity. Mini-blotting containers (Research Products International) were used for Western blots and polypropylene dishes (Ted Pella, Inc.) were employed for dot blots. Each of these containers were re-used for several experiments and no noticeable effects on the results

were observed. The CMWA protocols used a two-fold higher antibody concentration so lowering the volume requirements was of interest in making the technique economically viable. Early versions of the protocol used 1 ml of solution per step for dot blots and 20 ml for Western blots. In an effort to decrease the volume needed for Western blotting, containers were rendered hydrophilic by glow-discharging (in air) for 10 s at reduced atmospheric pressure immediately prior to use and this allowed a reduction in volume to 10 ml per step for Western blots. Dot blot containers were glow-discharged and still used 1 ml per step to allow total coverage of the membrane and to prevent background. It should be noted that CMWA Western blots did require a threefold increase in reagent use as compared to conventional protocols.

CMWA blotting used a six minute microwave cycle (2 min on, 2 min off, 2 min on) at a calibrated setting of 220W for blocking and antibody incubation steps compared to one hour or more for each step in conventional protocols. Blot development was performed at 21 °C as described for the conventional protocol. Dot blots processed concurrently using the CMWA protocol, but in the absence of microwave radiation did not produce a detectable signal (data not shown). The results of a CMWA Western blot using an anti-c-myc antibody demonstrated that specific proteins can be detected by the protocol and that non-specific proteins are not detected as a variant of lambda holin S105 bearing a His tag produced no signal. Analysis of dot blot and Western blots suggest that the uniform background corrected, integrated signal intensities in both the conventional and CMWA Western and dot blots are comparable. The complete CMWA protocol developed in our laboratory has been published (140).

Previous MWA protocols such as the ELISA protocol described by Van Dorp *et al*. (153) or the Western blot analyses reported by Li *et al*. (154) and Toyokuni *et al*. (155) utilized a microwave environment that does not provide a homogeneous, temperature-controlled microwave field at calibrated power settings (Watts). The latter studies could therefore not discount the involvement of microwave heat in addition to microwave energy and need to be seen in contrast to the CMWA protocol developed in our laboratory (140,141). In addition, the reports by Li *et al.* and Toyokuni *et al.* describe extended blocking and antibody incubation steps resulting in longer protocols.

2.2.4 *Arabidopsis thaliana* FtsZ assembly reactions promote two distinct types of filaments

Given its important role in chloroplast division, observation of FtsZ at a higher resolution than allowed by light microscopy is important to understand the morphology and manner in which they assemble. Similar studies using bacterial FtsZ revealed the morphology of filaments that assemble into the Z-ring. Bacterial studies also demonstrated that sheets, filaments and mini-ring assemblies are induced depending on the experimental conditions used and mutations made to bacterial FtsZ (100-102). One of the goals of this research is to examine the self-assembly capabilities of *Arabidopsis* FtsZ and compare them to the bacterial FtsZ results. *Arabidopsis* harbors two families of FtsZ proteins and each has to be investigated separately and in combination as a study using a yeast-two hybrid and bimolecular fluorescence complementation approach concluded that FtsZ1 and FtsZ2 interact with themselves and each other (113). Bacterial FtsZ studies have identified regions important for self-interaction (156).

FtsZ1 and FtsZ2 from *Nicotiana tabacum* have been expressed in *E. coli* (122) and while it was reported that FtsZ1 was able to self-assemble into filaments, FtsZ2 formed globular aggregates, which is in stark contrast to our observations. It is possible that *Nicotiana tabacum* and *Arabidopsis* FtsZ have different assembly properties, but a more likely explanation is that instead of the mature form of the proteins, the authors used recombinant proteins that included the N-terminal transit peptide. Olson *et al.* also reported that both FtsZ1 and FtsZ2 assembled into filaments as was observed in our studies (91).

Using a buffer system that was successful in the bacterial system, 100 mM MES, 1 mM EGTA, 5 mM magnesium acetate, pH 6.5 (MEMK) (157), *Arabidopsis* FtsZ assembly was demonstrated *in vitro* (90). Studies in our laboratory have investigated FtsZ protein assembly in equimolar concentrations and each protein individually in the absence and presence of GTP ($C_{10}H_{16}N_5O_{14}P_3$) and a nonhydrolyzable analog GTPγS ($C_{10}H_{16}N_5O_{13}P_3S$) that replaces an oxygen on the gamma phosphate with a sulfur (Fig. 2.3). Presence of both FtsZ1 and FtsZ2 promoted assembly, as did reactions with only one of the FtsZ species present. Two distinct types of filaments termed type-I and type-II were observed in both FtsZ1- and FtsZ2-only self-assemblies as well as in FtsZ1 and FtsZ2 mixtures (1:1) (Fig. 2.4) and initial analysis of the filaments hinted at their possible helical nature. FtsZ assembly assays lacking nucleotides or Mg^{2+} failed to

promote filament assembly in individual FtsZ preparations and when both proteins were present. Published reports indicate that without molecular crowding agents, the bacterial FtsZ self-assembly is not achieved in the presence of GTPγS (158,159). FtsZ1 and/or FtsZ2 assembly reactions containing GTPγS did not produce any assemblies except single particles. Assembly reactions containing GTPγS and polyethylene glycol (PEG) 1000 as a molecular crowding agent ranging from 1-8% did not produce larger condensates as observed in bacterial FtsZ (159). These experiments were repeated with a different assembly buffer successful with bacterial FtsZ assembly, HEPESAc (89), and the results were similar to those observed with MEMK.

An attempt to obtain more regular assemblies (filaments, helical tubes, two-dimensional crystalline sheets, etc.) that would facilitate data retrieval to higher resolution was conducted. Experimental variables included manipulating the relative FtsZ concentrations in the co-assembly procedure, supplementing the assembly buffer with Ca^{2+} which caused sheet formation in bacterial FtsZ and varying the concentration of Mg^{2+}. None of the conditions tested supported assemblies except the filament types described above. These results suggest the assembly pathway of bacterial and *Arabidopsis* FtsZ are mechanistically different.

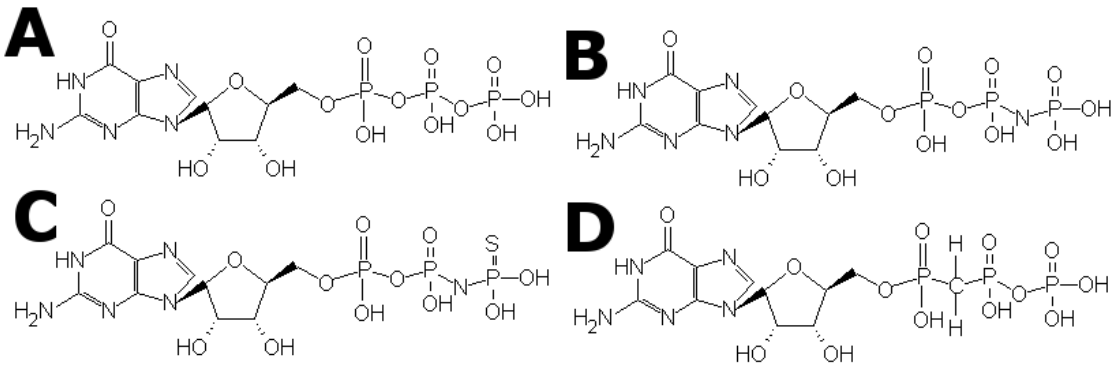

Figure 2.3 GTP and derivatives used in this study. (A) GTP, (B)GMP-PNP replaces the oxygen bridging the beta and gamma phosphates with a nitrogen, (C) GTPγS replaces the double bonded oxygen on the gamma phosphate with a sulfur, (D) GMPCPP replaces the oxygen bridging the alpha and beta phosphates with a methylene group.

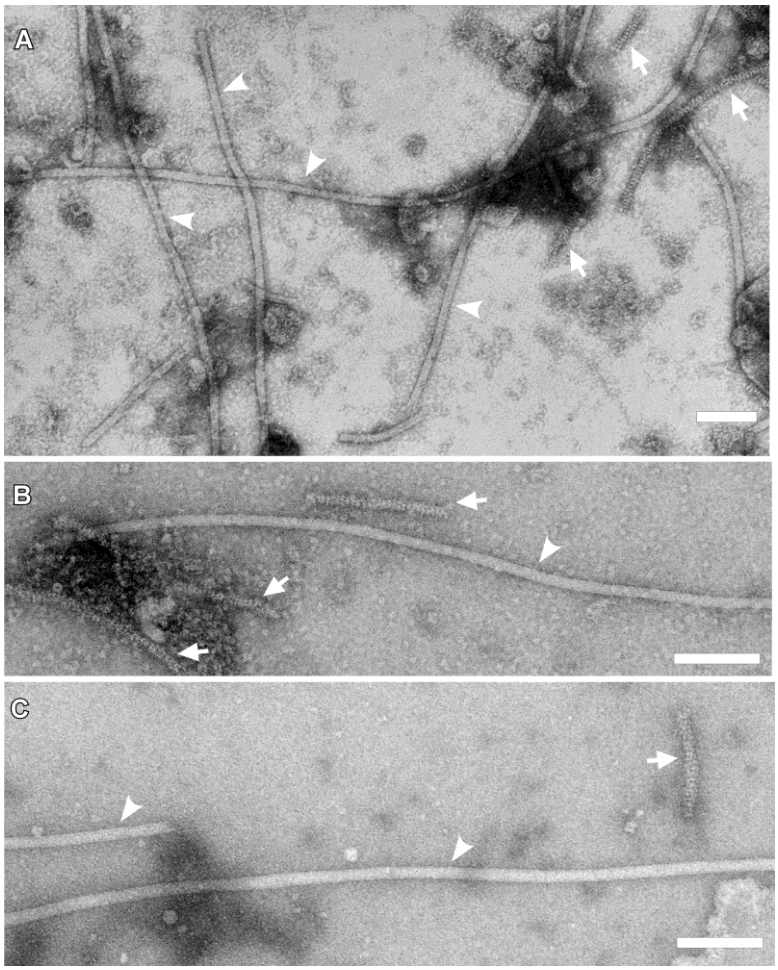

Figure 2.4. Electron micrographs of negatively stained FtsZ1 and FtsZ2 assemblies in the presence of GTP. For all panels, arrowheads highlight type-I filaments and arrows highlight type-II filaments. (A) Filaments from a reaction containing FtsZ1 and FtsZ2 in an equimolar mixture, (B) filaments from a reaction containing only FtsZ1, (C) filaments from a reaction containing only FtsZ2. The background displays filament precursors. Scale bars correspond to 100 nm (90).

2.2.5 Precursor assembly molecules are observed in assembly reactions

Assembly reactions in the presence of GTP have shown two distinct types of filaments while favoring type-II filaments (Table 2.2). Considerable heterogeneity in regards to particle types was observed (Fig. 2.5). The particles present when each protein was assembled alone and in combination are thought to comprise the soluble stromal FtsZ pool in chloroplasts. Using GDP in the assembly reactions favored the formation of type-I filaments (Table 2.2) with a significant background of unassembled intermediate particles. Upon surveying the sizes and shapes of the observed projections, it was noted that a fraction of the particle population displayed dimensions and shapes that were different from the ones observed under GTP-containing conditions and experiments lacking appropriate nucleotides (Figs. 2.5 and 2.6).

Fluorescence recovery after photobleaching (FRAP) was used to demonstrate that subunit exchange in and out of the Z-ring in *B. subtilis* and *E. coli* and the results reveal that it is rapid, indicating that the ring undergoes continuous remodeling (109,160) with half-time of FtsZ turnover $\mathbf{t_{1/2}}$ of approximately 8 s (160), similar to a rate of assembly determined by Förster resonance energy transfer with FtsZ labeled via small fluorescent dyes *in vitro* (161). Investigating whether these particles represent the stromal soluble FtsZ pool was studied and will be discussed in chapter III.

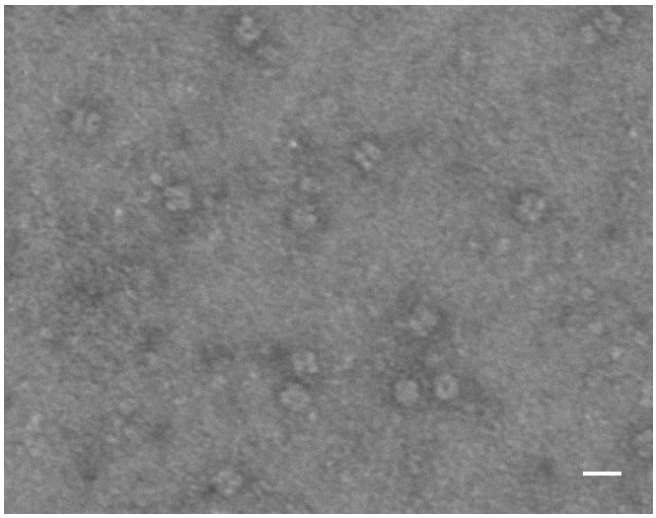

Figure 2.5. Overview electron micrograph of FtsZ2 assembly particles in the presence of GTP. Micrograph of a FtsZ2 assembly reaction in the presence of GTP displaying assembly intermediates in an area devoid of type-I and type-II filaments. Scale bar corresponds to 20 nm.

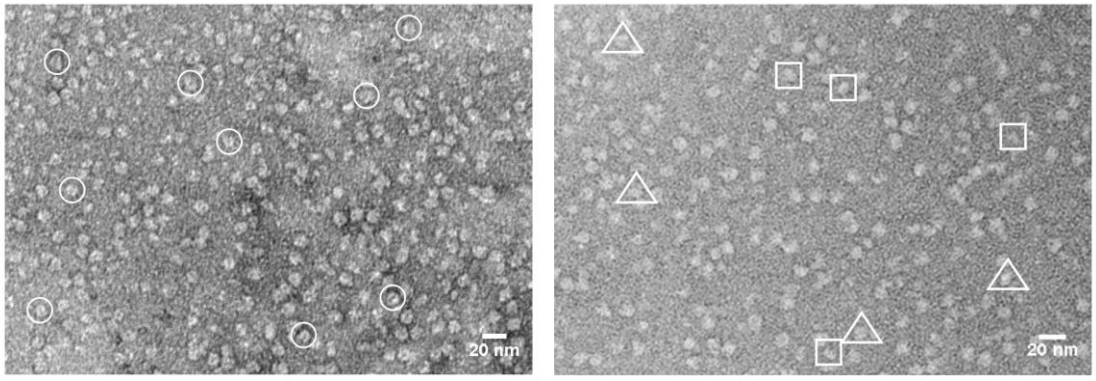

Figure 2.6 Overview electron micrographs of intermediates in assembly reactions lacking nucleotide and in the presence of GDP. The left panel represents a FtsZ1 assembly reaction lacking nucleotide. Projections resembling class averages discussed in chapter III are circled. The right panel displays an area from a FtsZ1 + GDP assembly assay devoid of filaments. Triangles highlight projections that could correspond to head-to-tail dimers as discussed in chapter III. Squares depict a minor species that does not appear in other assembly conditions. The dimensions of these particles are roughly consistent with a monomeric population.

Table 2.2. Distribution and diameter measurements of type-I and type-II filaments with GTP and GDP containing MEMK buffer and under assembly conditions.

	Type-I (%)[a]	Type-II (%)[a]
FtsZ 1+2 (GTP)	38	62
FtsZ 1 (GTP)	27	73
FtsZ 2 (GTP)	41	59
FtsZ1+2 (GDP)	71	29
FtsZ 1 (GDP)	66	34
FtsZ 2 (GDP)	58	42
Filament Diameter[b]	14.4 nm ± 0.8	11.2 nm ± 0.3

[a] n = 100
[b] n = 70
Standard deviation for type-II filaments in GTP is 6.01
Standard deviation for type-I filaments in GDP is 5.35

2.2.6 Type-I and type-II filaments are promoted in the presence of GTP and GDP at different rates

Negatively stained FtsZ1, FtsZ2 or the FtsZ co-assembly in the presence of either GDP or GTP were examined by EM to determine the relative abundance of the two types of filaments observed. While type-II filaments were favored in the presence of GTP, type-I filaments were more abundant in GDP assemblies. These trends hold true for the individual FtsZ protein assemblies as well as the FtsZ co-assembly and the results are summarized (Table 2.2).

In all of our *in vitro* experiments, FtsZ1 and FtsZ2 consistently formed straight or slightly undulating type-I and type-II filaments in assembly reactions containing either GDP or GTP and no evidence of GDP-dependent curvature was found as was described in the bacterial literature (102). Data presented here supports the idea that FtsZ1 or FtsZ2 alone or in combination with each other are unlikely to provide force for constriction of the chloroplasts.

2.2.7 *Arabidopsis thaliana* FtsZ are GTPases

One of the hallmarks of bacterial FtsZ is GTPase activity and plant FtsZ proteins have been expected to be GTPases due to their homology (96). In particular, the presence of the tubulin signature motif suggested that nucleotide binding occurred. A continuous GTPase assay was used as a gauge of functionality for the purified FtsZ proteins (162). This assay avoids substrate depletion and ensures accurate representation of data in the case of a lag in GTPase activity that are both potential problems in a fixed time point

assay. It has been previously used for *S. cerevisiae* mitochondrial division protein Dnm1 (162) and for bacterial FtsZ (106).

The recombinant, purified FtsZ1 and FtsZ2 each displayed a GTPase activity, 66 ± 1.5 nmoles GTP hydrolyzed · min^{-1} · mg^{-1} protein and 12 ± 0.5 nmoles GTP hydrolyzed · min^{-1} · mg^{-1} protein, respectively (Fig. 2.7) (90). When equal amount of both proteins were mixed, the activity was substantially lower (16.5 ± 0.3 nmoles GTP hydrolyzed/min/mg protein) as compared to a simple average of the individual activities (39 nmoles GTP hydrolyzed/min/mg protein), suggesting that GTPase activity of FtsZ1 may be moderated upon its interaction with FtsZ2. The GTPase activities are comparable to that reported for bacterial/archaeal FtsZ, which ranges from ~13 nmol/min/mg of protein in *Mycobacterium tuberculosis* (163) to ~90 nmol/min/mg of protein in *E. coli* (164). FtsZ GTPase activity was lower when GTP was replaced by the slowly hydrolyzable analog β-γ-methyleneguanosine 5' triphosphate (GMPPCP) ($C_{11}H_{18}N_5O_{13}P_3$) that replaces the bridging oxygen between the beta and gamma phosphates of GTP with a methylene group (Fig. 2.3) (165). Recent reports show that archaeal FtsZ GTPase is suppressed in the presence of sodium ions (100). This was also the case in plant FtsZ1 and FtsZ2: when the potassium component of the GTPase buffering system was replaced with sodium, GTP hydrolysis fell to essentially zero (data not shown).

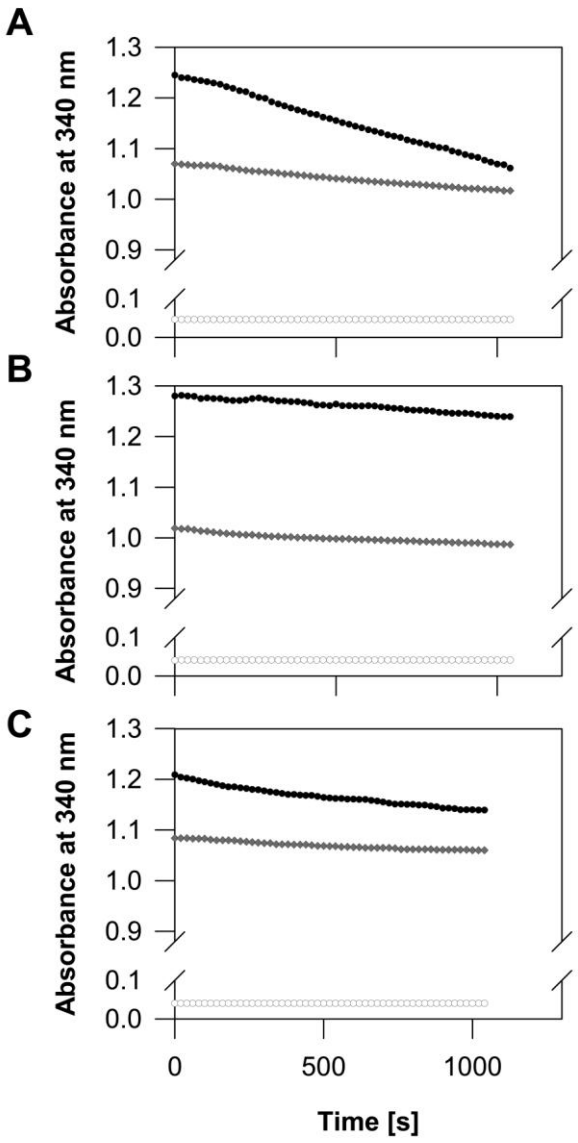

Figure 2.7. GTPase activity of FtsZ1 and FtsZ2. Enzyme-coupled assay monitoring NADH oxidation vs. time for (A) FtsZ1, (B) FtsZ2, and (C) FtsZ1 and FtsZ2 in the presence of GTP (top black line). Two controls were carried; FtsZ in the presence of GMPCPP (middle gray line) to show significance of GTP and an empty well control (bottom white line) to ensure experimental compatibility between different experimental set-ups (i.e. this report versus Ingerman *et al*. [18]). Readings were taken every 20 s for at least 15 min. The slope was subsequently used to calculate GTPase activity as described (see section 2.4.4) (90).

2.2.8 Determination of the critical concentration of the FtsZ co-assembly and FtsZ assembly efficiency

In vitro biochemical properties of bacterial FtsZ proteins have been characterized in terms of critical concentration, assembly efficiency and dynamics (164,166). The availability of soluble *Arabidopsis* FtsZ protein allowed characterization of these parameters. Determination of the percentage of protein incorporated into filaments and the critical concentration required for filament formation is important especially in light of the recent report in which molar concentrations and stoichiometry of FtsZ1 and FtsZ2 in *Arabidopsis* chloroplasts have been quantified (117).

The critical concentration was determined for the FtsZ1+FtsZ2 co-assembly (1:1) in the presence of GTP by ultracentrifugation and densitometry of the pellet (assemblies) after SDS-PAGE and Coomassie staining (Fig. 2.8). A bovine serum albumin (BSA) dilution series was used for calibration and to confirm linearity of the assay. Similar to the method used to determine the critical concentration of bacterial FtsZ, the amount of FtsZ in the pellet was plotted against the initial amount of FtsZ protein and the critical concentration was calculated as the x-intercept of the linear regression. The critical concentration for the FtsZ co-assembly was 82.75 µg/ml (= 1.95 µM), comparable to that for bacterial FtsZ measured using light scattering (167) (2.5 µM), sedimentation (166) (1.5 µM) or isothermal calorimetry (157) (0.3 µM).

The assembly efficiency of FtsZ proteins in the presence of GTP was monitored by gel densitometry analysis of pellet and supernatant fractions following sedimentation. Assembly efficiency of FtsZ2 was 42.2 ±1.9% , which is similar to that of *E. coli* FtsZ

(51%) under GTP containing conditions (166). The assembly efficiency of FtsZ1, which is more divergent from the bacterial protein, was substantially lower, and reached only 14.3 ± 2.5%, while co-assembly of FtsZ1 and FtsZ2 at an equimolar ratio gave intermediate results, 33.4 ± 0.9% (Fig. 2.9).

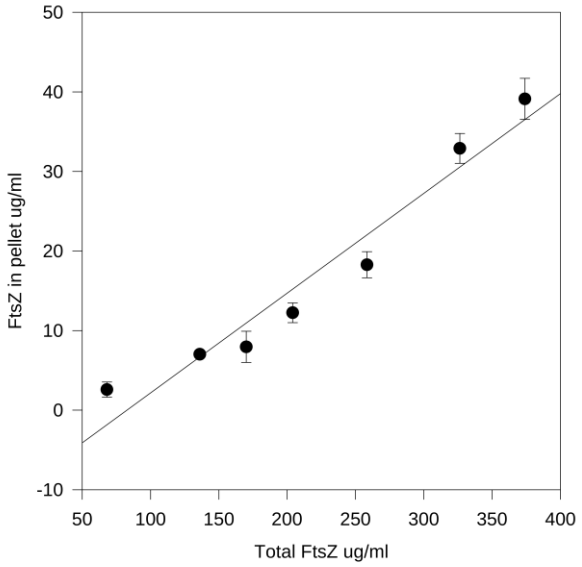

Figure 2.8. Critical concentration of the FtsZ1 and FtsZ2 co-assembly in the presence of GTP. Total FtsZ concentration is plotted on the X-axis and FtsZ found in the pellet fraction after sedimentation is plotted on the Y-axis. The X-intercept (82.75 μg/ml) is given as the critical concentration of FtsZ needed for assembly as described previously (166). The correlation coefficient was determined to be 0.944.

2.2.9 Volume measurements of the subunits of type-II filaments

Type-II filaments were markedly different than type-I filaments and displayed discrete, easily identifiable densities that appeared to constitute the subunits - i.e. the smallest repeating units - from which the filaments have assembled. Each of these filament subunits are elliptical in projection with the long axis measuring 6.1 nm and the short

axis 4 nm. Assuming a prolate ellipsoid as the three-dimensional subunit shape and a partial specific volume (υ) of 0.74 ml/g (168,169), the molecular mass (m) can be estimated according to the formula m (Da) = volume of the protein (ml) x Avogadro's number x 1/υ (170). Using this approach, one arrives at a molecular mass of 41.5 kDa per subunit which is in excellent agreement with the molecular mass of either FtsZ1 or FtsZ2. The molecular dimensions also agree well with the X-ray data for bacterial FtsZ where the bulk of the protein along the three principal axes measures approximately 3.5 x 4 x 6 nm (94).

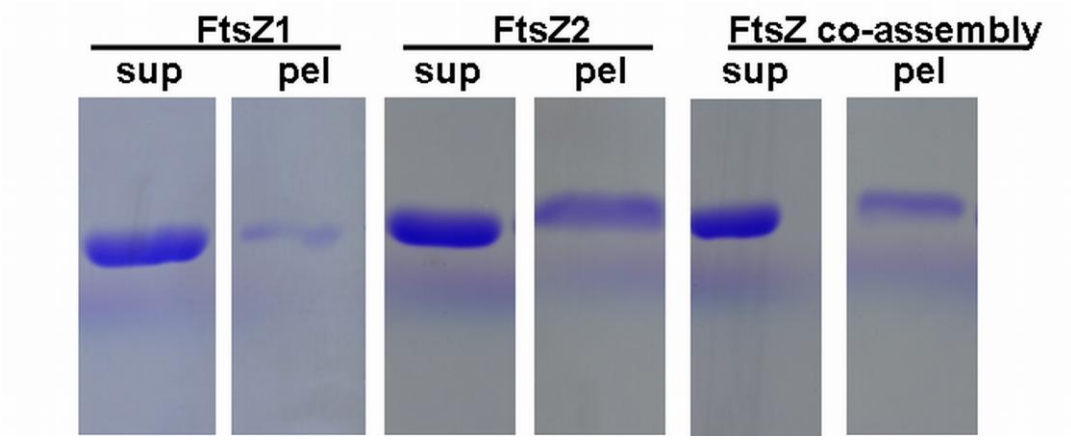

Figure 2.9. Assembly efficiency of FtsZ proteins. Following assembly procedures and centrifugation, supernatant fractions were recovered and pellet fractions were resuspended in fresh polymerization buffer. Fractions were subjected to SDS-PAGE as described previously (90). Representative SDS-PAGE bands for supernatant (sup) and pellet (pel) fractions for FtsZ1, FtsZ2 and the FtsZ co-assembly are shown.

2.3 DISCUSSION

2.3.1 Soluble FtsZ allows for biochemical characterization

Our laboratory and others have designed protocols that allow expression and purification of adequate amounts of FtsZ and partial characterization of the assembly mechanism and biochemical properties have been reported (90,91,122). The other reports used plant FtsZ expressed in *E. coli*. Overexpressing FtsZ from plants in bacterial systems has previously been shown to decrease growth rate, produce long filaments and change cell morphology with overexpression of FtsZ2 having a more severe effect (122). The proteins in *E. coli* were mostly misfolded and sequestered into inclusion bodies, making purification of functional FtsZs difficult, albeit possible (100,102,122). Whether bacterial and plant FtsZ can interact through self-assembly domains is unknown and a control has not been included in published reports.

To overcome the shortfalls of bacterial FtsZ expression and to increase protein yield, the *Pichia pastoris* yeast expression system has been used in our current studies. *Pichia* does not have endogenous FtsZ, thus overexpression of the protein is not toxic to the cell and use of a eukaryotic expression system would allow relevant posttranslational modifications of the expressed proteins that more closely represent native characteristics. The commercial *Pichia* expression vector pPICZ yields proteins C-terminally tagged with both myc and 6xHis tags to facilitate purification and detection. Small tags have been demonstrated not to affect biological activity with bacterial FtsZ (171).

El-Kafafi *et al.* concluded that FtsZ2 did not assemble into filaments which is not in agreement with the work presented here and Olson *et al.* observed that both FtsZ1 and

FtsZ2 assembled into filaments though not the morphologies observed in our studies (91,122). It should be noted that El-Kafafi *et al.* used FtsZ from *Nicotiana tabacum* and not *Arabidopsis* though the FtsZ between these species is well conserved at the protein level. Our work and Olson *et al.* demonstrate GTPase activities for both FtsZ families and critical concentrations of 1.95 µM and approximately 0.75 µM, respectively while El-Kafafi *et al.* did not include these experiments in their analysis (91,122).

2.3.2 Microwave-assisted protocols can be applied to other molecular techniques

Early users of MWA protocols faced difficulty in reproducing results in part due to inhomogeneities in the strength of the microwave field and uncontrolled heating (148,150,172,173). These problems were largely solved with the ColdSpot™ technology (developed by Ted Pella, Inc.) that creates uniform microwave irradiation and allows a rigorous temperature control of the sample (174). Earlier attempts to incorporate MWA principles into conventional techniques did not use the ColdSpot™ technology and had extended blocking and antibody incubation steps (154,155). Protocols using CMWA technology employ identical chemistry when compared to conventional techniques and may be adapted for a wide range of other screening/visualization applications. An example is the CMWA enzyme-linked immunosorbent assay (ELISA) protocol that was developed in our laboratory (140).

CMWA dot blotting is an attractive choice for screening large numbers of protein-expressing strains in a rapid fashion. In our experience, the same volumes of reagents are used and considerable time savings are achieved. However, CMWA Western blotting requires more antibody than conventional protocols owing to increased

volume requirements. This may pose a problem for laboratories dealing with an antibody that is in short supply, though the time savings may make the CMWA protocol more cost effective.

This line of experimentation provided further evidence in support of a microwave radiation effect versus a thermal effect. CMWA and corresponding microwave-unassisted experiments were carried out under the same conditions with regards to blocking steps, buffer composition, incubation steps and antibody concentration. A signal was detected only in the presence of microwave radiation, suggesting that antibody-antigen interactions are improved solely by microwave radiation. Experiments that were carried out at increased temperatures observed a further signal enhancement likely owing to an additional thermal effect.

2.3.3 The precursor molecules constitute the soluble pool that remodelss the Z-ring

Plant FtsZ has been actively researched at the organelle level using LM and other techniques and a large collection of phenotypic mutants is available to the research community. However, a lack of purified and biologically active protein has led to a lack of information at the molecular level. The expression protocols developed in our laboratory and by others will allow inquiries at the molecular level and structure-function relationships to be examined.

Bacterial FtsZ has been shown to contain a cytoplasmic soluble pool of FtsZ that constantly exchanges molecules in the Z-ring (109). A soluble FtsZ pool had been hypothesized to exist in chloroplasts and evidence of dynamic exchange in *Arabidopsis* Z-rings was recently provided by FRAP experiments in our laboratory (Carol B. Johnson

and Stanislav Vitha, manuscript in preparation). These experiments did not identify the FtsZ pool in terms of the oligomeric states present. Assembly experiments in the absence of appropriate nucleotides, Mg^{2+} or an assembly procedure did not promote filaments but many particles were observed in the background that possibly were precursor molecules to filament formation. Particles, representing assembly intermediates, were observed in assembly reactions in the presence of nucleotides in lesser numbers.

The prolate ellipsoid calculation given above for type-II filaments suggested that the observed densities incorporated into these filaments were in the size range of FtsZ1 and FtsZ2. The mechanism of incorporation of precursor molecules into type-I and type-II filaments is not currently understood. Chapter III of this work concerns itself chiefly with understanding the mechanism of *Arabidopsis* FtsZ assembly and identifying the oligomeric states present in the FtsZ soluble pool.

2.3.4 Type-I filaments may be helical and type-II filaments have distinct sub-filament units

While type-II filaments displayed identifiable densities that appeared to constitute the subunits, type-I filaments were smoothly delineated but often revealed a longitudinal striped pattern (marked by arrowheads in Fig. 2.10). Using Fourier peak filtering, a map (Fig. 2.11B) was calculated that emphasizes a 3.5 nm separation between stain-excluding densities that typically appear at type-I filament ends (highlighted by arrows in Fig. 2.11A). Given the generalized shape and dimension of archaeal FtsZ (*Methanococcus jannaschii*) monomers being a prolate ellipsoid of 3.5 x 4 x 6 nm (94), it is conceivable that each stain-excluding density corresponds to a FtsZ monomer in an

end-on projection of the ellipsoid, i.e. when viewed perpendicular to its short half-axis. Regarding their overall appearance, type-I *Arabidopsis* filaments were comparable to those assembled from *Nicotiana tabacum* FtsZ1 by El-Kafafi *et al.* (122) and to *B. subtilis* FtsZ filaments assembled in a GTP-containing environment (175). It is interesting to note that FtsZ filaments from *B. subtilis* displayed a striped pattern similar to those observed using *Arabidopsis* FtsZ under similar experimental conditions (compare right and left panels in Fig. 2.10). The separation between the striped densities was calculated as approximately 4 nm in *Arabidopsis* filaments (Fig. 2.11B) and approximately 4.3 nm in *B. subtilis* filaments, which suggests a similar protofilament arrangement. This thought is further supported by structural studies of bacterial FtsZ demonstrating protofilament widths between 4.2 and 4.7 nm (100,102,176,177). In contrast to type-I, type-II filaments had easily identifiable subunits and Fourier analysis suggested a separation of 6 nm between the units (Fig. 2.11C, D). This dimension agrees well with the overall monomer dimensions given above but would argue for a different packing. While in type-I FtsZ molecules are assembled with the short axes of the molecule aligned parallel to the filament axis, in type-II the positioning appears to have changed so that the long 6-nm axis of the molecule runs parallel with the filament.

At this point one has to differentiate between the fate of FtsZ molecules once incorporated into the filament and the process of incorporation of molecules into the filament. While this section describes the static assembled product, chapter III will be concerned with defining the components and the timing relevant for the dynamic mechanism of FtsZ assembly. The chapter will also allude to a structural evaluation of

the precursors prior to incorporation but en route to filament assembly. Proposed models for FtsZ incorporation into type-I and type-II filaments are presented in chapter III.

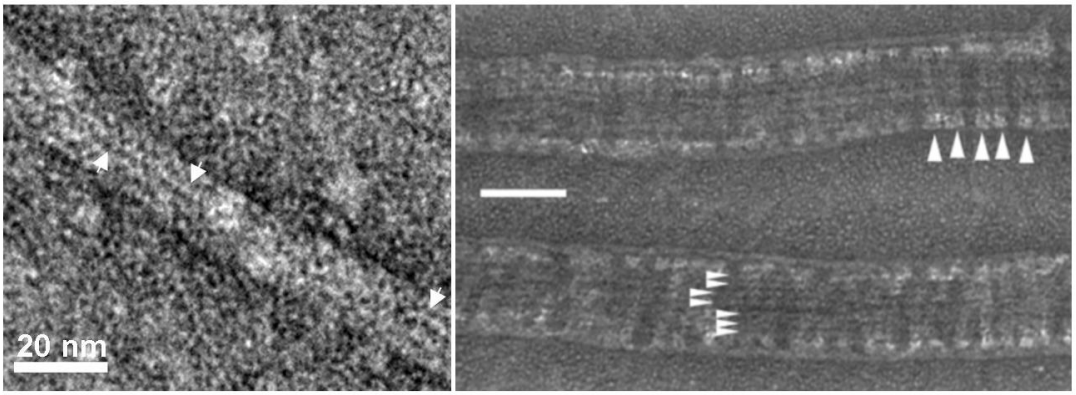

Figure 2.10. Type-I filament co-assembly in the presence of GTP. Reocurring striped pattern is highlighted by arrowheads in both panels. Left panel displays an *Arabidopsis* FtsZ1 type-I assembly in the presence of GTP. Right panel displays a *B. subtilis* FtsZ filament assembly in the presence of GTP. Scale bar for right panel corresponds to 50 nm (175).

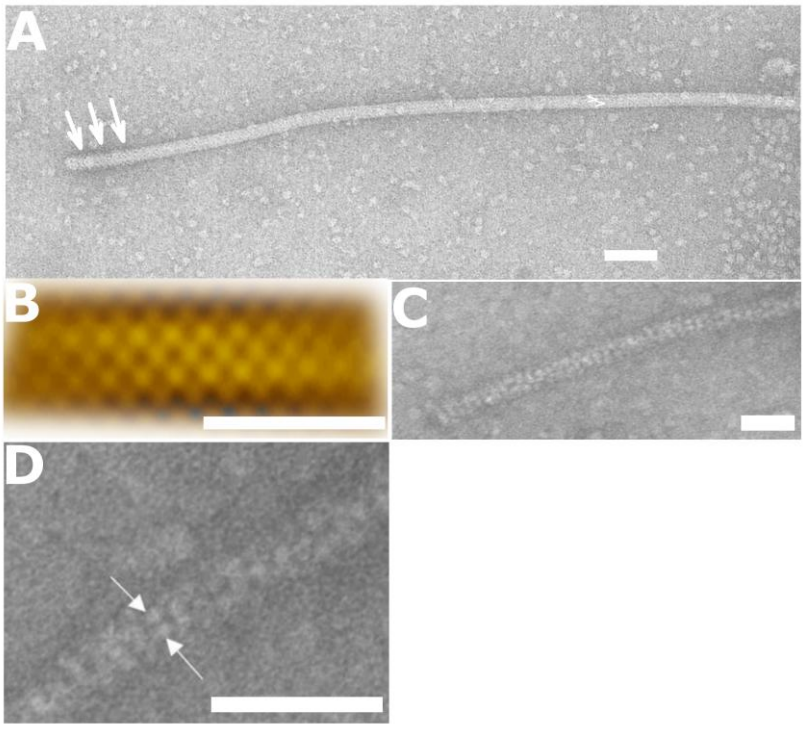

Figure 2.11. Electron microscopic analysis of negatively stained *in vitro* FtsZ1+ GTP assemblies. (A) Type-I filament displaying helical (arrows) ends and striped (arrow-heads) mid-filament patterns. (B) Fourier peak filtered map suggesting a helical architecture and emphasizing a 3.5 nm subunit separation found in type-I filament ends. It is interesting to note that the striated pattern observed at mid-filament locations (marked by arrowheads in A, and arrows in Figure 2.9) also shows a 3.5 nm repeat. The morphology of type-II filaments is strikingly different (C,D) readily revealing individual sub-filament units (arrows). Fourier analysis of type-II filaments suggests a subunit separation of 6 nm along the filament axis. Scale bars correspond to 20 nm.

2.3.5 FtsZ most likely does not supply the power needed for chloroplast constriction in a manner similar to bacterial constriction

An important aim of plastid division research is to determine the components that power the process by supplying energy for generating the constriction force necessary for division. Identifying the relevant proteins allows for inquiries into their functions as they relate to the division process. Bacterial Z-ring constriction is thought to occur by ring curvature triggered by a transition from straight filaments to curved filaments powered by GTP hydrolysis as straight filaments were observed in the presence of GTP and a nonhydrolyzable analog while assemblies in the presence of GDP produced curved filaments (87). Reconstitution experiments in liposomes using relevant bacterial components to show curvature has been published (89) and a potential experiment using *Arabidopsis* proteins is described in chapter IV.

A similar pattern of filament assembly was not observed in our studies as filaments were promoted in the presence of both GTP and GDP but no filament curvature was noted in the later suggesting that bacterial and plastid division derives constriction force from different sources. This is in agreement with current models for plastid division that imply ARC5 for this role. ARC5, in conjunction with PDV1 and PDV2, comprises the cytosolic division ring (37,70). Late stages of chloroplast constriction have been shown to be arrested in the absence of ARC5 (67). The possibility of a coordinated mechanism between the stromal and cytosolic rings can not be discarded at this time but could be addressed in the proposed reconstitution experiments.

2.3.6 The role of GTP hydrolysis in FtsZ assembly remains unresolved

The results from the assembly studies suggest that interaction with guanine nucleotides is necessary for FtsZ1 and/or FtsZ2 assembly since reactions performed without GTP/GDP or with a non-hydrolysable analog in bacterial FtsZ, GTPγS, did not yield any assemblies. However, the role of GTP hydrolysis in relation to FtsZ assembly remains unknown. Previous reports have demonstrated that another non-hydrolysable analog, guanylyl-imidodiphosphate (GMP-PNP) ($C_{10}H_{13}N_6O_{13}P_3$) (Fig. 2.3), is not a suitable substrate for bacterial FtsZ (158,178) and glutathione *S*-transferase tagged *E. coli* FtsZ does not polymerize when GTP is replaced by GMP-PNP (179). GMP-PNP is differentiated from GTP by replacing the oxygen atom bridging the beta and gamma phosphates with a nitrogen atom.

While further work is needed to address the complete role of GTP hydrolysis, the lack of filaments in assembly reactions devoid of nucleotides demonstrates that the filaments observed in the presence of GTP and GDP are the result of an active FtsZ protein assembly and not due to a contaminant or aggregates of misfolded, denatured protein. If GTPγS is a true substrate for *Arabidopsis* FtsZs, the results herein would hint at GTP hydrolysis as an essential requirement for assembly *in vitro* as no filaments were observed in GTPγS reactions. The nucleotide binding region, the T7 loop, has been identified in bacterial studies and is conserved in plant FtsZ families. A rigorous mutational study examining this region and monitoring affects on FtsZ assembly under different conditions would provide answers to some of the outstanding questions.

2.4 EXPERIMENTAL PROCEDURES

2.4.1 Plasmid constructs

FtsZ1 cDNA (Genbank Accession U39877) nt 180 to end, corresponding to the predicted mature protein without the chloroplast targeting sequence, was amplified using 5'-atgaattctataatgtctagaatcagtcaattccg-3' (forward), and 5'-gaggtaccgagaagaaaagtctacgggg-3' (reverse) primers and the Pfx50 proofreading DNA polymerase (Invitrogen, Carlsbad, CA). The forward primer introduces an *Eco*RI restriction site (underlined) and an initiation ATG as part of a yeast consensus sequence (double underlined) (180). The reverse primer was designed to remove a stop codon and to introduce a *Kpn*I restriction site. Similarly, FtsZ2 cDNA (NM_129183) fragment containing nt 220 to 1435 of coding sequence, without the predicted chloroplast targeting sequence, was amplified using primers 5'-atgaattctataatgtcttgaaccttcacccggaa-3' (forward) and 5'- gaggtaccgagactcggggataacgag-3'(reverse).

Each PCR product was cloned into *Sma*I-digested pBluescript II KS+ cloning vector (Stratagene, La Jolla, CA) and the lack of PCR errors was verified by sequencing. The FtsZ fragment was then excised with *Kpn*I and *Eco*RI, gel-purified and cloned in-frame into the pPICZ B expression vector (Invitrogen, Carlsbad, CA) for intracellular recombinant protein expression. In-frame junction of the vectors and inserts was confirmed by sequencing. The resulting expression constructs were then isolated, linearized with *Sma*I and used for transformation of *Pichia pastoris* strains X33, GS115, and KM71H with the Easy Select *Pichia* expression kit (Invitrogen, Carlsbad, CA). Protocols were carried out as described in the user manual. Transformants were selected

on YPD plates supplemented with 18.2% (w/v) sorbitol and zeocin at 100 μg/ml as a selection medium. Integration and expression were verified by PCR analysis and Western blotting.

The FtsZ1 cDNA (U39877) contains a mutation resulting in S115F substitution. The Serine at this position is conserved in most plant and many bacterial FtsZ sequences and is close to conserved residues that in *Methanococcus jannaschii* are known to contact guanine nucleotides (97). Therefore, an error-free FtsZ1 cDNA (AY113896) was also obtained and amplification and expression vector preparation was performed as above.

2.4.2 Protein expression and purification

Pichia X-33 strain expressing FtsZ1 or FtsZ2 were grown in 250 ml cultures using buffered methanol complex medium (1% (w/v) yeast extract, 2% (w/v) peptone, 100 mM potassium phosphate (pH 6.0), 1.34% (w/v) yeast nitrogen base, 4 x 10^{-5}% (w/v) biotin, and 1% (v/v) methanol) and supplemented with 3% (v/v) methanol every 12 h for a total growth time of 60 h at 30 °C. Cell lysates were prepared by centrifuging the culture and resuspending in 10 ml of breaking buffer (50 mM sodium phosphate (pH 7.4), 1 mM phenyl-methylsulfonyl fluoride (PMSF), 1 mM ethylenediaminetetraacetic acid (EDTA), and 5% (v/v) glycerol). An equal volume of 0.5 μm glass beads were added and the sample was vortexed for eight 30 s cycles interspersed by 30 s on ice. The proteins were purified under native conditions using Ni–NTA agarose beads (Invitrogen, Carlsbad, CA) as follows. Cell lysates were poured over a 10 ml Ni-NTA column to selectively purify the tagged protein. After addition of the lysate, it was allowed to bind

under gentle agitation for 30 min at 4 °C. Subsequently, four washes were performed with 8 ml of native wash buffer (50 mM sodium phosphate, 0.5 M sodium chloride, and 20 mM imidazole, pH 8.0) and collected by gravity filtration. Finally, the protein was eluted using native elution buffer (50 mM sodium phosphate, 0.5 M sodium chloride, and 250 mM imidazole, pH 8.0) and collected in 1-ml fractions. Subsequently, fractions determined to contain the respective FtsZ protein by SDS-PAGE were dialyzed against a buffer comprised of 50 mM NaMES (2-(*N*-morpholino) ethanesulfonic acid), 100 mM potassium chloride, 1 mM EGTA (ethylene glycol tetraacetic acid) and 2.5 mM magnesium acetate (pH 6.5) using SnakeSkin® pleated dialysis tubing (Pierce, Rockford, IL) with a 10,000 molecular weight cutoff. Protein concentrations were determined using a NanoDrop 1000 (Thermo Scientific, Rockford, IL), the bicinchoninic acid protein assay (Pierce, Rockford, IL) (181) or by the Bradford method (182). Collected fractions were subjected to SDS-PAGE and Western blotting to identify pure aliquots for assembly reactions.

2.4.3 Conventional Western and dot blots

For Western blotting, the proteins were first separated by SDS–PAGE (10% separating and 4% stacking gels) using a Mini-PROTEAN 3 system (Bio-Rad, Hercules, CA) (143) and the Precision Plus protein standards (Bio-Rad, Hercules, CA). The protein was

transferred onto 0.2 µm nitrocellulose at 1 A for 50 min in 25 mM Tris–glycine/20% methanol (v/v) (pH 8.3) using a Genie blotter (Idea Scientific, Minneapolis, MN). All incubation steps were performed at room temperature (21 ºC) unless indicated otherwise. Blocking for 1 h with 2% (v/v) cold water fish gelatin (Sigma, St. Louis, MO) in TBST (50 mM Tris-HCl (pH 7.4), 200 mM sodium chloride, 0.2% (v/v) Tween-20 (Research Products International, Mt. Prospect, Illinois)) was followed by an overnight incubation at 4 ºC with mouse monoclonal anti-c-myc antibody (Invitrogen, Carlsbad, CA) at a 1:5000 dilution in TBST, three washes in TBST 10 min each, and a 45-min incubation with mouse anti-rabbit alkaline phosphatase conjugate (Invitrogen, Carlsbad, CA). Developing was carried out with 10 ml of reaction buffer (100 mM sodium chloride, 5 mM magnesium chloride, and 100 mM Tris–HCl (pH 8.8)), 60 µl of 5% (w/v) aqueous BCIP solution (Research Products International, Mt. Prospect, Illinois) and 10 µl of 7.5% (w/v) NBT (nitroblue tetrazolium, Research Products International) in 100% (v/v) methanol at 21 ºC. Individual washes of membranes were carried out for 10 min in Tris-buffered saline (50 mM Tris and 200 mM NaCl (pH 7.4)) or TBST.

2.4.4 GTPase assay

GTPase activity was measured using a continuous, regenerative GTPase assay (162) (Fig. 2.12) at 37 °C with 50 µl reaction volumes in a 384-well plate (Greiner Bio-One, Monroe, NC). This assay was modified from an earlier ATPase measuring protocol (183). Absorbances at 340 nm were monitored using a Synergy HT Multi-Mode Microplate Reader (BioTek Instruments, Inc., Winooski, VT). Data were plotted using Microsoft Excel and corrected against a sample containing no protein. GTPase activities

given are derived from triplicate experiments. In control reactions, GTP was substituted by GMPCPP, which is hydrolyzed at a much slower rate than GTP (165). GTPase activity was calculated as follows (example provided is for FtsZ2).

The slope of the FtsZ2 curve was 5×10^{-5} and that of a no protein added curve was 2×10^{-5} resulting in a corrected slope of 3×10^{-5}. Division by the molar NADH extinction coefficient [6220 $M^{-1}cm^{-1}$] yields 2.89×10^{-7} min/ M cm and division by the path length of a 384-well plate [0.391 cm] results in 7.4×10^{-7} M/min. Relating this to total protein [0.003 mg] yields 12.34 nmoles of GTP/min x mg protein.

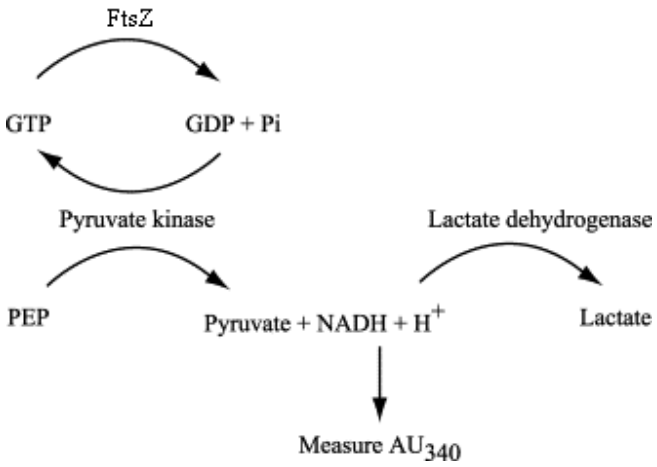

Figure 2.12. The continuous GTPase assay schematic. The active GTPase, in this case FtsZ, hydrolzes GTP to GDP and the newly formed GDP and phospho(enol)pyruvate participate in a reaction catalyzed by pyruvate kinase that yields GTP and pyruvate. The GTP allows the first reaction to be continuous and the pyruvate is reduced to lactate and the cosubstrate NADH is oxidized to NAD^+. The oxidation results in a measurable decrease at an absorbance of 340 nm that is directly proportional to the rate of GTP hydrolysis. This assay was used previously to ascertain the GTPase of bacterial FtsZ (106). Adapted from (162).

2.4.5 FtsZ assembly reactions and electron microscopy

Assembly reactions were carried out with either 100 mM morpholine-ethanesulfonicacid, 1 mM EGTA, and 5 mM magnesium acetate (adjusted with potassium hydroxide to pH 6.5) (MEMK) (184) or 50 mM HEPES, supplemented with 5 mM magnesium acetate and 350 mM potassium acetate (pH 7.7) (HEPESAc) (89). Reactions contained 0.6 mg of FtsZ protein per ml and either 2 mM GTP, 2 mM GMPPNP, 2 mM GMPPCP, 2 mM GMP-PNP or no nucleotide and assembly conditions consisted of a 10 min incubation on ice followed by a 10 min incubation at 37 °C. For electron microscopic analysis 2-5 µl of the reaction mixture was adsorbed onto a freshly glow-discharged carbon-coated formvar grid, washed briefly in water and negatively stained with a 2% (w/v) aqueous solution of uranyl acetate (pH 4.5). Specimens were observed in a JEOL 1200 EX transmission electron microscope operated at an acceleration voltage of 100 kV. Electron micrographs were recorded at a calibrated magnification (24,390 x) on Kodak electron image sheet film 4489. Negatives were digitized at 10 µm increments using an Epson Perfection 4490 flatbed scanner corresponding to 0.41 nm/pixel at the specimen level.

2.4.6 Blot quantification

Integrated densities in the dot and Western blots were quantified using Image J routines (185). Briefly, the digitized data were converted to 8-bit grayscale images, uniform background features subtracted using a 25 pixel rolling-ball algorithm, and the densities inverted to yield pixel values close to zero. The speckled background features observed with the conventional dot blots were assessed using the Digital Map routine within the

image processing software package CRISP (132). Two representative background areas were cropped and their density distributions evaluated for maximum and minimum values. The change in density variations were compared between the CMWA and conventional dot blot background areas and found to amount to18 and 42, respectively, suggesting that the CMWA protocol provides an approximately two-fold lower background noise.

2.4.7 Microwave assisted blotting

The protocol using CMWA technology involved identical reagents but made use of a PELCO BioWave® Pro Laboratory Tissue Processing System equipped with a ColdSpot™ temperature control system. Processing temperature was set at 37 °C or 21 °C (temperature cutoff at 42 °C or 25 °C, respectively) and blocking and antibody incubations were cycled for 6 min (2 min on, 2 min off, 2 min on) using a calibrated power output of 220W. Washing step times were reduced to 1 min each. Dot blots were carried out by placing 2-5 µl droplets of a 0.2 mg/ml protein sample onto a 0.2 µm nitrocellulose membrane (Bio-Rad, Hercules, CA). Polypropylene dishes (Ted Pella, Inc., Redding, CA, 50mm dia. x 12mm deep) were used for dot blots and mini-blotting containers (Research Products International, 9 x 6.4 x 2.1 cm) for Western blotting. Wattage was calibrated by placing a glass beaker containing 1 liter of water inside the cavity without the ColdSpot™ and incubating for 2 min at a nominal power setting of 250W. The temperature difference prior to and after the incubation (ΔT) multiplied by 35 gave the true wattage output.

CHAPTER III

STRUCTURAL STUDIES OF THE FtsZ ASSEMBLY MECHANISM

3.1 INTRODUCTION

As alluded to in chapter II, this section deals with FtsZ assembly dynamics. To this end, it becomes important to further differentiate between the *ab initio* assembly dynamics defined above and the steady-state dynamics of already existing filaments. The latter process is known in the literature as dynamic exchange and involves exchange between a soluble pool of FtsZ intermediates and the assembled filaments in the Z-ring. Previous reports showed that 50% of FtsZ molecules in the Z-ring are turned over within approximately 7 s in *E. coli* and *B. subtilis* (160), or within approximately 25 and 60 s for *Mycobacterium smegmatis* (186) and *Mycobacterium tuberculosis* (103), respectively. Recent results in our laboratory demonstrate that *Arabidopsis* FtsZ1 and FtsZ2 also undergoes dynamic exchange with the Z-ring although at a slower rate than the bacterial Z-ring and FtsZ1 and FtsZ2 displayed different turnover dynamics (Carol B. Johnson and Stanislav Vitha, manuscript in preparation). While the driving force behind the slower turnover rate was not readily apparent, the existence of this turnover activity prompted an investigation into the components of the FtsZ soluble pool by EM, native PAGE and gel chromatography using precursor molecules occurring in the presence of GTP under assembly conditions. The omission of assembly conditions and appropriate nucleotides, i.e. GTP, granted an opportunity to observe FtsZ molecules prior to filament assembly endowing this chapter with the first insights into the dynamic

exchange between the Z-ring and the soluble FtsZ pool and the assembly mechanism for FtsZ in *Arabidopsis*.

3.2 RESULTS

3.2.1 FtsZ1 and FtsZ2 under non-assembly conditions are homodimers

A soluble stromal FtsZ pool had been thought to perform dynamic exchange with the Z-ring in plastid division similar to the cytoplasmic FtsZ pool present in bacterial systems, confirmation of its existence was demonstrated using FRAP experiments in our laboratory (Carol B. Johnson and Stanislav Vitha, manuscript in preparation). A model of bacterial Z-ring dynamic exchange suggests that the cytoplasmic pool may consist of monomers (109). Bacterial FtsZ has been shown to assemble into ribbons that are one monomer thick in a GTP-dependant manner as determined using atomic force microscopy (187). It is currently unknown if *Arabidopsis* FtsZ behaves in a similar manner.

To better understand the population of *Arabidopsis* FtsZ that participates in Z-ring turnover, the oligomeric state of non-assembled FtsZ1 and FtsZ2 particles were determined. Previous results demonstrated that *Arabidopsis* FtsZ assembles into two filament types in the presence of GTP with one of them displaying discrete subunits that when assumed to be a prolate ellipsoid yielded a volume of 41.5 kDa which is in agreement with a monomer (90,169). No filaments were observed in the absence of the assembly procedure and nucleotides.

FtsZ1 and FtsZ2 were purified to homogeneity using a Ni-NTA column and analyzed for purity by subsequent SDS-PAGE analysis (90). Protein in the absence of

assembly procedures and nucleotides was then subjected to gel permeation chromatography using a Superdex-200 column to separate potential different oligomeric orientations of FtsZ. Only one major peak was observed on the gel chromatograph for each FtsZ protein and corresponded to approximately 78 kDa for FtsZ1 and approximately 80 kDa for FtsZ2 which are close to the calculated molecular mass of dimers suggesting that the molecules are homodimers prior to assembly. This result suggests that *Arabidopsis* FtsZ can dimerize in the absence of added GTP as was shown for bacterial FtsZ (188,189). A smaller peak (approximately 3 kDa) was present in both chromatographs and most likely represents residual imidazol carried over from previous purification steps (Figs. 3.1 and 3.2). The ~78 kDa and ~80 kDa proteins were each spread over two fractions and both were kept for analysis. The smaller peak fractions were adsorbed to carbon-coated grids, negatively stained using an aqueous solution of 2% (w/v) uranyl acetate (pH4.5) and observed using TEM. No apparent protein densities similar to those observed in FtsZ reactions were present. In order to determine if protein subjected to chromatography remained biologically active, fractions representing the 78 kDa and 80 kDa proteins were used in assembly reactions in the presence of GTP and/or GDP. Both types of filaments were present in these reactions suggesting the proteins remained active following chromatography. This allowed for examination of precursor molecules beyond those found in the unassembled state. Experiments with the dimeric FtsZ1 and FtsZ2 fractions under non-assembly conditions and in the absence of nucleotides did not yield filaments as judged by TEM over a wide range of concentrations (from 25 - 500 µg/ml FtsZ).

Native gel electrophoresis was used as an independent method to confirm the oligomeric state of unassembled FtsZ proteins. The basic native PAGE gel displayed one prominent broad band. The median of this band corresponds to approximately 80 kDa which is in agreement with the major peak from the gel chromatograph (Fig. 3.3). An alternative interpretation could be that the broadness of the band harbors two density maxima corresponding to two masses, one at slightly higher and the other at slightly lower mobility. This difference could originate from two protein populations that are of similar mass but exhibit differences in electrophoretic mobility. Such differences are due to variations in the charge to mass ratio regimes as conferred by e.g. configurational changes. No contaminating bands were observed except for a high molecular weight band that most likely represents the filamentous assemblies previously seen using EM (Fig 2.4). Taken together, these results suggest that FtsZ1and FtsZ2 are homodimers prior to assembly and are the building blocks used in FtsZ assembly. However, the possibility of formation of heterodimers (FtsZ1 and FtsZ2) can not be excluded at this time.

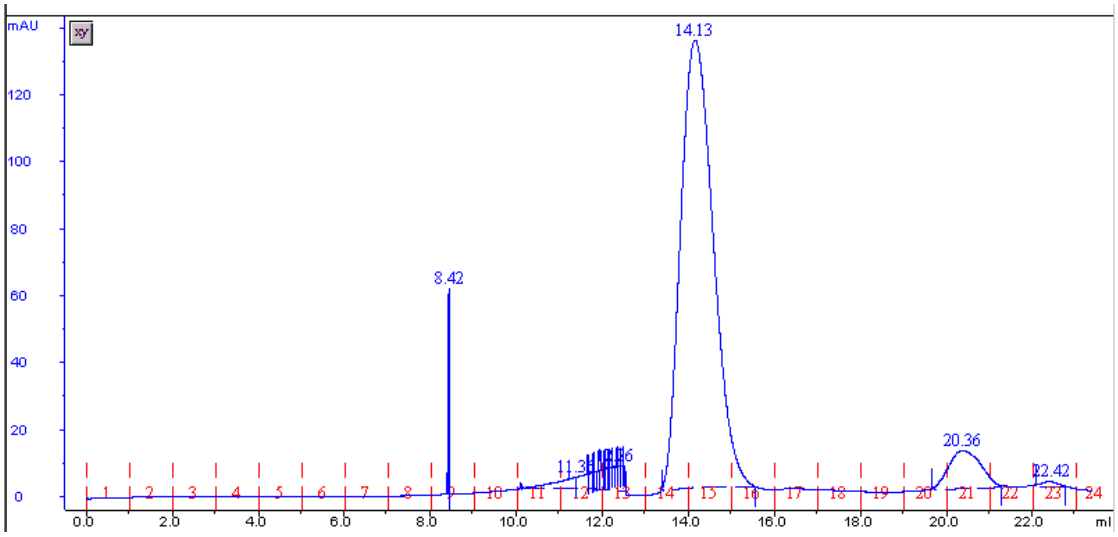

Figure 3.1. Gel filtration chromatography of nucleotide-free FtsZ1. Elution profile of FtsZ1. The mobility of the front (right) peak corresponds to ~2.7 kDa, the rear (left) peak is estimated as ~79 kDa, using molecular mass standards (Bio-Rad).

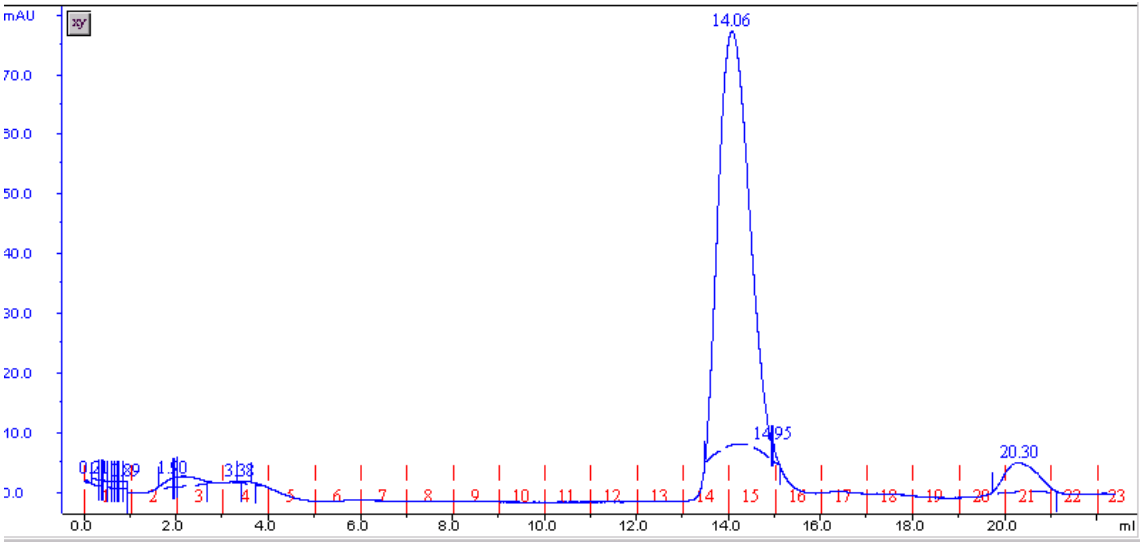

Figure 3.2. Gel filtration chromatography of nucleotide-free FtsZ2. Elution profile of FtsZ2. The mobility of the front (right) peak corresponds to ~2.7 kDa, the rear (left) peak is estimated as ~81 kDa, using molecular mass standards (Bio-Rad).

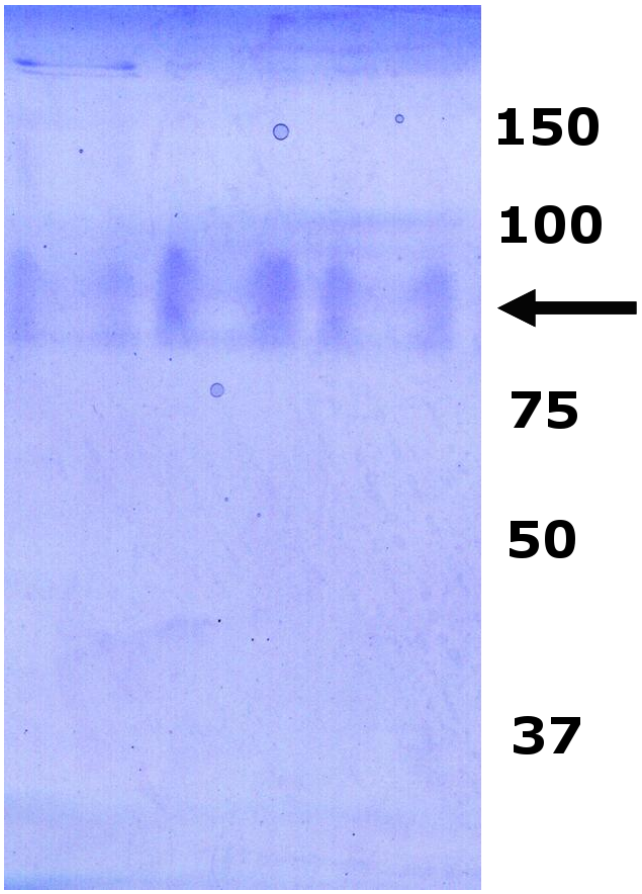

Figure 3.3. Basic native PAGE of FtsZ proteins. Native gel showing single bands for FtsZ1 (left lane) and FtsZ2 (middle and right lanes) at approximately 80 kDa (arrow) which corresponds to a dimer. Molecular weight marker positions are given in kDa.

3.2.2 FtsZ under non-assembly conditions has C2 symmetry

Following purification and Superdex-200 column work, the relevant fractions were adsorbed to grids, negatively stained with 2% (w/v) uranyl acetate and micrographs were recorded on a JEOL 1200X electron microscope with an optically coupled 3k slowscan Charge-Coupled Device (CCD) camera. Image quality was evaluated using the FFT

algorithm in the CRISP software (132). Those micrographs exhibiting no drift or astigmatism and of similarly suitable defocus (i.e. close to Scherzer focus) were selected to be used for particle selection using the Boxer program included in the EMAN software package (123). Boxer allows the user to manually or semi-automatically select the desired particles for reconstruction. The semi-automatic routine was used with the data sets presented in this report as this method lead to a larger and more diverse data set and eliminated the possibility of user bias. Smaller data sets that were picked manually were also used for reconstruction and gave similar final reconstructions but at lower resolutions (~30-35 Å) as compared to the reconstructions presented below.

Following particle selection, all data were normalized and low-pass filtered within the framework of EMAN (Fig. 3.4 top panel). The data set was aligned by reference-free alignment into class averages (Fig. 3.4 middle panel) (190). Initial reconstructions were created using a subset of class averages without imposed symmetry. Iterative refinement was carried out until no further increase of resolution was observed. Examination of the back-projections used to create the final reconstructions revealed that these projections showed features that agreed with those present in the class averages (Fig. 3.4 bottom panel).

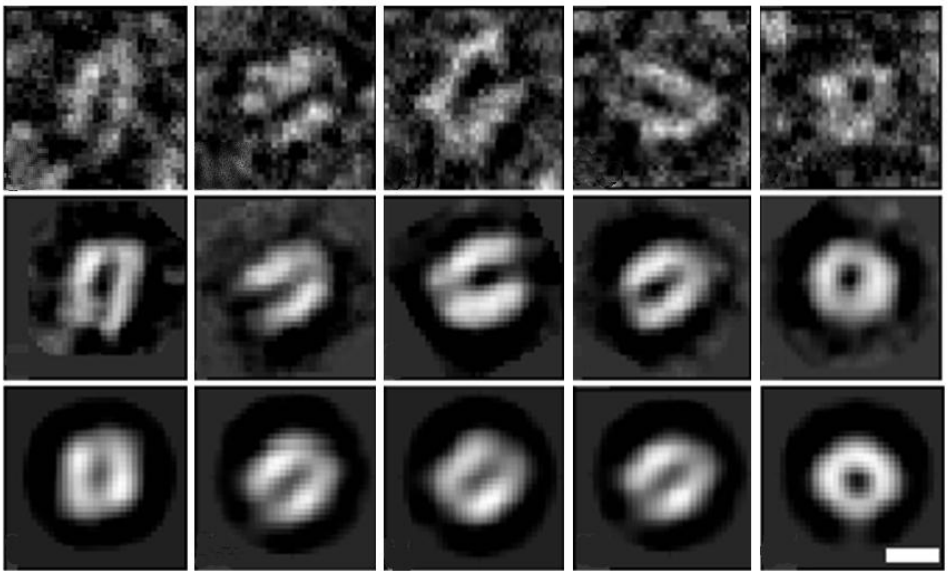

Figure 3.4. Image analysis of the FtsZ1 unassembled particles. Top row: raw particles. Middle row: representative class averages harboring the raw particles presented in the top row as members. Bottom row: back-projections from the final 3-D reconstruction. Scale bar corresponds to 10 nm.

The validity of three-dimensional reconstructions can be qualitatively determined by several methods. Asymmetric triangles are useful in determining whether a sufficient number of views are present during reconstruction with each point of the triangle representing an orthogonal view. The asymmetric triangle presented here demonstrates that many views of the particle are reflected in the reconstruction and that the three-dimensional space has been well sampled (Fig. 3.5A). FSC curves help determine whether reconstructions converge and provide an approximate resolution. Similar FSC curves between iterations are a mark of convergence. The curves for eight iterations of unassembled FtsZ1 are shown in Figure 3.5B. Similar results were generated using the FtsZ2 reconstruction (data not shown).

The reconstruction after the eighth iterative round of refinement displayed two gourd-shaped structures with a wide gap between the structures at the base (Fig. 3.6). Volume measurements estimate the molecular mass of the reconstruction at approximately 85 kDa as shown. Resolution for the final reconstruction is approximately 26 Å. The point where the monomers contact each other is likely to contain the FtsZ self-interaction domain. Separate studies using *E. coli* FtsZ suggest that the self-interaction domain is contained between amino acid residues 175 to 323 (156) or residues 100 to 326 (191). This region is well conserved between bacteria and *Arabidopsis* FtsZ. This seems to support the idea that *Arabidopsis* FtsZ would be able to dimerize in the absence of nucleotide binding as shown for bacterial FtsZ (161,186). It should be noted that the tubulin signature motif, essential for nucleotide binding, is located upstream of the region described by Di Lallo and colleagues (156). A report utilizing *Staphylococcus aureus* FtsZ showed that a nine amino acid region (residues 202 to 210) of FtsZ and a single residue, L270, are necessary for self-interaction (192). Three amino acids are conserved in both *Arabidopsis* FtsZ families in the 202 to 210 region and are also conserved in *E. coli* FtsZ (Fig. 3.7) and the L270 residue is conserved in FtsZ2 but not FtsZ1. Future experiments employing mutational analysis of these regions/residues coupled with gel chromatography to determine the oligomeric state of the mutants will allow identification of the critical residues in *Arabidopsis*. All together, these results further suggest that homodimers are a building block of the FtsZ filament assembly mechanism in GTP containing environments.

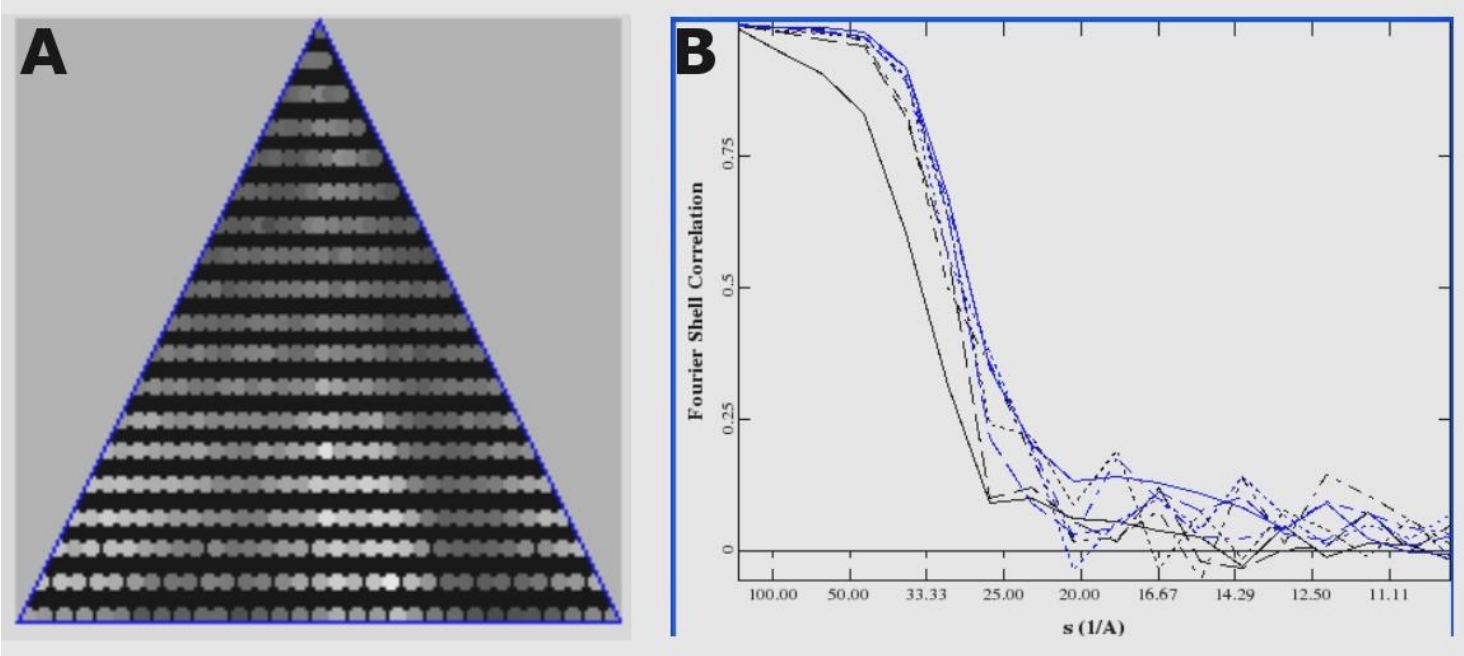

Figure 3.5. Asymmetric triangle and FSC curves for FtsZ1 unassembled particles. (A) Asymmetric triangle from the final round of refinement, (B) FSC curves for eight iterative cycles. Estimated resolution for the final reconstruction is approximately 26 Å.

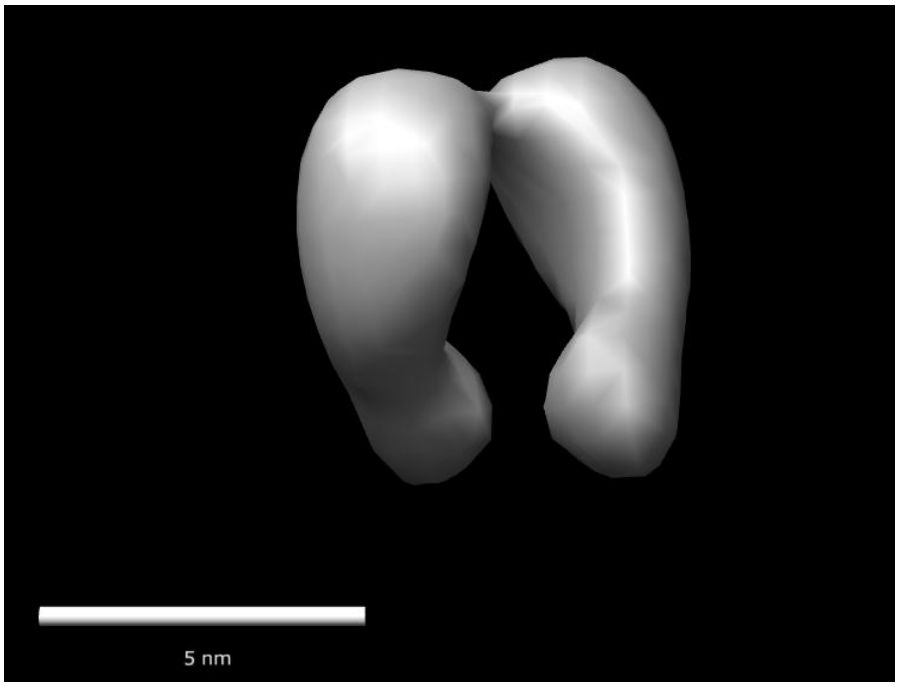

Figure 3.6. FtsZ1 unassembled reconstruction. Rendering of the final three dimensional reconstruction with C2 symmetry imposed.

Arabidopsis thaliana FtsZ2
QGVRGISDIITIPGLVNVDFADVRAIMANAGSSLMGIGTATGKSRARDAALNAIQSPLLD 360

Arabidopsis *thaliana* FtsZ1
QGVQGISDIITIPGLVNVDFADVKAVMKDSGTAMLGVGVSSSKNRAEEAAEQATLAPLIG 313

E. coli FtsZ
GAVQGIAELITRPGLMNVDFADVRTVMSEMGYAMMGSGVASGEDRAEEAAEMAISSPLLE 250

Staphylococcus aureus FtsZ
QGVQGISDLIAVSGEVNLDFADVKTIMSNQGSALMGIGVSSGENRAVEAAKKAISSPLLE 251

Figure 3.7. Alignment of region identified as necessary for FtsZ self-interaction in *S. aureus*. Residues 202-210 were reported to be necessary for self-interaction and are highlighted in red. Three conserved residues in this region in *E. coli* and *Arabidopsis* FtsZ are highlighted in blue.

3.2.3 The most abundant FtsZ assembly precursor molecule is a tetramer

FtsZ1 and FtsZ2 assembly reactions were conducted as described above, adsorbed onto carbon-coated grids and processed with EMAN as described for the FtsZ unassembled particles. Native PAGE of assembly reactions revealed that there are intermediate oligomeric forms between the homodimer and assembled filaments. In addition to the high molecular weight band seen in the native PAGE gel, at least two additional oligomeric forms were observed (Fig 3.8). It is unclear if the additional band is a true intermediate or a degradation product. Analysis of the most frequently occurring intermediate is described in this section. Initial reconstructions were created using a subset of class averages without imposed symmetry and from the raw data set with C4 symmetry imposed (Fig. 3.9 top and middle panels) and back projections used in the final reconstruction were contained in the class averages (Fig. 3.9 bottom panel). Iterative refinement was carried out separately with each initial reconstruction yielding similar results. The results of a refinement using imposed symmetry are reflected in the asymmetric triangle (Fig. 3.10A) and FSC curves for eight iterations of refinement (Fig. 3.10B). No further gain in resolution was observed using additional iterative cycles.

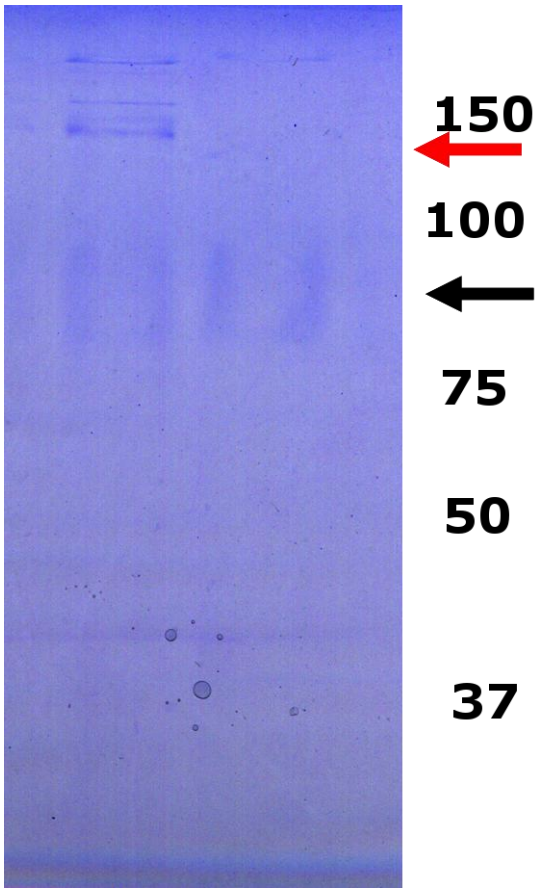

Figure 3.8 Native gel of assembly reaction. Left lane shows assembly reaction in the presence of GTP and 2 µl 2% (w/v) ammonium molybdate as a stabilizing agent and the presence of additional oligomeric intermediates. Right lane shows bands for an assembly reaction without stabilizing agent and no additional intermediates are observed. Molecular weight marker positions are given in kDa. The black arrow corresponds to 75 kDa and the red arrow to 150 kDa.

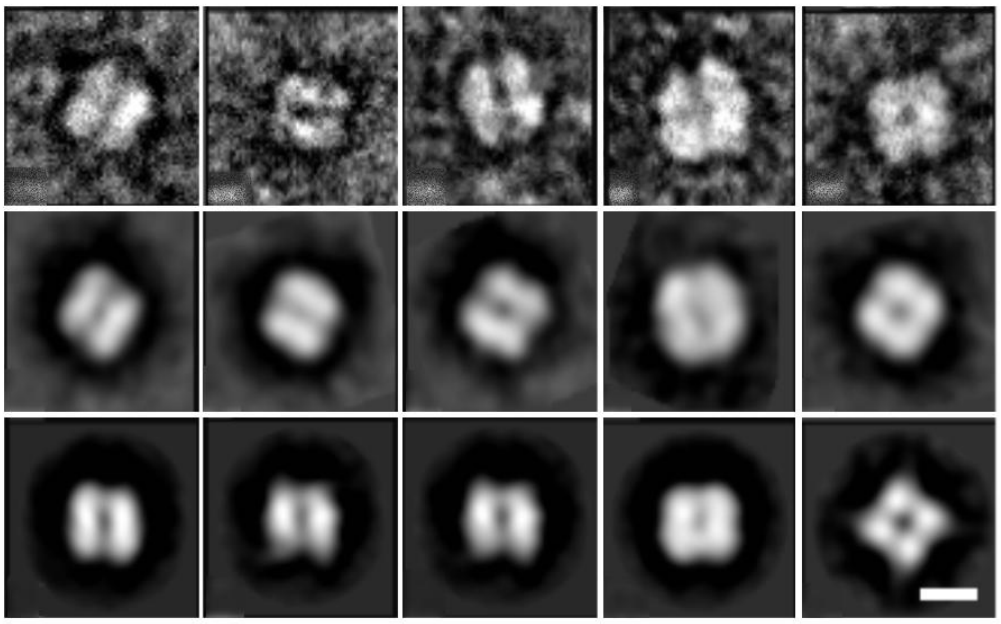

Figure 3.9. Image analysis of the FtsZ1 assembly particles. Top row: raw particles. Middle row: representative class averages harboring the raw particles presented in the top row as members. Bottom row: back-projections from the final three dimensional reconstruction. Scale bar corresponds to 10 nm.

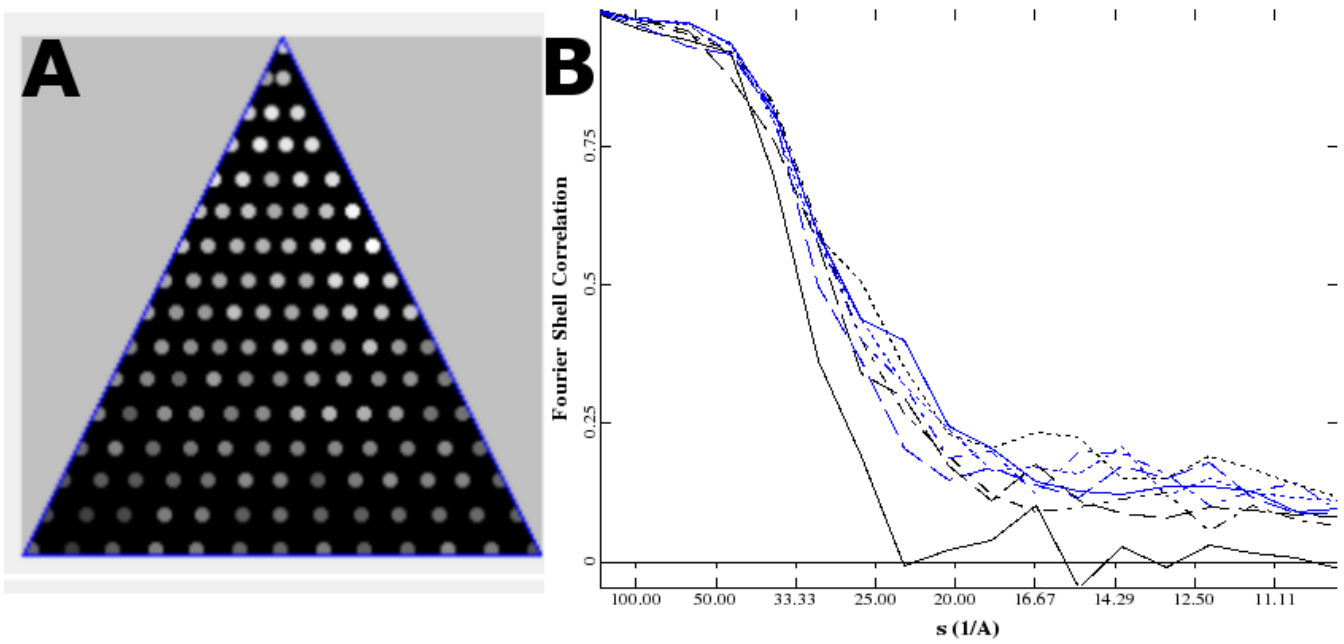

Figure 3.10. Asymmetric triangle and FSC curves for FtsZ1 assembly particle. (A) Asymmetric triangle from the final round of refinement, (B) FSC curves for eight iterative cycles. Estimated resolution for the final reconstruction is approximately 30Å.

The final three-dimensional reconstruction has C4 symmetry imposed and dimensions of approximately 12x12x12 nm with a significant protein deficit of ~5nm across the base of the structure (Fig. 3.11). Four protomers are connected at the base and the protein density is contiguous at the base. Each protomer extends from the base approximately 6 nm and measures 4 nm across. The reconstruction presented here is estimated to be 175 kDa suggesting that the molecule is a tetramer. Reconstructions imposing D4 symmetry, which would produce an octamer, did not produce back-projections consistent with the class averages. An octamer could therefore be excluded as the most prevalent assembly intermediate.

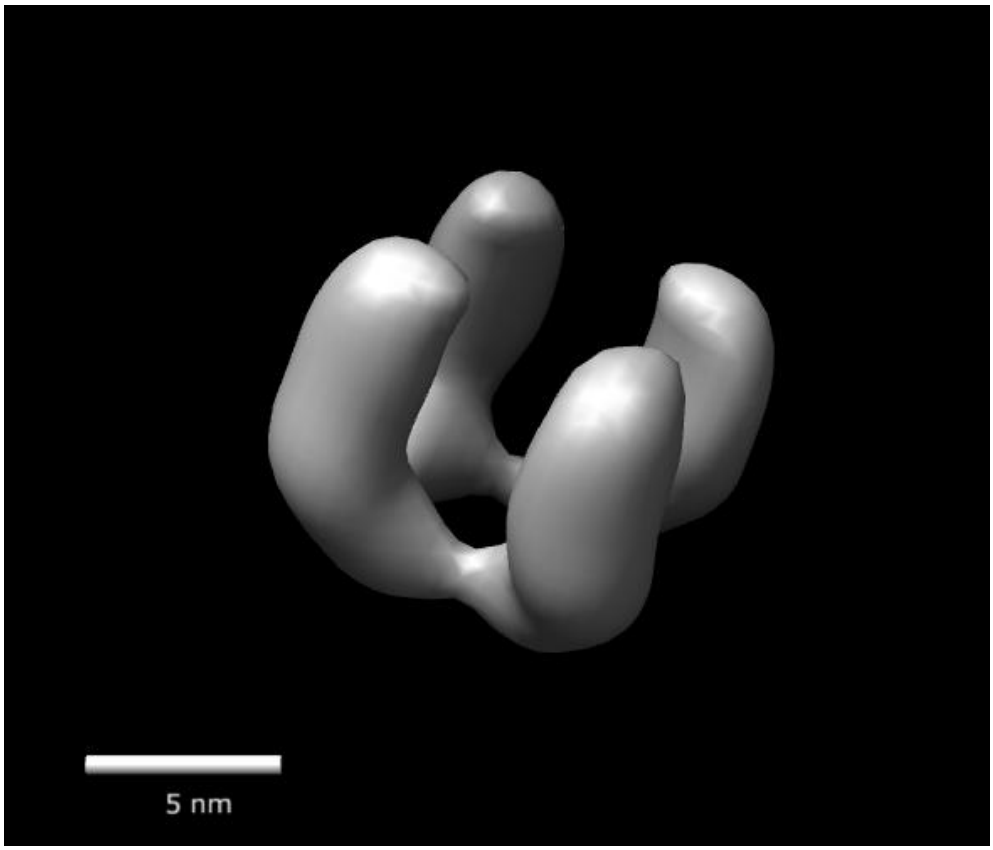

Figure 3.11. FtsZ1 assembly intermediate reconstruction. Rendering of the final three dimensional reconstruction with C4 symmetry imposed.

3.3 DISCUSSION

3.3.1 The dimer and tetramer intermediates may represent consecutive steps in the assembly mechanism

The current literature and our own experiments suggest that a stromal FtsZ pool is present, but the results presented here are the first to examine the composition of the soluble FtsZ pool. These experiments investigated the oligomeric state of *Arabidopsis* FtsZ prior to assembly events and following initiation of the assembly events. Native gel electrophoresis and gel chromatography results demonstrate that the smallest identifiable building block of FtsZ assembly is a dimer and native gel and image analysis suggest that a tetramer is present under GTP assembly conditions. Additional oligomeric states were not detected in the data sets used for the reconstructions presented here. However, particles that possess dimensions consist with monomeric FtsZ particles were detected in assembly reactions using GDP. Gel chromatography studies with GDP assembly reaction intermediates will be useful in determining if these particles are FtsZ monomers. Under GTP assembly conditions, image processing with the EMAN software revealed tetramers to be the most abundant species in FtsZ assembly reactions. This raises the questions as to whether the dimer and tetramer are consecutive steps in the assembly pathway and what is the ultimate fate of the tetramer during filament assembly.

It is noteworthy that in none of the GTP containing *in vitro* assembly reactions has monomeric FtsZ been detected by EM, native PAGE or gel permeation

chromatography. This is in stark contrast to bacterial FtsZ, for which a monomeric population was reported *in vitro* (193) based on sedimentation equilibrium centrifugation. Those authors also propose the linear assembly of monomers into 4.3 nm wide single-stranded filaments. The absence of a distinct population of FtsZ monomers could be due to a pronounced instability. It has, for instance, been argued that the simple association of two identical monomeric protein molecules into a dimer confers thermodynamic benefits, i.e. freedom for rotational motion and mutual vibration of the monomers in the dimer in conjunction with a possible gain in entropy ($\Delta S_{solvent}$) (based on the loss of protein surface area available for binding water molecules) and a decrease in binding enthalpy (ΔH) (194-196). In a similar vein, forming a larger ordered assembly would offer the same or even more pronounced overall negative free energy (ΔG) values. Following on from this, it is conceivable that the monomeric pool undergoes prompt self-assembly into protofilaments and filaments. If this were true, one would expect to see filaments that exhibit inter-profilament spacings in the order of 4 nm based on the findings published for bacterial FtsZ. Upon closer inspection of FtsZ type-I filaments (see Fig. 2.10 left panel), which appear overall void of finer structural details, striations occurring at 4-nm periodicities have been noted. It is plausible that type-I filaments consists of protofilament bundles and that each protofilament resulted from a linear self-association starting with the formation of head-to-tail dimers in which there is significant overlap between the monomeric units (Fig. 3.12). However, the results in the

presence of GTP demonstrate that type-II filaments are favored in the assembly reactions (Table 2.2) implying that head-to-tail dimers would be the less prevalent dimeric form in the population and that head-to-head, arc-shaped dimers (see below) are the driving force behind type-II filament formation, i.e. dimers that do not assemble into protofilaments. The head-to-head dimers (lateral association) are distinct from the head-to-tail dimers (longitudinal association) and do not engage in dovetailing along the 6-nm axis as demonstrated by the given reconstruction (Fig. 3.6). Through this different association, the head-to-head dimers would have less solvent-accessible surface area available for interaction. It is interesting to note that with bacterial FtsZ the same two types of dimers have been observed albeit in different species, head-to-tail dimers in M*ethanococcus jannaschii* (197) and arc-shaped head-to-head dimers in *Mycobacterium tuberculosis* (198). Under assembly conditions, the head-to-head dimer should be considered a first intermediate *en route* to type-II filament formation with a second intermediate being likely a tetramer. To this end, it was noted that a significant number of FtsZ molecules occurred in a tetrameric state under GTP assembly conditions. However, as equilibrium concentrations are lower for tetramers than for dimers (199) a dichotomic fate may be expected: tetramers could either revert to dimers or proceed to a higher order assembly. Electron microscopic characterization of the tetramer led to the calculation of a three- dimensional structure (Fig. 3.11). In this structure, the four protomers extending from the base form a square when viewed face-on projecting down

towards the base. In this projection, the center-to-center distance between the protomers measures 5.7 nm. This value agrees well with the calculated subunit separation in type-II filaments. In addition, one can discern the tetrameric footprint within the sub-filament units (Fig. 2.11D) which means that it is possible that tetramers are indeed assembled into type-II filaments. The model for FtsZ assembly described above follow the two-state model reaction proposed by Neet and Timm who suggest that stable monomers do not exist in significant concentrations at equilibrium (Fig. 3.12) (196,200).

The experiments described here investigated FtsZ1 and FtsZ2 assembly separately though the proteins are known to colocalize in FtsZ rings *in vivo* (23). The results demonstrate that both FtsZ1 and FtsZ2 form homodimers prior to assembly events though it remains unknown if heterodimers can be formed and used for filament incorporation. The possibility that a mixture of homodimers and heterodimers may be necessary to assemble the filaments observed in the assembly experiments cannot be excluded. A clearer picture of the incorporation of the precursor molecules into filaments may be revealed following filament reconstruction and further work with GDP and GTP analogs.

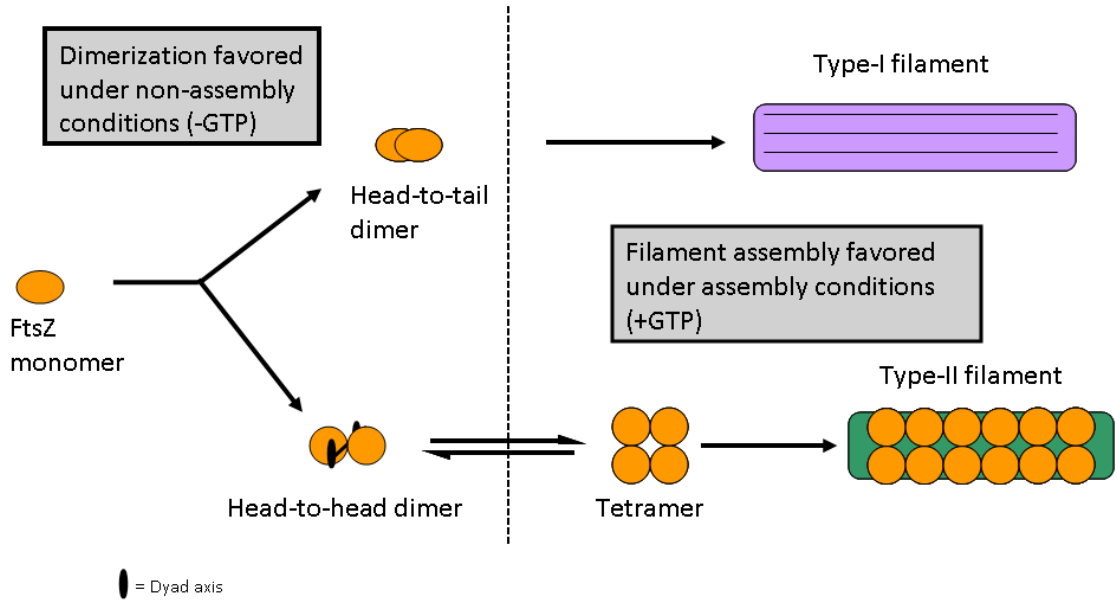

Figure 3.12. Proposed two-state FtsZ assembly mechanism in a GTP environment. Schematic representation of the proposed two-state FtsZ assembly mechanisms. The FtsZ monomer assembles into dimers that are packed differently for each filament type. The type-I filaments are assembled as a result of dimers that slightly overlap each other and type-II filaments are exclusively assembled from tetramers.

3.3.2 Implications for the model of chloroplast division

Bacterial FtsZ dynamic exchange between the Z-ring and the soluble cytoplasmic pool involves monomers (109,193). Disassembly of the bacterial filaments is not dependent on GTP-hydrolysis, but the rate of disassembly is enhanced with hydrolysis (201). One aim of this research is to determine if these models could be applied to plastid division. However, no monomers were detected in our experiments using GTP. It is currently unclear which oligomeric form(s) would participate in the dynamic exchange in chloroplasts.

An updated model of FtsZ assembly postulates that assembly of protofilaments using molecules from the stromal FtsZ pool is driven by GTP binding and enhanced by GTP hydrolysis. Chloroplast division is initiated by formation of a Z-ring from the protofilaments. Prior research has suggested that chloroplast division is most likely powered by ARC5 (dynamin-like) as mutants have led to initiation but incomplete chloroplast constriction (67,202,203). PDV1 also has a role at the division site and PDV1 in conjunction with PDV2 recruits ARC5 to the division site late in constriction.

3.3.3 Accessory proteins ARC3 and ARC6 may regulate relative rates of FtsZ assembly

Plants and algae encode two conserved FtsZ families, FtsZ1 and FtsZ2, which arose by gene duplication after the cyanobacterial endosymbiosis (72,204) and are both required for normal plastid division (71,120,205). FtsZ2 closely resembles its cyanobacterial ancestor, while FtsZ1 lost a conserved C-terminal core domain (97,204,206) known to mediate interactions with proteins involved in Z-ring stabilization and tethering to the membrane in both prokaryotes (FtsA,(98)) and plants (ARC6, (207)). The loss of this domain may play a role in FtsZ assembly and the relative rate of assembly between the two FtsZ families.

Previous data has shown that both FtsZ1 and FtsZ2 assembly reactions promote the same types of filament formation (90). Subsequent work demonstrated filaments with different morphologies but also report that FtsZ1 and FtsZ2 were each capable of assembling into similar filaments (91). Given this data it is not surprising that both proteins have similar assembly mechanisms. This work does not address the relative

amounts of FtsZ1 and FtsZ2 being incorporated into the filaments. However, FtsZ1 has been shown to interact with a destabilizing factor ARC3 (36) and due to a lack of the C-terminal core domain (97,116,206) does not interact with the Z-ring stabilizing factor ARC6 (70). This suggests that ARC3 may play a role in reducing the efficiency of FtsZ1 assembly *in vivo* which is in line with the observed 1:2 FtsZ1/FtsZ2 ratio present in *Arabidopsis* chloroplasts (117). A line of experiments to test this hypothesis are described in chapter IV. Additionally, *in vivo* experiments in our laboratory that aim to elucidate the relative amounts of FtsZ in assembled filaments is underway.

3.4 EXPERIMENTAL PROCEDURES

3.4.1 Plasmid constructs and protein purification

Pichia pastoris X-33 strains expressing *At*FtsZ1 or *At*FtsZ2 with C-terminal c-myc and 6x His tags were grown and cell lysates prepared using 0.5 μm glass beads as described in section 2.4.2. Lysates were poured over a 10-ml Ni-NTA column to selectively purify the tagged protein and eluted with 250 mM imidazole. Collected fractions were subjected to SDS-PAGE and Western blotting to identify pure aliquots for assembly reactions. When homogenous populations were desired, purified protein was subjected to a Superdex-200 column.

3.4.2 FtsZ assembly reactions and electron microscopy

Assembly reactions were carried out with 0.6 mg of protein and MEMK (184) assembly buffer in a GTP containing environment. Samples were placed on ice for 10 min followed by 10 min at 37°C. Samples were adsorbed onto carbon-coated formvar grids for up to 5 minutes and negatively stained with 2% (w/v) uranyl acetate. Specimens were

observed on a Jeol 1200 EX TEM operated at 100 kv. Images were captured using an optically coupled 3k slow scan CCD camera (SIA, Duluth, GA model 15C) and Maxim DL imaging software.

3.4.3 Image processing

Images were processed with CRISP to evaluate initial image quality (132). Suitable micrographs (absence of drift, astigmatism, etc.) were further processed within the framework of the EMAN software package (123). Images of selected particles were bandpass-filtered and aligned by reference-free alignment (190). Classes of particles representing identical orientations were determined by multivariate statistical analysis and hierarchical ascendant classification using complete linkage. Resolution was assessed by using the standard Fourier shell correlation (FSC) criterion (135,136). The angular refinement process was stopped when no further increase of resolution was observed. The three dimensional reconstructions were visualized and manipulated using the Chimera software packages (208).

3.4.4 Native gel electrophoresis

Discontinuous native gel electrophoresis was carried out according to a protocol developed at the Wolfson Centre for Applied Structural Biology at The Hebrew University of Jerusalem (http://wolfson.huji.ac.il/). Basic-native gels were run in buffer containing 0.38M Glycine, 0.05M Trizma and pH adjusted to 8.9. Loading buffer consisted of two parts 100% glycerol (v/v), one part 0.5M Tris-HCl pH 6.8 (v/v), one part dH_2O (v/v) and trace amounts of bromophenol blue. In some cases 2 ul of 2% ammonium molybdate (w/v) (pH 7.0) was added following assembly reactions to

stabilize intermediates. Ten percent resolving and four percent separating gels were cast and FtsZ protein was loaded into the wells. Gels were initially ran at 50 V and increased to 100 V after protein entered the resolving gel. Staining used 50% (v/v) Methanol, 40% (v/v) dH_2O, 10% (v/v) acetic acid and 0.25% (w/v) Coomassie Brilliant Blue R and gels were shaken in stain for ~1 h-overnight. Destaining solution consisted of 15% Methanol (v/v), 10% acetic acid (v/v) and 75% dH_2O (v/v) and was carried out with several changes until bands were readily visible.

CHAPTER IV

CONCLUSIONS AND FUTURE DIRECTIONS

4.1 CONCLUSIONS AND IMPACT ON FIELD

The research described here allows for several contributions to the literature in the field of plastid division and advancements in blotting that is applicable to multiple fields of research. Prior to this work, a report had expressed FtsZ1 and FtsZ2 from *Nicotiana tabacum* in an *E. coli* system and did not characterize the biochemical parameters apart from demonstrating self-assembly for FtsZ1 (122). Protocols allowing expression and purification of *Arabidopsis* FtsZ in a eukaryotic system were developed during this project (90). Using protein purified from these strains, our laboratory provided evidence of FtsZ1 and FtsZ2 self-assembly which is in contrast to the earlier report. A later report using *Arabidopsis* FtsZ expressed in *E. coli* demonstrated self-assembly in FtsZ1 and FtsZ2 albeit with different morphologies (91). Our results also provide evidence of different GTPase activities for each family, a critical concentration for FtsZ co-assembly and FtsZ assembly efficiencies. Unpublished observations indicate that filaments are promoted in the presence of GDP and a similar result was reported in Olson *et al*. (91).

Chapter III describes research that examines structure-function relationships at a molecular level. The composition of the stromal soluble pool of *Arabidopsis* FtsZ that undergoes dynamic exchange had not been investigated previously. Image processing software and gel chromatography were useful in providing the first data relating to oligomeric states of the soluble FtsZ pool that is incorporated into FtsZ assemblies. This

line of research will be expanded in the future to include the effect of accessory proteins (e.g. ARC3) on FtsZ assembly. Further assembly experiments using GTP analogs and GDP will be conducted and their effects on the oligomeric state of the intermediates investigated.

CMWA protocols developed in our laboratory and previously published hold the potential to be applied to techniques that are useful in several fields of research (140). The microwave steps included do not introduce additional reagents and allow for identical chemistry to conventional protocols. Our publications have outlined protocols for Western blotting, dot blotting and ELISA (140). Other laboratories have developed protocols for diverse applications such as decalcification of bone (209), resin polymerization for electron microscopy (151) and antibody labeling of fixed biological tissue (152).

4.2 DETERMINATION OF FTSZ ACCESSORY PROTEIN EFFECTS ON THE ASSEMBLY PATHWAY

The FtsZ families in *Arabidopsis* each have an accessory protein that specifically binds only one of the families. ARC3, a factor shown to perform some functions similar to MinC in bacteria and has destabilizing effects regarding FtsZ assembly (36), binds to FtsZ1. An additional interaction occurs between ARC3 and PARC6 that may affect FtsZ1. A stabilizing factor, ARC6, binds to FtsZ2 in addition to tethering the FtsZ ring to the membrane. Whether these interactions also play a role in regulating the efficiency of the FtsZ assembly pathway is currently not understood.

A direct way to test the effects of these accessory proteins involves expressing each accessory protein *in vitro* using the *Pichia pastoris* expression system described or another suitable system. Once purified, these proteins will be used in assembly reactions harboring different combinations of proteins. For example, (i) FtsZ1 and ARC3, (ii) FtsZ1, ARC3 and PARC6, and (iii) FtsZ2 and ARC6 are combinations that could potentially provide valuable information. These reactions would be monitored by TEM to determine if novel assemblies are promoted and by dynamic light scattering to obtain the relative rates of polymerization.

Controls for these experiments will include using combinations of proteins that are known to not interact *in vivo* such as (i) ARC3 and FtsZ2, (ii) ARC6 and FtsZ1, (iii) PARC6 and FtsZ2, etc. The relative rates of FtsZ assembly and assembly morphology are not expected to significantly change from wild-type rates under these conditions. This line of experimentation also allows the possibility of reconstructing the accessory proteins in a similar manner to the process outlined above or using cryo-EM to obtain higher resolution structures. The results from this line of inquires may provide valuable information on the relative effects of the accessory proteins on FtsZ assembly which would allow a more detailed model than the current hypothesis presented in the literature.

4.3 MUTATIONAL ANALYSIS OF FTSZ ACCESSORY PROTEIN BINDING DOMAINS

The availability of an *in vitro* expression system allows inquiries into the structure and function of *Arabidopsis* FtsZ by mutagenesis after taking into consideration that several

important residues or regions in plant and bacterial FtsZ have been identified (71,100,164,210,211). The report by Yoder *et al.* focused on *Arabidopsis* FtsZ1 plastid division mutants and observed defects in chloroplast division ranging from a severe phenotype, G267R, with 1 chloroplast per cell to a mutant (G366A) with 23 chloroplasts per cell as opposed to 55 chloroplasts per cell in the wild-type (71). Bacterial studies revealed relevant mutations that decrease GTPase activity (164) and affect cell division frequency, placement and morphology (211).

Several of the published mutants are single or a few residue changes and a commercially available kit such as Quickchange (Stratagene) may be a valuable tool for rapidly constructing these mutants in our laboratory. Larger changes such as domain truncations will most likely require mutagenesis by PCR using the original FtsZ constructs as templates. Aside from plastid division mutants, other relevant FtsZ regions including the C-terminal core domain of FtsZ2 will be probed for functional consequences. For example, a recent report used point mutations in *Methanococcus jannaschii* FtsZ to produce a set of mutants that had phenotypes such as increased GTPase activity, reduced assembly and stabilized assembly (212). Protein sequence alignments reveal that eight of these point mutants are conserved in either FtsZ1 or FtsZ2. The relevant residues will be mutated to alanine for these experiments and their effect on assembly of type-I or -II filaments, the distribution of filament types or the occurrence of assemblies not yet observed will be monitored by TEM and rates of assembly analyzed by dynamic light scattering. Mutant proteins will be purified as described above and analyzed for their assembly pathway and intermediates. Particularly

interesting mutants will serve as candidates for three-dimensional reconstruction to compare to the wild-type structure.

4.4 RECONSTITUTION OF FTSZ ASSEMBLY IN LIPOSOMES

Recent reports have characterized the FtsZ tethering mechanism in bacteria identifying FtsA as the major *in vivo* membrane-tether (213). With *Arabidopsis thaliana,* ARC 6 is proposed to act as the envelope anchor (68) and reconstitution experiments using different combinations of FtsZ, ARC and PDV proteins could be used in a liposome environment to examine force generation in a cell-free system. A similar experiment using bacterial cell division machinery has been recently reported (89). These experiments clearly showed Z-ring constriction and relaxation using the liposome environment (Fig. 4.1).

The major players that have been identified to participate in plant ring formation are the proteins FtsZ1, FtsZ2, ARC3, ARC5, ARC6, PARC6, PDV1 and PDV2. The target proteins are thought to organize into a coordinated structure that allows ring constriction. These experiments seek to determine the architecture of the coordinated ring structure, identify the component(s) that generate the force for ring constriction and gather information about the assembly properties of the ARC proteins.

To accomplish these ends, ARC3, ARC5, ARC6, PARC6, PDV1 and PDV2 will be expressed and purified. FtsZ proteins tagged with YFP or CFP will be expressed for this experiment to visualize reconstituted rings. A variant of ARC6 has been expressed that lack the predicted transmembrane domain and will be used to examine the effects of membrane tethering on constriction force generation. A full-length variant of ARC6 was

recently expressed and purified in our lab and shown to be capable of assembly *in vitro* (Fig. 4.2). The initial liposome used will be a mixture of monogalactosyldiacylglycerol (~50%), digalactosyldiacylglycerol (~20%), phosphatidylcholine (~15%), phosphatidylglycerol (10%) and sulfoquinovosyldiacylglycerol (5%) as this mixture corresponds to the approximate lipid conditions found in the *Arabidopsis thaliana* chloroplast envelope (214). A liposome composed of a mixture of 1,2-dioleoyl- *sn* -glycero-3-phospho- *rac* -(1-glycerol) and egg phosphatidylcholine was used for the bacterial reconstitution system and this liposome will be used to determine if the bacterial liposome environment can support the plant chloroplast division machinery.

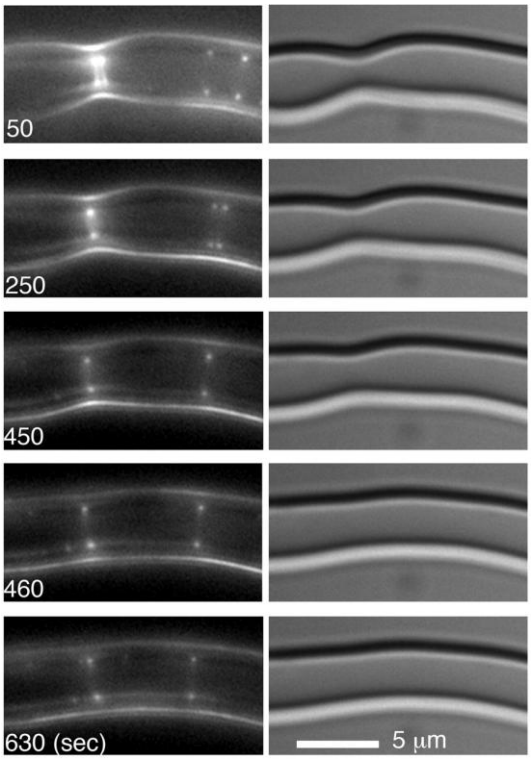

Figure 4.1. A Z ring and its constriction abruptly relaxes. For this preparation, the GTP concentration was 100 mM and should have been exhausted in ~20 min. The first image was obtained ~10 min after mixing liposomes with *E. coli* FtsZ and GTP, and images were taken every 10 s for another 60 min. Elapsed times after the first image are indicated on the frames (89).

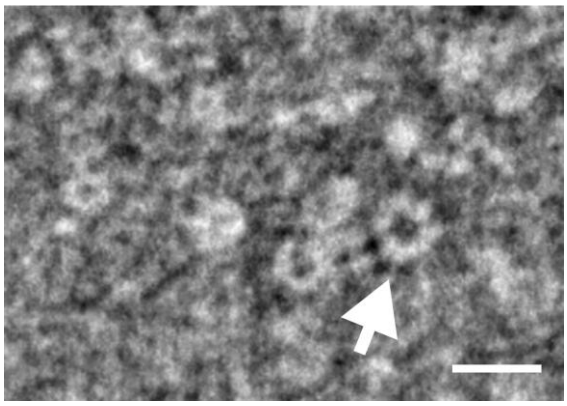

Figure 4.2. Electron micrograph of negatively stained ARC6 molecules. The arrow highlights a single ARC6 particle viewed face-on. Scale bar corresponds to 10 nm.

In the bacterial system, only FtsZ and GTP were needed to generate a ring constriction force and this line of experiments will determine the minimal machinery required to generate this force in *Arabidopsis*. Experiments will be conducted by mixing proteins with the liposomes, placing onto a coverslip and monitoring for liposome constriction at the LM level (Zeiss Axiophot). Experiments will be conducted in several combinations: (i) each FtsZ protein alone, (ii) both FtsZ1 and FtsZ2, (iii) FtsZ proteins with ARC3, PARC6 and ARC6, (iv) FtsZ proteins with ARC3, PARC6, ARC6 and ARC5 (v) FtsZ proteins with ARC3, PARC6, ARC6, ARC5, PDV1 and PDV2. No constriction is expected for experiments using FtsZ proteins in the absence of accessory proteins. These experiments would provide a tool to test the current model of chloroplast constriction presented in the literature.

Currently there are no published reports of ARC3, ARC5, PARC6, ARC6, PDV1 and PDV2 being expressed in an *in vitro* system and biochemical characterization of these proteins would prove beneficial to the FtsZ field. Assembly properties will be

monitored by EM and possible GTPase activity will be determined in a similar method to the FtsZ proteins. ARC5 is a member of the dynamin-related protein family and is expected to have a GTPase activity (67).

REFERENCES

1. Marinos, N. G. (1967) *J Ultrastruct Res* **17**, 91-113
2. McFadden, G. I. (1999) *Current Opinion in Plant Biology* **2**, 513-519
3. Mereschkowsky, C. (1905) *Biol. Centralbl.* **25**, 593-604
4. Austin, J., and Webber, A. N. (2005) *Photosynthesis Research* **85**, 373-384
5. Koniger, M., Delamaide, J. A., Marlow, E. D., and Harris, G. C. (2008) *J Exp Bot* **59**, 2285-2297
6. Yun, M. S., and Kawagoe, Y. (2009) *Plant Cell Physiol* **50**, 1617-1626
7. de Pater, S., Caspers, M., Kottenhagen, M., Meima, H., ter Stege, R., and de Vetten, N. (2006) *Plant Biotechnology Journal* **4**, 123-134
8. Johnson, L. A., Hardy, C. L., Baumel, C. P., Yu, T. H., and Sell, J. L. (2001) *Cereal Foods World* **46**, 472-481
9. Blanchard, P. H. (1992) *Technology of Corn Wet Milling and Associated Processes.*, Elsevier, New York
10. Davis, S. C., and Diegel, S. W. (2004) *Transportation Energy Data Book.* Oak Ridge National Laboratory, Oak Ridge, TN
11. Ramirez, E. C., Johnston, D. B., McAloon, A. J., and Singh, V. (2009) *Biotechnol Biofuels* **2**, 1-9
12. Gallagher, P. W., Brubaker, H., and Shapouri, H. (2005) *Biomass & Bioenergy* **28**, 565-571
13. Wu, Y. V. (1992) *Cereal Chemistry* **69**, 343-347

14. Chandrashekar, A., and Mazhar, H. (1999) *Journal of Cereal Science* **30**, 193-207

15. Bryan, T. (2005) *Ethanol Producer Magazine* **11**, 58-63

16. Singh, V., and Eckhoff, S. R. (1997) *Cereal Chemistry* **74**, 462-466

17. Redei, G. P. (1975) *Annu Rev Genet* **9**, 111-127

18. Meyerowitz, E. M. (2001) *Plant Physiol* **125**, 15-19

19. Pyke, K. A., and Leech, R. M. (1992) *Plant Physiol* **99**, 1005-1008

20. Boyes, D. C., Zayed, A. M., Ascenzi, R., McCaskill, A. J., Hoffman, N. E., Davis, K. R., and Gorlach, J. (2001) *Plant Cell* **13**, 1499-1510

21. Clough, S. J., and Bent, A. F. (1998) *cePlant Journal* **16**, 735-743

22. Erickson, H. P. (1997) *Trends in Cell Biology* **7**, 362-367

23. Vitha, S., McAndrew, R. S., and Osteryoung, K. W. (2001) *Journal of Cell Biology* **153**, 111-119

24. Adams, D. W., and Errington, J. (2009) *Nat Rev Microbiol* **7**, 642-653

25. Margolin, W. (2005) *Nat Rev Mol Cell Biol* **6**, 862-871

26. Machida, M., Takechi, K., Sato, H., Chung, S. J., Kuroiwa, H., Takio, S., Seki, M., Shinozaki, K., Fujita, T., Hasebe, M., and Takano, H. (2006) *PNAS* **103**, 6753-6758

27. Garcia, M., Myouga, F., Takechi, K., Sato, H., Nabeshima, K., Nagata, N., Takio, S., Shinozaki, K., and Takano, H. (2008) *Plant Journal* **53**, 924-934

28. Makarova, K. S., and Koonin, E. V. (2010) *Biol Direct* **5**, 33

29. Bernander, R., and Ettema, T. J. G. (2010) *Current Opinion in Cell Microbiology* **13**, 1-6

30. Scheffers, D. J. (2008) *FEBS Letters* **582**, 2601-2608

31. Adler, H., Fisher, H. I., Cohn, A., and Hardigree, A. A. (1967) *PNAS* **57**, 321-326

32. Shih, Y.-L., Le, T., and Rothfield, L. (2003) *PNAS* **100**, 7865-7870

33. Rothfield, L., Taghbalout, A., and Shih, Y. L. (2005) *Nat Rev Microbiol* **3**, 959-968

34. Nakanishi, H., Suzuki, K., Kabeya, Y., Okazaki, K., and Miyagishima, S. Y. (2009) *Commun Integr Biol* **2**, 400-402

35. Shimada, H., Koizumi, M., Kuroki, K., Mochizuki, M., Fujimoto, H., Ohta, H., Masuda, T., and Takamiya, K.-i. (2004) *Plant Cell Physiol* **45**, 960-967

36. Maple, J., Vojta, L., Soll, J., and Møller, S. G. (2007) *EMBO Reports* **8**, 293-299

37. Glynn, J. M., Miyagishima, S., Yoder, D. W., Osteryoung, K. W., and Vitha, S. (2007) *Traffic* **8**, 451-461

38. Nakanishi, H., Suzuki, K., Kabeya, Y., and Miyagishima, S. (2009) *Current Biology* **19**, 151-156

39. Erickson, H. P. (2001) *Current Opinion in Cell Biology* **13**, 55-60

40. Pichoff, S., and Lutkenhaus, J. (2002) *EMBO J* **21**, 685-693

41. Hale, C. A., and de Boer, P. A. J. (1997) *Cell* **88**, 175-185

42. Hale, C. A., Rhee, A. C., and de Boer, P. A. J. (2000) *J Bacteriol* **182**, 5153-5166

43. RayChaudhuri, D. (1999) *EMBO J* **18**, 2372-2383

44. Geissler, B., Elraheb, D., and Margolin, W. (2003) *PNAS* **100**, 4197-4202

45. Levin, P. A., Kurtser, I. G., and Grossman, A. D. (1999) *PNAS* **96**, 9642-9647

46. Ishikawa, S., Kawai, Y., Hiramatsu, K., Kuwano, M., and Ogasawara, N. (2006) *Mol Microbiol* **60**, 1364-1380

47. Gueiros-Filho, F. J., and Losick, R. (2002) *Genes Dev.* **16**, 2544-2556

48. Ebersbach, G., Galli, E., Moller-Jensen, J., Lowe, J., and Gerdes, K. (2008) *Mol Microbiol* **68**, 720-735

49. Haeusser, D. P., Schwartz, R. L., Smith, A. M., Oates, M. E., and Levin, P. A. (2004) *Mol Microbiol* **52**, 801-814

50. Weart, R. B., Lee, A. H., Chien, A. C., Haeusser, D. P., Hill, N. S., and Levin, P. A. (2007) *Cell* **130**, 335-347

51. Huisman, O., and Dari, R. (1981) *Nature* **290**, 797-799

52. Justice, S. S., Garcia-Lara, J., and Rothfield, L. I. (2000) *Mol Microbiol* **37**, 410-423

53. Bi, E., and Lutkenhaus, J. (1993) *J Bacteriol* **175**, 1118-1125

54. Mukherjee, A., Cao, C., and Lutkenhaus, J. (1998) *PNAS* **95**, 2885-2890

55. Dajkovic, A., Mukherjee, A., and Lutkenhaus, J. (2008) *J Bacteriol* **190**, 2513-2526

56. Handler, A. A., Lim, J. E., and Losick, R. (2008) *Mol Microbiol* **68**, 588-599

57. Maple, J., and Møller, S. G. (2007) *Annals of Botany* **99**, 565-579

58. Maple, J., and Møller, S. G. (2007) *FEBS Letters* **581**, 2162-2167

59. Tveitaskog, A. E., Maple, J., and Moller, S. G. (2007) *J Biol Chem* **388**, 937-942

60. Miyagishima, S., Takahara , M., Mori, T., Kuroiwa, H., Higashiyama, T., and Kuroiwa, T. (2001) *Plant Cell* **13**, 2257-2268

61. Osteryoung, K. W., and Vierling, E. (1995) *Nature* **376**, 473-474

62. Pyke, K. A. (1999) *Plant Cell* **11**, 549-556

63. Pyke, K. A., and Leech, R. M. (1991) *Plant Physiol* **96**, 1193-1195

64. Pyke, K. A., Rutherford, S. M., Robertson, E. J., and Leech, R. M. (1994) *Plant Physiol* **106**, 1169-1177

65. Pyke, K. A., Rutherford, S. M., Robertson, E. J., and Leech, R. M. (1994) *J Cell Sci* **108**, 2937-2944

66. Marrison, J. L., Rutherford, S. M., Robertson, E. J., Lister, C., Dean, C., and Leech, R. M. (1999) *Plant Journal* **18**, 651-662

67. Gao, H., Kadirjan-Kalbach, D., Froehlich, J. E., and Osteryoung, K. W. (2003) *PNAS* **100**, 4328-4333

68. Vitha, S., Froehlich, J. E., Koksharova, O., Pyke, K. A., van Erp, H., and Osteryoung, K. W. (2003) *Plant Cell* **15**, 1918-1933

69. Glynn, J. M., Yang, Y., Vitha, S., Schmitz, A. J., Hemmes, M., Miyagishima, S. Y., and Osteryoung, K. W. (2009) *Plant Journal* **59**, 700-711

70. Glynn, J. M., Froehlich, J. E., and Osteryoung, K. W. (2008) *Plant Cell* **20**, 2460-2470

71. Yoder, D. W., Kadirjan-Kalbach, D., Olson, B. J. S. C., Miyagishima, S. Y., DeBlasio, S. L., Hangarter, R. P., and Osteryoung, K. W. (2007) *Plant and Cell Physiol* **48**, 775-791

72. Stokes, K. D., and Osteryoung, K. W. (2003) *Gene* **320**, 97-108

73. Fujiwara, M. T., Nakamura, A., Itoh, R., Shimada, Y., Yoshida, S., and Moller, S. G. (2004) *J Cell Sci* **117**, 2399-2410

74. Fulgosi, H., Gerdes, L., Westphal, S., Glockmann, C., and Soll, J. (2002) *PNAS* **99**, 11501-11506

75. Wallin, I. E. (1923) *The American Naturalist* **57**, 255-261

76. Kuroiwa, T. (1998) *Bioessays* **20**, 344-354

77. Terui, S., Kuninori, S., Takahashi, H., Itoh, R., and Kuroiwa, T. (1995) *J. Phycol.* **31**, 958-961

78. Eckardt, N. A. (2003) *Plant Cell* **15**, 577-579

79. Schaefer, D., Zryd, J. P., Knight, C. D., and Cove, D. J. (1991) *Molecular & General Genetics* **226**, 418-424

80. Engel, P. P. (1968) *American Journal of Botany* **55**, 438-446

81. Ashton, N. W., and Cove, D. J. (1977) *Molecular & General Genetics* **154**, 87-95

82. Ashton, N. W., Grimsley, N. H., and Cove, D. J. (1979) *Planta* **144**, 427-435

83. Martin, A., Lang, D., Hanke, S. T., Mueller, S. J. X., Sarnighausen, E., Vervliet-Scheebaum, M., and Reski, R. (2009) *Molecular Plant* **2**, 1359-1372

84. Beech, P. L., Nheu, T., Schultz, T., Herbert, S., Lithgow, T., Gilson, P. R., and McFadden, G. I. (2000) *Science* **287**, 1276-1279

85. Takahara, M., Takahashi, H., Matsunaga, S., Miyagishima, S., Takano, S., Sakai, A., Kawano, S., and Kuroiwa, T. (2000) *Mol Gen Genet* **7**, 245-251

86. Gilson, P. R., Yu, X. C., Hereld, D., Barth, C., Savage, A., Kiefel, B. R., Lay, S., Fisher, P. R., Margolin, W., and Beech, P. L. (2003) *Eukaryot Cell* **2**, 1315-1326

87. Lu, C. L., Reedy, M., and Erickson, H. P. (2000) *J Bacteriol* **182**, 164-170

88. Li, Z., Trimble, M. J., Brun, Y. V., and Jensen, G. J. (2007) *EMBO J* **26**, 4694-4708

89. Osawa, M., Anderson, D. E., and Erickson, H. P. (2008) *Science* **320**, 792-794

90. Smith, A. G., Johnson, C. B., Vitha, S., and Holzenburg, A. (2010) *FEBS Letters* **584**, 166-172

91. Olson, B. J., Wang, Q., and Osteryoung, K. W. (2010) *J Biol Chem* **285**, 20634-20643

92. Miyagishima, S., Nishida, K., Mori, T., Matsuzaki, M., Higashiyama, T., Kuroiwa, H., and Kuroiwa, T. (2003) *Plant Cell* **15**, 655-665

93. Hirota, Y., Ryter, A., and Jacob, F. (1968) *Cold Spring Harbor Symposia on Quantitative Biology* **33**, 677-693

94. Löwe, J. (1998) *Journal of Structural Biology* **124**, 235-243

95. Rossman, M. G., Moras, D., and Olsen, K. W. (1974) *Nature* **250**, 194-199

96. de Boer, P., Crossley, R., and Rothfield, L. (1992) *Nature* **359**, 254-256

97. Osteryoung, K. W., and McAndrew, R. S. (2001) *Annu. Rev. Plant Physiol Plant Mol. Biol.* **52**, 315-333

98. Ma, X. L., and Margolin, W. (1999) *J Bacteriol* **181**, 7531-7544

99. Bi, E., and Lutkenhaus, J. (1991) *Nature* **354**, 161-164

100. Oliva, M. A., Huecas, S., Palacios, J. M., Martin-Benito, J., Valpuesta, J. M., and Andreu, J. M. (2003) *J Biol Chem* **278**, 33562-33570

101. Löwe, J., and Amos, L. A. (2000) *Biological Chemistry* **381**, 993-999

102. Erickson, H. P., Taylor, D. W., Taylor, K. A., and Bramhill, D. (1996) *PNAS* **93**, 519-523

103. Srinivasan, R., Mishra, M., Wu, L., Yin, Z., and Balasubramanian, M. K. (2008) *Genes Dev.* **22**, 1741-1746

104. RayChaudhuri, D., and Park, J. T. (1994) *J Biol Chem* **269**, 22941-22944

105. Lu, C., Stricker, J., and Erickson, H. P. (2001) *BMC Microbiology* **1**, 7

106. Margalit, D. N., Romberg, L., Mets, R. B., Hebert, A. M., Mitchison, T. J., Kirschner, M. W., and RayChaudhuri, D. (2004) *PNAS* **101**, 11821-11826

107. Jaiswal, R., Beuria, T. K., Mohan, R., Mahajan, S. K., and Panda, D. (2007) *Biochemistry* **46**, 4211-4220

108. Niu, L., and Yu, J. (2008) *Biophys J* **95**, 2009-2016

109. Stricker, J., Maddox, P., Salmon, E. D., and Erickson, H. P. (2002) *PNAS* **99**, 3171-3175

110. Mingorance, J., Tadros, M., Vicente, M., Gonzalez, J. M., Rivas, G., and Velez, M. (2005) *J Biol Chem* **280**, 20909-20914

111. Osteryoung, K. W., Stokes, K.D., Rutherford, S.M., Percival, A.L., and Lee, W.Y. (1998) *Plant Cell* **10**, 1991-2004

112. Schmitz, A. J., Glynn, J. M., Olson, B. J. S. C., Stokes, K. D., and Osteryoung, K. W. (2009) *Mol. Plant* doi:10.1093/mp/ssp1077

113. Maple, J., Aldridge, C., and Møller, S. G. (2005) *Plant J* **43**, 811-823

114. Osteryoung, K. W., Stokes, K. D., Rutherford, S. M., Percival, A. L., and Lee, W. Y. (1998) *Plant Cell* **10**, 1991-2004

115. McAndrew, R. S., Froehlich, J. E., Vitha, S., Stokes, K. D., and Osteryoung, K. W. (2001) *Plant Physiol* **127**, 1656-1666

116. Miyagishima, S. Y., Nozaki, H., Nishida, K., Matsuzaki, M., and Kuroiwa, T. (2004) *J Mol Evol* **58**, 291-303

117. McAndrew, R. S., Olson, B. J. S. C., Kadirjan-Kalbach, D. K., Chi-Ham, C. L., Vitha, S., Froehlich, J. E., and Osteryoung, K. W. (2008) *Biochemical Journal* **412**, 367-378

118. Rensing, S., Kiessling, J., Reski, R., and Decker, E. (2004) *J Mol Evol* **58**, 154-162

119. Stokes, K. D., McAndrew, R. S., Figueroa, R., Vitha, S., and Osteryoung, K. W. (2000) *Plant Physiol* **124**, 1668-1677

120. Schmitz, A. J., Glynn, J. M., Olson, B. J. S. C., Stokes, K. D., and Osteryoung, K. W. (2009) *Mol. Plant* **2**, 1211-1222

121. Vitha, S., Holzenburg, A., and Osteryoung, K. W. (2005) *Microscopy and Microanalysis* **11 (Suppl 2)**, 1154CD-1155CD

122. El-Kafafi, S., Mukherjee, S., El-Shami, M., Putaux, J. L., Block, M. A., Pignot-Paintrand, I., Lerbs-Mache, S., and Falconet, D. (2005) *Biochemical Journal* **387**, 669-676

123. Ludtke, S. J., Baldwin, P. R., and Chiu, W. (1999) *J Struct Biol* **128**, 82-97

124. Vanheel, M. G. (1979) *Ultramicroscopy* **4**, 117-117

125. van Heel, M., Harauz, G., Orlova, E. V., Schmidt, R., and Schatz, M. (1996) *J Struct Biol* **116**, 17-24

126. Vanheel, M., and Keegstra, W. (1981) *Ultramicroscopy* **7**, 113-130

127. Frank, J., Shimkin, B., and Dowse, H. (1981) *Ultramicroscopy* **6**, 343-357

128. Frank, J., Radermacher, M., Penczek, P., Zhu, J., Li, Y. H., Ladjadj, M., and Leith, A. (1996) *Journal of Structural Biology* **116**, 190-199

129. Ludtke, S. J., Chen, D. H., Song, J. L., Chuang, D. T., and Chiu, W. (2004) *Structure* **12**, 1129-1136

130. Menetret, J. F., Schaletzky, J., Clemons, W. M., Osborne, A. R., Skanland, S. S., Denison, C., Gygi, S. P., Kirkpatrick, D. S., Park, E., Ludtke, S. J., Rapoport, T. A., and Akey, C. W. (2007) *Mol. Cell* **28**, 1083-1092

131. Chen, C., Ko, Y., Delannoy, M., Ludtke, S. J., Chiu, W., and Pedersen, P. L. (2004) *J. Biol. Chem.* **279**, 31761-31768

132. Hovmoller, S. (1992) *Ultramicroscopy* **41**, 121-135

133. Chiu, C. Y., Cary, R. B., Chen, D. J., Peterson, S. R., and Stewart, P. L. (1998) *J. Mol. Biol.* **284**, 1075-1081

134. Thuman-Commike, P. A. (2001) *FEBS Letters* **505**, 199-205

135. Harauz, G., and Vanheel, M. (1986) *Optik* **73**, 146-156

136. Saxton, W. O., and Baumeister, W. (1982) *Journal of Microscopy-Oxford* **127**, 127-138

137. Bottcher, B., Wynne, S. A., and Crowther, R. A. (1997) *Nature* **386**, 88-91

138. Baumeister, W., and Steven, A. C. (2000) *Trends Biochem. Sci.* **25**, 624-631

139. Sun, J., Savva, C. G., Deaton, J., Kaback, H. R., Svrakic, M., Young, R., and Holzenburg, A. (2005) *Arch Biochem Biophys* **434**, 352-357

140. Smith, A. G., Jayaram, J., Johnson, C. B., Ellis, E. A., Vitha, S., Collisson, E. W., and Holzenburg, A. (2009) *Methods in Molecular Biology* **536**, 533-543

141. Smith, A. G., Johnson, C. B., Ann Ellis, E., Vitha, S., and Holzenburg, A. (2008) *Analytical Biochemistry* **375**, 313-317

142. Emanuelsson, O., Nielsen, H., and von Heijne, G. (1999) *Protein Sci* **8**, 978-984

143. Laemmli, U. K. (1970) *Nature* **227**, 680-685

144. Towbin, H., T.Staehelin, and Gordon, J. (1979) *PNAS* **76**, 4350-4354

145. Mayers, C. P. (1970) *J. Clin Pathol.* **23**, 273-275

146. Kok, L. P., Visser, P. E., and Boon, M. E. (1988) *Histochem J* **20**, 323-328

147. Schwan, H.P. (1960). *In Medical Physics*, vol. 3, ed. Glasser, Chicago, Year Book Inc,. 52-63

148. Giberson, R. T., Demaree, R.S., Jr. (1995) *Microsc. Res. Tech.* **32**, 246-254

149. Login, G. R., and Dvorak, A. M. (1994) *Prog Histochem Cytochem* **27**, 1-127

150. Giberson, R. T., Demaree Jr., R.S. and Nordhausen, R.W. (1997) *J. Vet. Diagn. Invest.* **9**, 61-67

151. Demaree, R. S., Jr., Giberson, R.T., Smith, R.L. (1995) *Scanning* **17 (Suppl. 5)**, 25-26

152. Chicoine, L., and Webster, P. (1998) *Micros. Res. Tech.* **42**, 24-32

153. Van Dorp, R., Kok, P.G., Marani, E., Boon, M.E. and Kok, L.P. (1991) *J. Clin. Lab. Immunol.* **34**, 87-96

154. Li, W., Murai, Y., Okada, E., Matsui, K., Hayashi, S., Horie, M., and Takano, Y. (2002) *Pathology International* **52**, 234-238

155. Toyokuni, S., Kawaguchi, W., Akatsuka, S., Hiroyasu, M., and Hiai, H. (2003) *Pathology International* **53**, 259-261

156. Di Lallo, G., Anderluzzi, D., Ghelardini, P., and Paolozzi, L. (1999) *Mol Microbiol* **32**, 265-274

157. Caplan, M. R., and Erickson, H. P. (2003) *J Biol Chem* **278**, 13784-13788

158. Scheffers, D. J., den Blaauwen, T., and Driessen, A. J. (2000) *Mol Microbiol* **35**, 1211-1219

159. Popp, D., Iwasa, M., Narita, A., Erickson, H. P., and Maeda, Y. (2009) *Biopolymers* **91**, 340-350

160. Anderson, D., Guerios-Filho, F., and Erickson, H. (2004) *J Bacteriol* **186**, 5775-5781

161. Chen, Y. D., and Erickson, H. P. (2005) *J Biol Chem* **280**, 22549-22554

162. Ingerman, E., and Nunnari, J. (2005). *Methods Enzymol.*, vol. 404, eds. W.E. Balch, C.J. Der, and A. Hall, New York, Academic Press, 611-619.

163. Gupta, P., Anand, S. P., Srinivasan, R., Rajeswari, H., Indi, S., and Ajitkumar, P. (2004) *Microbiology* **150**, 3906-3908

164. Mukherjee, A., Saez, C., and Lutkenhaus, J. (2001) *J Bacteriol* **183**, 7190-7197

165. Hyman, A. A., Salser, S., Drechsel, D. N., Unwin, N., and Mitchison, T. J. (1992) *Molecular Biology of the Cell* **3**, 1155-1167

166. Mukherjee, A., and Lutkenhaus, J. (1998) *EMBO J* **17**, 462-469

167. Mukherjee, A., and Lutkenhaus, J. (1999) *J Bacteriol* **181**, 823-832

168. Harris, J. R., and Holzenburg, A. (1989) *Micron and Microscopica Acta* **20**, 223-238

169. Holzenburg, A., Jones, P. C., Franklin, T., Pali, T., Heimburg, T., Marsh, D., Findlay, J. B., and Finbow, M. E. (1993) *European Journal of Biochemistry* **213**, 21-30

170. Holzenburg, A., Bewley, M. C., Wilson, F. H., Nicholson, W. V., and Ford, R. C. (1993) *Nature* **363**, 470-472

171. Lu, C., and Erickson, H. P. (1998) *Methods Enzymol* **298**, 305-313

172. Kok, L., and Boon, M. (1992). *Microwave cookbook for microscopists: art and science of visualization*. 3rd ed. Leiden, Coulomb Press,

173. Giberson RT, A. R., Charlesworth J, Adamson G, Herrera GA. (2003) *Ultrastruct Pathol.* **27**, 187-196

174. Sanders, M. A. (2002) *Microsc. Microanal. Proc.* ***8*** *Suppl. 2*, 158-159

175. Gündoğdu, M. E., Kawai, Y., Pavlendova, N., Ogasawara, N., Errington, J., Scheffers, D. J., and Hamoen, L. W. (2011) *EMBO J* **30**, 617-626

176. Huecas, S., Llorca, O., Boskovic, J., Martin-Benito, J., Valpuesta, J. M., and Andreu, J. M. (2008) *Biophys. J.* **94**, 1796-1806

177. Oliva, M. A., Cordell, S. C., and Lowe, J. (2004) *Nat Struct Mol Biol* **11**, 1243-1250

178. Erickson, H. P., Anderson, D. E., and Osawa, M. (2010) *Microbiol Mol Biol Rev* **74**, 504-528

179. Lockhart, A., and Kendrick-Jones, J. (1998) *FEBS Letters* **430**, 278-282

180. Romanos, M. A., Scorer, C. A., and Clare, J. J. (1992) *Yeast* **8**, 423-488

181. Smith, P. K., Krohn, R. I., Hermanson, G. T., Mallia, A. K., Gartner, F. H., Provenzano, M. D., Fujimoto, E. K., Goeke, N. M., Olson, B. J., and Klenk, D. C. (1985) *Analytical Biochemistry* **150**, 76-85

182. Bradford, M. M. (1976) *Analytical Biochemistry* **72**, 248-254

183. Renosto, F., Seubert, P. A., and Segel, I. H. (1984) *J. Biol. Chem.* **259**, 2113-2123

184. Erickson, H. P. (2000) *Journal of Cell Biology* **148**, 1103-1106

185. Abramoff, M. D., Magelhaes, P. J., and S.J. Ram. (2004) *Biophotonics Intl.* **11**, 36-42

186. Chen, Y., Anderson, D. E., Rajagopalan, M., and Erickson, H. P. (2007) *J Biol Chem* **282**, 27736-27743

187. Gonzalez, J. M., Jimenez, M., Velez, M., Mingorance, J., Andreu, J. M., Vicente, M., and Rivas, G. (2003) *J Biol Chem* **278**, 37664-37671

188. Chen, Y., Anderson, D. E., Rajagopalan, M., and Erickson, H. P. (2007) *J Biol Chem* **282**, 27736-27743

189. Chen, Y. D., and Erickson, H. P. (2005) *J Biol Chem* **280**, 22549-22554

190. Penczek, P., Radermacher, M., and Frank, J. (1992) *Ultramicroscopy* **40**, 33-53

191. Wang, X., Huang, J., Mukherjee, A., Cao, C., and Lutkenhaus, J. (1997) *J Bacteriol* **179**, 5551-5559

192. Yan, K., Sossong, T. M., and Payne, D. J. (2001) *Biochem. Biophys. Res. Commun.* **284**, 515-518

193. Rivas, G., Lopez, A., Mingorance, J., Ferrandiz, M. J., Zorrilla, S., Minton, A. P., Vicente, M., and Andreu, J. M. (2000) *J Biol Chem* **275**, 11740-11749

194. Steinberg, I. Z., and Scheraga, H. A. (1963) *J Biol Chem* **238**, 172-181

195. Chothia, C., and Janin, J. (1975) *Nature* **256**, 705-708

196. Tsai, C. J., Lin, S. L., Wolfson, H. J., and Nussinov, R. (1997) *Protein Sci* **6**, 53-64

197. Löwe, J., and Amos, L. A. (1999) *EMBO J* **18**, 2364-2371

198. Leung, A. K., Lucile White, E., Ross, L. J., Reynolds, R. C., DeVito, J. A., and Borhani, D. W. (2004) *J Mol Biol* **342**, 953-970

199. Erickson, H.P. (1980). *Electron Microscopy at Molecular Dimensions*, eds. W. Baumeister and W. Vogell, Berlin: Springer, 309-317

200. Neet, K. E., and Timm, D. E. (1994) *Protein Sci* **3**, 2167-2174

201. Lan, G., Dajkovic, A., Wirtz, D., and Sun, S. X. (2008) *Biophys J* **95**, 4045-4056

202. Pyke, K. A., and Leech, R. M. (1994) *Plant Physiol* **104**, 201-207

203. Robertson, E. J., Rutherford, S. M., and Leech, R. M. (1996) *Plant Physiol* **112**, 149-159

204. Miyagishima, S. Y., Nozaki, H., Nishida, K., Nishida, K., Matsuzaki, M., and Kuroiwa, T. (2004) *J. Mol. Evol.* **58**, 291-303

205. Osteryoung, K. W., Stokes, K. D., Rutherford, S. M., Percival, A. L., and Lee, W. Y. (1998) *Plant Cell* **10**, 1991-2004

206. Osteryoung, K. W., and Nunnari, J. (2003) *Science* **302**, 1698-1704

207. Glynn, J. M., Froehlich, J. E., and Osteryoung, K. W. (2008) *Plant Cell* **20**, 2460-2470

208. Pettersen, E. F., Goddard, T. D., Huang, C. C., Couch, G. S., Greenblatt, D. M., Meng, E. C., and Ferrin, T. E. (2004) *J Comput Chem* **25**, 1605-1612

209. Madden, V. J., Henson, M.M. (1997) *Hearing Research* **111**, 76-84

210. Romberg, L., and Levin, P. A. (2003) *Annu Rev Microbiol* **57**, 125-154

211. Feucht, A., and Errington, J. (2005) *Microbiology* **151**, 2053-2064

212. Martin-Galiano, A. J., Buey, R. M., Cabezas, M., and Andreu, J. M. (2010) *J Biol Chem* **285**, 22554-22565

213. Pichoff, S., and Lutkenhaus, J. (2007) *Mol Microbiol* **64**, 1129-1138

214. Browse, J., and Somerville, C. R. (eds). (1994) *Glycerolipids*, Cold Spring Harbor Laboratory Press Plainview, NY

VITA

Name: Aaron Gene Smith

Email: agsmith4@hotmail.com
Address: The Microscopy and Imaging Center, Biological Sciences Building West (BSBW), Texas A&M University, College Station, Texas 77843-2257

Education: Bachelor of Science in Biochemistry, 2003
Oakland University, Rochester, Michigan

Awards: 2003 Merck/AAAS Undergraduate Science Research Program (USRP) scholar
2008 Microscopy Society of America Presidential Student Award
2009 Microscopy Society of America student poster award (Applications of Microscopy & Microanalysis - Biological, 1st. prize)

Publications:

1. Chaudhry, G.R., Yao, D., Smith, A. and Hussain, A. (2004). Osteogenic cells derived from embryonic stem cells produced bone nodules in three-dimensional scaffolds. *Journal of Biomedicine and Biotechnology*, **2004** (4): 203-210.

2. Yao, D.G., Smith, A., Nagarajan, P., Vasquez, A., Dang, L. and Chaudhry, G.R. (2006). Fabrication of polycaprolactone scaffolds using a sacrificial compression-molding process. *Journal of Biomedical Materials Research Part B-Applied Biomaterials* **77B**, 287-295.

3. Mohammad, M.M., Donti, T.R., Yakisich, J.S., Smith, A.G. and Kapler, G.M. (2007). Tetrahymena ORC contains a ribosomal RNA fragment that participates in rDNA origin recognition. *EMBO J* **26**, 5048-5060.

4. Smith, A.G., Johnson, C.B., Ellis E.A., Vitha, S., and Holzenburg A. (2008). Protein screening using cold microwave technology. *Analytical Biochemistry* **375**, 313-317.

5. Smith, A. G., Jayaram, J., Johnson, C. B., Ellis, E. A., Vitha, S., Collisson, E. W. and Holzenburg, A. (2009) Improved protein detection using cold microwave technology. *Methods in Molecular Biology* **536**, 533-43.

6. Smith, A. G., Johnson, C. B., Vitha, S. and Holzenburg, A. (2010) Plant FtsZ1 and FtsZ2 expressed in a eukaryotic host: GTPase activity and self-assembly. *FEBS Letters* **581**: (1), 166-172.